Coordination Chemistry Reviews 253 (2009) 526–563

Contents lists available at ScienceDirect

Coordination Chemistry Reviews

journal homepage: www.elsevier.com/locate/ccr

Review

Prediction of molecular properties and molecular spectroscopy with density functional theory: From fundamental theory to exchange-coupling

Frank Neese

Lehrstuhl für Theoretische Chemie, Universität Bonn, Institut für Physikalische und Theoretische Chemie, Wegelerstrasse 12, D-53115 Bonn, Germany

E-mail address: neese@thch.uni-bonn.de.

0010-8545/$ – see front matter
doi:10.1016/j.ccr.2008.05.014

ARTICLE INFO

Article history:
Received 5 March 2008
Accepted 23 May 2008
Available online 29 May 2008

Keywords:
Density functional theory
Linear response theory
Molecular properties
Inorganic spectroscopy
Spin states
Exchange coupling

ABSTRACT

This review provides a detailed account of density functional theory (DFT) and its application to the calculation of molecular properties of inorganic compounds. After introducing some fundamental quantum mechanical concepts, the foundations of DFT and their realization in the framework of the Kohn–Sham construction are described. Following a brief exposition of the computational machinery required to carry out large-scale DFT calculations, the application of analytic derivative theory to DFT is developed in some detail. The cases covered include geometric, electric, magnetic and time-dependent perturbations. The developed theoretical apparatus is then applied to the calculations of molecular structures, vibrational energies as well as a wide variety of properties including absorption, circular dichroism, magnetic circular dichroism, resonance Raman, X-ray absorption, Mössbauer and electron paramagnetic resonance spectroscopies. Finally, the important subjects of spin state energetics and exchange couplings in oligomeric transition metal clusters is discussed.

1. Introductory remarks

The present volume is devoted to the use of density functional theory (DFT) in (bio)-inorganic chemistry. In fact, DFT has enjoyed an enormous popularity in this field over the past two decades (for reviews see [1–16]) and has found many users that range from hard-core theoretical chemists to experimentalists who wish to employ DFT alongside with their experimental studies. Parallel with the impressive development of computational hardware the quantum chemical software that is required to perform DFT calculations has progressed to a state where calculations can be performed with high efficiency and in a user friendly manner. Consequently, at least a dozen of major program packages are available, either commercially or free of charge, that allow for DFT calculations on large molecules (Table 1). The notion of a 'large' molecule in quantum chemistry is a moving target. At the time of writing molecules with around 100 atoms can be treated routinely with DFT methods and molecules with around 200 atoms with some effort. Even larger molecules belong to a specialist domain and will usually require 'linear-scaling' or mixed classical/quantum mechanical (QM/MM) techniques in order to be approachable. Such techniques have been extensively developed but have not yet found their way into the standard arsenal of the practicing computational chemist.

The present chapter is intended to provide the theoretical background that is necessary to appreciate the physical content of DFT. It is neither intended to be a complete guide into the technical aspects of DFT nor it is intended to be a comprehensive description of the entire theory of DFT. Rather, the aim of the chapter is to provide the main lines of thought that led to present day DFT, to briefly touch the most frequently used methods and to describe how the existing DFT methods can be used to calculate structures, energies and spectroscopic parameters of molecules of bio-inorganic interest.

It is hoped that the material contained in this chapter proves to be useful for theoretical Ph.D. students at the beginning of their thesis work and for spectroscopists who already had contact with DFT calculations and wish to learn more about the background of the calculations that they are doing. The physical principles of the various spectroscopies that are treated in this chapter can, of course, not be described and the reader is referred to several excellent compilations [17,18]. Extended examples of DFT applications will be amply covered in the other articles of this volume and will therefore only receive a cursory treatment here.

2. Theoretical background

2.1. The molecular Hamiltonian

The molecular Hamiltonian operator that describes the vast majority of chemistry is deceptively simple—it just contains the Coulombic interactions between the charged nuclei and electrons together with the kinetic energy of the electrons. In atomic units[1] it reads for a system with N electrons and M nuclei [19,20]:

$$\begin{aligned}\hat{H}_{\mathrm{BO}} &= T_e + V_{eN} + V_{ee} + V_{NN} \\ &= -\frac{1}{2}\sum_{i=1}^{N}\nabla_i^2 - \sum_{i=1}^{N}\sum_{A=1}^{M}\frac{Z_A}{|\mathbf{r}_i - \mathbf{R}_A|} \\ &\quad + \frac{1}{2}\sum_{i=1}^{N}\sum_{\substack{j=1 \\ j\neq i}}^{N}\frac{1}{|\mathbf{r}_i - \mathbf{r}_j|} + \frac{1}{2}\sum_{A=1}^{M}\sum_{\substack{B=1 \\ A\neq B}}^{M}\frac{Z_A Z_B}{|\boldsymbol{R}_A - \boldsymbol{R}_B|} \\ &\equiv \sum_i h(i) + \frac{1}{2}\sum_{i\neq j} g(i,j) + V_{NN}\end{aligned} \tag{1}$$

[1] One atomic unit of energy (1 E_h) is equivalent to ~27.21 eV or ~627 kcal/mol. The atomic unit of length is equivalent to 0.529 Å. In these units the numerical values of $\hbar$ and $4\pi\varepsilon_0$ are unity.

Table 1
Alphabetic list of major program packages used for performing DFT calculations

Program	Leading authors	Homepage	Commercial
ADF	Baerends, Ziegler	http://www.scm.com/	Yes
DALTON	Helgaker, Jörgensen, Ruud, Agren, Salek	http://www.kjemi.uio.no/software/dalton/dalton.html	No
DGauss	Andzelm, Wimmer	http://cachesoftware.com/index_main.php	Yes
DeMon	Salahub, Casida, Köster	http://www.demon-software.com/public_html/index.html	No
DMol	Delly	http://www.accelrys.com/products/mstudio/modeling/quantumandcatalysis/dmol3.html	Yes
Gamess	Gordon, Schmidt	http://www.msg.ameslab.gov/GAMESS/	No
Gaussian	Frisch, Pople, Gill	http://www.gaussian.com/	Yes
Jaguar	Friesner	http://www.schrodinger.com/ProductDescription.php	Yes
NWChem	Kendall, Windus	http://www.emsl.pnl.gov/docs/nwchem/	No
ORCA	Neese	http://www.thch.uni-bonn.de/tc/orca/	No
QChem	Head-Gordon, Gill	http://www.q-chem.com/	Yes
TurboMole	Ahlrichs, Häser, Furche, Hättig	http://www.cosmologic.de/QuantumChemistry/main_turbomole.html	Yes

where i, j sum over electrons at positions $\boldsymbol{r}_i$ and A, B over nuclei at positions $\boldsymbol{R}_A$ with nuclear charges Z_A. The term $(-1/2)\nabla_i^2 = (1/2)p_i^2$ is the quantum mechanical form of the kinetic energy operator of the ith electron with momentum $\boldsymbol{p}_i$. Note that this Hamiltonian corresponds to the Born–Oppenheimer (BO) approximation in which the kinetic energy of the nuclei is dropped and the nuclear positions enter as fixed parameters in the equations. The BO approximation is assumed to be valid throughout this chapter.

Associated with the N-electron Hamiltonian is a time-independent N-electron Schrödinger equation:

$$\hat{H}_{\mathrm{BO}}\Psi(\mathbf{x}_1,\ldots,\boldsymbol{x}_{\mathrm{N}}|\boldsymbol{R}_1,\ldots,\boldsymbol{R}_{\mathrm{M}}) = E\Psi(\boldsymbol{x}_1,\ldots,\boldsymbol{x}_{\mathrm{N}}|\boldsymbol{R}_1,\ldots,\boldsymbol{R}_{\mathrm{M}}) \quad (2)$$

Here $\boldsymbol{x}_{\mathrm{i}}$ collectively denotes the three spatial degrees of freedom ($\boldsymbol{r}_{\mathrm{i}}$) and the spin-degree of freedom (σ_i) for the ith electron. Eq. (1) constitutes a high-dimensional differential equation that can – in principle – be solved at any nuclear configuration $\boldsymbol{R}=\boldsymbol{R}_1,\ldots,\boldsymbol{R}_{\mathrm{M}}$ for the exact eigenstates $\Psi_0(\boldsymbol{x}|\boldsymbol{R}),\Psi_1(\boldsymbol{x}|\boldsymbol{R}),\ldots$ ($\boldsymbol{x}=\boldsymbol{x}_1,\ldots,\boldsymbol{x}_N$) with energies $E_0, E_1,\ldots$ that represent the ground- and the electronically excited states of the system as a function of molecular geometry. The interpretation of the many-electron wavefunction is:

$\Psi_I(\mathbf{x}|\mathbf{R})\Psi_I(\mathbf{x}|\mathbf{R})^*\,\mathrm{d}\mathbf{x}$ = probability for finding the electrons in an infinitesimal volume element $\mathrm{d}x$ around configuration $\mathbf{x}$ if the nuclei are at rest at positions $\mathbf{R}$ and the system is in the electronic eigenstate I

The set of many-electron wavefunctions Ψ_I define the maximum amount of information that can be gained about the molecular system according to the laws of quantum mechanics. Unfortunately, the complexity of the N-electron problem defeats exact solution and consequently, approximations are needed. The best approximations that can nowadays be generated provide energies within <1 kJ/mol of their exact values [21–25]. However, the associated methods are computationally so demanding that they can only be applied to very small systems that are irrelevant to (bio)inorganic chemistry.

2.2. Reduced density matrices

The many electron wavefunctions $\Psi_I(\boldsymbol{x}|\boldsymbol{R})$ are objects of bewildering complexity that can not be pictured or easily understood. We will now drop the subscript 'I' and refer to the electronic ground state until otherwise noted. As a matter of fact, these many-electron wavefunctions contain far more information than is necessary in order to deduce all observable properties of the system. Since the BO Hamiltonian does not contain more than two-particle operators, it is in fact sufficient to know the distribution of *pairs* of electrons. This information about the *pair distribution function* is contained in the second-order reduced density-matrix associated with the wavefunction $\Psi(\boldsymbol{x}|\boldsymbol{R})$. It is defined by

$$\Gamma(\boldsymbol{x}_1,\boldsymbol{x}_2) = \frac{N(N-1)}{2}\int \Psi(\boldsymbol{x}_1,\boldsymbol{x}_2,\ldots,\boldsymbol{x}_N|\boldsymbol{R}) \times\Psi(\boldsymbol{x}_1,\boldsymbol{x}_2,\ldots,\boldsymbol{x}_N|\boldsymbol{R})^*\,\mathrm{d}\boldsymbol{x}_3\ldots\mathrm{d}\boldsymbol{x}_N \quad (3)$$

The integral evaluates to the probability of finding a pair of electrons in the arrangement $(\boldsymbol{x}_1,\boldsymbol{x}_2)$ irrespective of the positions of the remaining electrons. The normalization factor is chosen such that the integral of $\Gamma(\boldsymbol{x}_1,\boldsymbol{x}_2)$ over all arrangements $(\boldsymbol{x}_1,\boldsymbol{x}_2)$ returns the number of electron pairs. Analogously, the single particle density matrix is defined by

$$\gamma(\boldsymbol{x}_1,\boldsymbol{x}_1')=N\int \Psi(\boldsymbol{x}_1,\boldsymbol{x}_2,\ldots,\boldsymbol{x}_N|\boldsymbol{R})\Psi(\boldsymbol{x}_1',\boldsymbol{x}_2,\ldots,\boldsymbol{x}_N|\boldsymbol{R})^*\mathrm{d}\boldsymbol{x}_2\ldots\mathrm{d}\boldsymbol{x}_N \quad (4)$$

Here we have applied a small trick and have introduced a new set of primed variables $\mathbf{x}_1'$ that only enters into ψ^* but not into ψ. The reason for this somewhat unusual manipulation will become apparent below. The 'diagonal element' of the first order density matrix $\rho(\boldsymbol{x})=\gamma(\boldsymbol{x},\boldsymbol{x})$ is simply the electron density at configuration $\boldsymbol{x}$ as it may be measured by electron diffraction techniques. As long as we disregard relativistic effects, $\rho(\boldsymbol{x})$ can be decomposed into contributions from spin-up and spin-down electrons as

$$\rho(\boldsymbol{r}) = \int \rho(\boldsymbol{x})\,\mathrm{d}s = \rho^{\alpha}(\boldsymbol{r}) + \rho^{\beta}(\boldsymbol{r}) \quad (5)$$

where the 'integration' over the spin-variable s amounts to a summation over the two possible argument $s=\pm(1/2)$ of a function defined in one-particle spin-space. The electron density $\rho(\boldsymbol{r})$ simply represents N times the probability for finding an electron at position $\boldsymbol{r}$ irrespective of its spin. The *spin-density* $\rho^{\alpha-\beta}(\boldsymbol{r})=\rho^{\alpha}(\boldsymbol{r})-\rho^{\beta}(\boldsymbol{r})$ represents the distribution of unpaired spins and is normalized to $N_\alpha - N_\beta$.

Note that $\gamma(\boldsymbol{x}_1,\boldsymbol{x}_1')$ can be obtained from a generalization of $\Gamma(\boldsymbol{x}_1,\boldsymbol{x}_2)$ to $\Gamma(\boldsymbol{x}_1,\boldsymbol{x}_2,\boldsymbol{x}_1',\boldsymbol{x}_2')$ as

$$\gamma(\boldsymbol{x}_1,\boldsymbol{x}_1') = \frac{2}{N-1}\int \Gamma(\boldsymbol{x}_1,\boldsymbol{x}_2,\boldsymbol{x}_1',\boldsymbol{x}_2)\,\mathrm{d}\boldsymbol{x}_2 \quad (6)$$

In terms of these density matrices, the exact energy $E = \langle\psi|H|\psi\rangle$ can be written as

$$E = V_{NN} - \frac{1}{2}\int_{\boldsymbol{x}_1=\boldsymbol{x}_1'} \nabla^2\gamma(\boldsymbol{r}_1,\boldsymbol{r}_1')\,\mathrm{d}\boldsymbol{x} - \sum_A \int \rho(\boldsymbol{r}) Z_A r_{iA}^{-1}\,\mathrm{d}\boldsymbol{r} + \int\int \Gamma(\boldsymbol{r}_1,\boldsymbol{r}_2) r_{12}^{-1}\,\mathrm{d}\boldsymbol{x}_1\,d\boldsymbol{x}_2 \quad (7)$$

The spin-free density matrices used in this expression are obtained by simply integrating over the spin-variables:

$$\gamma(\boldsymbol{r},\boldsymbol{r}') = \int_{s_1=s_1'} \gamma(\boldsymbol{x}_1,\boldsymbol{x}_1')\,\mathrm{d}s = \gamma^{\alpha}(\boldsymbol{r},\boldsymbol{r}') + \gamma^{\beta}(\boldsymbol{r},\boldsymbol{r}') \quad (8)$$

$$\Gamma(\boldsymbol{r}_1,\boldsymbol{r}_2) = \int\int \Gamma(\boldsymbol{x}_1,\boldsymbol{x}_2)\,\mathrm{d}s_1\,\mathrm{d}s_2 = \Gamma^{\alpha\alpha}(\boldsymbol{r}_1,\boldsymbol{r}_2) + \Gamma^{\beta\beta}(\boldsymbol{r}_1,\boldsymbol{r}_2) + \Gamma^{\alpha\beta}(\boldsymbol{r}_1,\boldsymbol{r}_2) + \Gamma^{\beta\alpha}(\boldsymbol{r}_1,\boldsymbol{r}_2) \quad (9)$$

From this discussion, it becomes apparent that once the pair-distribution function Γ is known, all properties of the system (in the given electronic state) can be calculated exactly by evaluating the appropriate one- and two-electron integrals. Obviously, Γ, γ and in particular ρ are *much* simpler objects than the N-electron wavefunction itself. Hence, an old dream of quantum chemistry is to *directly* calculate these density matrices *without* the "detour" of the many electron wavefunction. Perhaps one could formulate a variational principle that allows the variation of a trial Γ in order to obtain a 'best' approximation to the true Γ within the given Ansatz. However, so far this dream has been proven to be elusive although there has been progress along these lines [26]. The reason is the N-representability problem: in order to obtain a physically allowed Γ it must be derivable (in principle) from a physically allowed N-electron wavefunction Ψ. The necessary and sufficient conditions on Γ to be N-representable, are, however, not known.

In DFT one does not attempt to calculate or approximate Γ. Instead, it will be motivated below that – in principle – it is enough to know $\rho(\boldsymbol{r})$ in order to fully determine the exact E.

2.3. Hartree–Fock theory

If one proceeds along a systematic route the most obvious choice is to use the variational principle in order to obtain an optimum approximate Ψ from which Γ, γ and E are calculated. The term in the Hamiltonian that prevents an exact solution is the electron–electron interaction. Without this term, the Hamiltonian would be simply a sum of one-particle contributions and its eigenfunctions would be a product of single-electron wavefunctions, e.g. $\Psi(\boldsymbol{x}_1,\ldots,\boldsymbol{x}_N) = \psi_1(\boldsymbol{x}_1),\ldots,\psi_N(\boldsymbol{x}_N)$. However, such a Hartree product violates the Pauli principle and hence the appropriate form for a system of noninteracting electrons is a single *Slater determinant*:

$$\Psi_{\mathrm{SD}}(\boldsymbol{x}_1,\ldots,\boldsymbol{x}_N) = \frac{1}{\sqrt{N!}}\begin{vmatrix} \psi_1(\boldsymbol{x}_1) & \psi_2(\boldsymbol{x}_1) & \cdots & \psi_N(\boldsymbol{x}_1) \\ \psi_1(\boldsymbol{x}_2) & \psi_2(\boldsymbol{x}_2) & \cdots & \psi_N(\boldsymbol{x}_2) \\ \vdots & \vdots & \ddots & \vdots \\ \psi_1(\boldsymbol{x}_N) & \psi_2(\boldsymbol{x}_N) & \cdots & \psi_N(\boldsymbol{x}_N) \end{vmatrix} \quad (10)$$

Which, from the mathematical properties of determinants, is properly antisymmetric with respect to interchange of two sets of electronic variables and is usually abbreviated by $|\psi_1,\ldots,\psi_N|$.[2] The single-electron wavefunctions ψ_i that enter into Eq. (10) are, as of yet, unspecified, but should form an orthonormal set. They are called *orbitals*. The expectation value of the BO operator over such a Slater determinant is:

$$\langle\Psi_{\mathrm{SD}}|H_{\mathrm{BO}}|\Psi_{\mathrm{SD}}\rangle = V_{NN} + \sum_i \langle\psi_i|h|\psi_i\rangle + \frac{1}{2}\sum_{i,j}\langle\psi_i\psi_j||\psi_i\psi_i\rangle \quad (11)$$

where the one- and two-electron integrals are defined as[3]:

$$\langle\psi_i|h|\psi_i\rangle = \int \psi_i^*(\boldsymbol{x})h(\boldsymbol{x})\psi_i(\boldsymbol{x})\,\mathrm{d}\boldsymbol{x} \quad (12)$$

$$\begin{aligned}\langle\psi_i\psi_j||\psi_i\psi_j\rangle &= \langle\psi_i\psi_j|\psi_i\psi_j\rangle - \langle\psi_i\psi_j|\psi_j\psi_i\rangle \\ &= \int\int \psi_i^*(\boldsymbol{x}_1)\psi_j^*(\boldsymbol{x}_2)r_{12}^{-1}[\psi_i(\boldsymbol{x}_1)\psi_j(\boldsymbol{x}_2) - \psi_i(\boldsymbol{x}_2)\psi_j(\boldsymbol{x}_1)]\,\mathrm{d}\boldsymbol{x}_1\,\mathrm{d}\boldsymbol{x}_2\end{aligned} \quad (13)$$

Obviously, there are two types of electron–electron repulsion integrals. The Coulomb-integral $J_{ij} \equiv \langle\psi_i\psi_j|\psi_i\psi_j\rangle$ represents the electrostatic interaction of two-smeared out charge clouds $|\psi_i|^2$ and $|\psi_j|^2$ while the second integral $K_{ij} \equiv \langle\psi_i\psi_j|\psi_i\psi_j\rangle$ represent the self-repulsion of an 'interference-density' $\psi_i\psi_j$. As will be elaborated in Section 7.10, these 'exchange' integrals solely arise from the antisymmetry requirement of the wavefunction and have nothing to do with a genuine 'exchange interaction' between electrons. Both types of integrals are inherently positive. Since $J_{ii} = K_{ii}$ the negative sign of the exchange interaction cancels the spurious 'self-interaction' terms arising from the J_{ii} integrals.

The basic idea of Hartree–Fock theory is to use this *independent particle* model as an Ansatz for the full, interacting many electron system. By means of the *variational principle*:

$$E \le \frac{\langle\Psi_{\mathrm{trial}}|H|\Psi_{\mathrm{trial}}\rangle}{\langle\Psi_{\mathrm{trial}}|\Psi_{\mathrm{trial}}\rangle} \quad (14)$$

One seeks the single determinant that yields the lowest energy. Thus, one varies the *functional* $E[\{\psi\}]$ with respect to the form of the orbitals. The energy that one obtains is an upper bound to the true ground state energy of the system. However, one cannot perform a free variation of the orbitals, since these are required to stay orthonormal in the process. This is usually achieved by means of Lagrange multipliers [20]. The result is that all of the orbitals have to satisfy the same pseudo-one-electron *self-consistent field* (SCF) equations:

$$\hat{F}\psi_i(\boldsymbol{x}) = \varepsilon_i\psi_i(\boldsymbol{x}) \quad (15)$$

The operator $\hat{F}$ is the *Fock-operator*. It is a rather complicated integro-differential operator. For an arbitrary pair of orbitals ψ_p,ψ_q, the matrix elements of the Fock-operator are:

$$\langle\psi_p|F|\psi_q\rangle = \langle\psi_p|h|\psi_q\rangle + \sum_i \langle\psi_i\psi_p||\psi_i\psi_q\rangle \quad (16)$$

The interpretation of the orbital energy $\varepsilon_i = \langle\psi_i|F|\psi_i\rangle$ is that it provides the average energy of an electron that occupied ψ_i in the field of the nuclei and the average field of the other electrons. By Koopmans' theorem, it is approximately equal to minus the energy required to remove the electron from this orbital (i.e. $-\varepsilon_i$ approximates an ionization potential). It is obvious from Eq. (10) that the Fock-operator depends on its own eigenfunctions. Hence, the Hartree–Fock equations constitute a complicated set of nonlinear

[2] If one wants to specify the spin of a given one-electron function one writes it with an overbar in order to indicate a spin-beta spin factor, e.g. $|\psi_1\bar{\psi}_1\ldots\psi_N\bar{\psi}_N|$ for a closed shell system.

[3] We will also simply write $\langle pq|rs\rangle = \langle\psi_p\psi_q|\psi_r\psi_s\rangle$.

equations that cannot be solved directly.[4] Rather, the HF equations are solved by iterative methods as described in Section 5.

A very useful form of the HF equations can be readily derived and reads:

$$\hat{F}\hat{P} - \hat{P}\hat{F} = 0 \tag{17}$$

where $\hat{F}$ is the Fock operator and $\hat{P}$ is the so-called density operator $\hat{P} = \sum_i |\psi_i\rangle\langle\psi_i|$ that has the property of being idempotent ($\hat{P}^2 = \hat{P}$).

Hartree–Fock theory is surprisingly successful. Despite the crude Ansatz for the many-electron wavefunction HF theory is capable to recover around 99.9% of the exact ground state energy. However, the remaining fraction of ~0.1% still amounts to several Hartrees (>1000 kcal/mol) for a medium sized molecule. Thus, on a chemically relevant energy scale ($\sim 1\,\mathrm{m}E_\mathrm{h} = 10^{-3}\,E_\mathrm{h}$), the error of the HF approximation is, unfortunately, gigantic. Of course, in chemistry, what matters are energy differences rather than total energies. For these, the HF approximation can be much better and many chemically meaningful results can be obtained with it, in particular, if the number and identity of the bonds that are involved in the chemical process under study does not change drastically. Yet, the errors of the HF approximation in chemistry are still so large that it is seldom used in actual investigations.

While there are many ways to approach the subject, the most common definition of the *correlation energy* is, that it is the energy that is missing from the Hartree–Fock energy. Thus:

$$E_\mathrm{C} = E_\mathrm{exact} - E_\mathrm{HF} \tag{18}$$

In this definition, the correlation energy is always negative (except for one electron systems where it is zero). Physically speaking, the correlation energy arises from the electron–electron interactions that are not covered by the mean-field approach provided in the HF treatment. Thus, electron–electron correlation is an 'instantaneous' interaction and is of short range.

Much progress has been made in quantum chemistry with the development of 'post-HF' methods that recover sizeable fractions of the correlation energy (today these are essentially Coupled-Cluster and many-body perturbation theory [27,28], and their 'multireference' generalizations [29–35]). In fact, if high accuracy is required, these are the methods of choice. However, they have presently still not been developed to the stage where one could routinely treat molecules of interest for (bio)inorganic chemistry owing to the high- and steeply rising computational effort that is characteristic of these approaches.[5] Thus, these methods will not be covered in this chapter (see [36–38] for reviews in an inorganic chemistry context).

3. Foundations of DFT

Owing to the enormous rise in popularity in chemistry and physics DFT was rewarded with the Nobel prize for chemistry in 1998 to Walter Kohn (for developing DFT) and to John Pople (for his developments of computational methods in quantum chemistry in general). In fact, Kohn stated [39] "*DFT has found many useful applications when moderate accuracies* (*typically in the range* 10^{-3} to 10^{-1}) *are required. It is not a precision method which, in principle, can be pushed to arbitrary accuracy*". Viewed from this perspective, the success of DFT is truly remarkable and must be considered as very fortunate for the development of theory in chemistry. DFT, as we know it today, rests on the theorems of Hohenberg and Kohn which were formulated in the 1960s [40]. However, it should be recognized that DFT has been pursued by theoreticians since the cradle days of quantum mechanics. In fact, important ingredients that are used in practically all presently used functionals have been formulated in the 1930s by a combination of mathematical rigor and physical intuition [41]. The only thing that was not realized at that time was that these methods are approximate realizations of a formally exact theory.

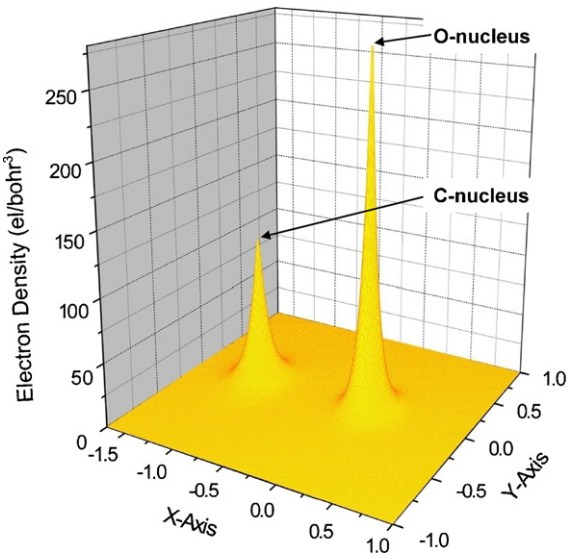

Fig. 1. Electron density of the CO molecule in the *X*–*Y* plane. The density shows characteristic cusps at the nuclear positions from which the position of the nuclei and their nuclear charge can be deduced.

3.1. Everything from the density?

It was stated in Section 2.2, that the true ground state energy could be calculated from the second-order density matrix if it could only be calculated without having to know the many electron wavefunction Ψ. DFT is based on a considerably more powerful theorem that proves that – in principle – the exact energy could be determined from the knowledge of the electron density $\rho(\boldsymbol{r})$ alone. It might still be considered surprising that such a theorem exists and since DFT is based on this theorem it is appropriate to investigate how it comes about. At first glance it seems counter-intuitive that one would be able to calculate the interactions of *electron pairs* without knowing the actual distribution of the pairs (a two-electron entity) but only the distribution of the electrons (e.g. $\rho(\boldsymbol{r})$; a one-electron entity).

The basic ideas are disarmingly simple and the mathematical elaboration of the theory (which we will not go into in this chapter [42]) is frustratingly complex. Consider the plot of the electron density of the CO molecule in Fig. 1.

It is a rather smooth function except at the positions of the nuclei where $\rho(\boldsymbol{r})$ has a cusp (Fig. 1). The cusp is finite and has values [43]:

$$\lim_{r\to 0}\left[\frac{\partial}{\partial r} + 2Z_A\right]\bar{\rho}(r) = 0 \tag{19}$$

where $\bar{\rho}(r)$ is the spherically averaged electron density. Qualitatively, the argument runs as follows (Fig. 2): (1) The BO Hamiltonian is completely determined by specifying the number of electrons and the 'external potential', v (in our case simply V_{eN}) which in turn

[4] It is not even known how many different solutions the Hartree–Fock equations have nor is it possible to mathematically prove the existence of such solutions. However, such fundamental questions are of no concern in the present context.

[5] In fact, these approaches are only highly accurate in conjunction with very large and flexible basis sets of at least triply-polarized triple-ζ quality. Such basis sets are not yet affordable for larger molecules. Correlated *ab initio* calculations with smaller basis sets cannot claim to have achieved high-accuracy and must be viewed with caution.

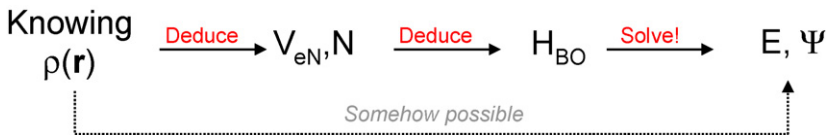

Fig. 2. The route from the density to the exact energy and wavefunction.

is fully specified once the nuclear positions and nuclear charges are known. (2) Given N and v, the Schrödinger equation has a unique ground state energy E (now regarded as a functional of N and v, $E[N, v]$) and associated many electron wavefunction Ψ.[6] (3) Since one can deduce N from the integral over $\rho(\boldsymbol{r})$ and the nuclear positions and charges from the cusps of $\rho(\boldsymbol{r})$ one can fully reconstruct the Hamiltonian from only the knowledge of $\rho(\boldsymbol{r})$. Since the Hamiltonian determines the energy, the wavefunction and also all associated properties, it must be possible to construct a functional $E[\rho]$ that provides the exact energy given the exact density. The existence of this functional is the subject of the first Hohenberg–Kohn theorem [44].

How would one start to construct such a functional? The obvious starting point is to see which terms in the exact energy expression can already be expressed in terms of $\rho(\boldsymbol{r})$ directly. A quick inspection shows that this is only true for the nuclear-electron attraction term (disregarding the trivial nuclear-nuclear repulsion term). The electronic kinetic energy involves a differential operator and consequently we need to know the more general first-order density *matrix* $\gamma(\boldsymbol{r}, \boldsymbol{r}')$ while the two-particle density $\Gamma(\boldsymbol{x}_1, \boldsymbol{x}_2)$ seems to be required in order to calculate the electron–electron repulsion. The most discouraging part is the latter interaction.

Insight into its dependence on the density can be obtained by studying the Hartree–Fock energy in terms of density matrices:

$$E_{\mathrm{HF}} = V_{NN} \underbrace{- \sum_A Z_A \int \rho(\boldsymbol{r}) r_{iA}^{-1} \, \mathrm{d}\boldsymbol{r}}_{V_{eN}[\rho]} + \underbrace{\frac{1}{2} \int\int \rho(\boldsymbol{r}_1)\rho(\boldsymbol{r}_2) r_{12}^{-1} \, \mathrm{d}\boldsymbol{r}_1 \, \mathrm{d}\boldsymbol{r}_2}_{J[\rho]} \underbrace{- \frac{1}{2} \int\int \gamma(\boldsymbol{r}_1, \boldsymbol{r}_2)\gamma(\boldsymbol{r}_1, \boldsymbol{r}_2) r_{12}^{-1} \, \mathrm{d}\boldsymbol{r}_1 \, \mathrm{d}\boldsymbol{r}_2}_{\mathrm{K}} \underbrace{- \frac{1}{2} \int_{\boldsymbol{r}'=\boldsymbol{r}} \nabla^2 \gamma(\boldsymbol{r}, \boldsymbol{r}') \, \mathrm{d}\boldsymbol{r}}_{\mathrm{T}} \tag{20}$$

This expression reveals that a part (in fact, typically 80–90%) of the electron–electron repulsion energy can be written as $J[\rho]$, the quasi-classical self-interaction energy of the charge-cloud $\rho(\boldsymbol{r})$. However, even in the Hartree–Fock model – that by definition contains no correlation – the exchange and kinetic energy terms require the knowledge of the entire one-particle density matrix. Yet, the first HK theorem states that it *must* be possible to somehow write these terms and the missing electron correlation in terms of the density. Thus, we may write:

$$E[\rho] = V_{NN} + V_{eN}[\rho] + J[\rho] + T[\rho] + E'_{\mathrm{XC}}[\rho] \tag{21}$$

where $T[\rho]$ is the (unknown) kinetic energy functional and $E'_{\mathrm{XC}}[\rho]$ is the (unknown) exchange-correlation functional. These latter two functionals are "universal" in the sense that they have a common (but unknown) form for every system.

If it is presumed that these functionals would be known, the second Hohenberg–Kohn theorem provides the necessary recipe to obtain the exact energy. It states that for any trial density $\tilde{\rho}$, the value of $E[\tilde{\rho}] \geq E[\rho]$ where the equality holds if $\tilde{\rho}$ matches the exact ρ. Thus, minimization of $E[\rho]$ over the range of allowed $\tilde{\rho}$ would yield the exact ground state density, energy and hence all other properties of the system.

[6] This discussion does only apply to orbitally non-degenerate states. The treatment of spin-degeneracy presents no problem. Since the eigenfunctions of the BO Hamiltonian are also eigenfunctions of the total-spin squared operator S^2, the condition is that the ground state is only $2S+1$-fold degenerate.

3.1.1. A point of concern

While the existence of the universal functional is remarkable, one should probably not overlook one fact: the one thing that we have so far achieved is to reconstruct the many electron Hamiltonian from the density. We are then faced with the fact that we can not solve the associated many-electron Schrödinger equation exactly. However, *we knew the Hamiltonian before and could not solve the associated Schrödinger equation*! The Hamiltonian is given by Eq. (1) in this review, in Eq. (1) of the famous book by Parr and Yang [44] and in pretty much "Eq. (1)" of any other exposition of quantum chemistry. Viewed from this perspective DFT brings oneself back to the start with one additional step: the reconstruction of the Hamiltonian from the density which, so far, has no practical relevance. The common situation is that the number and identity of atoms as well as the number of electrons in the system is known in advance and at least a reasonable guess of the initial nuclear positions is available.

Thus, depending on the taste of the reader, the existence of the universal functional might be taken as an inspiration for the development of new approximate approaches and as a source of physical insight – or – as an elaborate excuse for pursuing more or less elegant approximate methods that have, in their essence, been developed by physical reasoning much earlier.

3.2. The Kohn–Sham construction

One of the most difficult early problems has been to develop an accurate expression for the kinetic energy in terms of the density. Models like the well-known Thomas–Fermi method provide such an explicit expression [44]. However, it is unfortunately not accurate enough for chemical applications. Practically speaking, the kinetic energy predicted by the Hartree–Fock method is not a poor approximation to the exact kinetic energy. Thus, one may wonder whether it would not be possible to use some aspects of HF theory in constructing an appropriate expression that would still maintain the formal exactness of DFT. Indeed, the Kohn–Sham construction provides such a recipe [45]. Consider a fictitious system of non-interacting electrons. Such a system is described exactly by a single Slater determinant $\psi_{\mathrm{KS}}(\boldsymbol{x}) = |\psi_i \ldots \psi_{\mathrm{N}}|$. The electron density associated with this determinant is:

$$\rho_{\mathrm{KS}}(\boldsymbol{r}) = \sum_i \int |\psi_i(\boldsymbol{x})|^2 \, \mathrm{d}s \tag{22}$$

In order to make the connection to the formal DFT theory, it is required that $\rho_{\mathrm{KS}}(\boldsymbol{r}) = \rho(\boldsymbol{r})$; the fictitious system and the real system are required to share the same density. One may then re-write:

$$E[\rho] = V_{NN} + T_{\mathrm{s}}[\rho] + V_{eN}[\rho] + J[\rho] + E_{\mathrm{XC}}[\rho] \tag{23}$$

where the non-interacting kinetic energy (presumably the largest part of $T[\rho]$) is calculated from the Kohn–Sham orbitals:

$$T_s[\rho] = -\frac{1}{2}\sum_i \langle\psi_i|\nabla^2|\psi_i\rangle \tag{24}$$

This expression is, indirectly, a functional of the density since the Kohn–Sham orbitals themselves are also functionals of the density.[7] The exchange correlation functional is then redefined as

$$E_{XC}[\rho] = E'_{XC}[\rho] + T[\rho] - T_s[\rho] \tag{25}$$

It now contains the (presumably small) part of the kinetic energy that is not covered by $T_s[\rho]$. The big step forward achieved with this construction is that the second Hohenberg–Kohn theorem can now be applied to yield through variation of the density the single-particle (Kohn–Sham) equations:

$$\left\{-\frac{1}{2}\nabla^2 + v_{eff}(\boldsymbol{r})\right\}\psi_i(\boldsymbol{x}) = \varepsilon_i\psi_i(\boldsymbol{x}) \tag{26}$$

Importantly, the 'effective potential' seen by the electrons is given by

$$v_{eff}(\boldsymbol{r}) = -\sum_A Z_A|\boldsymbol{r} - \boldsymbol{R}_A|^{-1} + \int \rho(\boldsymbol{r}')|\boldsymbol{r} - \boldsymbol{r}'|^{-1}\mathrm{d}\boldsymbol{r}' + V_{XC}(\boldsymbol{r}) \tag{27}$$

The exchange-correlation *potential* is the functional derivative of the exchange-correlation energy with respect to the density[8]:

$$V_{XC}(\boldsymbol{r}) = \frac{\delta E_{XC}[\rho]}{\delta\rho(\boldsymbol{r})} \tag{28}$$

Obviously, the KS equations closely resemble the HF equations. The only difference is the replacement of the (nonlocal) exchange term by the (local) exchange-correlation potential. Thus, most of the powerful machinery worked out for Hartree–Fock calculations can be transferred with limited modifications to density functional programs. Yet, if the exchange-correlation potential would be exactly known, the KS procedure would yield the exact ground state energy. However, despite its frequent use, this is an empty statement unless the form of $E_{XC}[\rho]$ is actually specified.

A particular Ansatz that has provided much insight is to write the two-particle density of the real system in terms of the two-particle density of the non-interacting system (known from HF theory) and a correction. The correction is called the 'exchange-correlation hole':

$$\Gamma(\boldsymbol{r}_1, \boldsymbol{r}_2) = \rho(\boldsymbol{r_1})\rho(\boldsymbol{r}_2)[1 + h_{XC}(\boldsymbol{r}_1, \boldsymbol{r}_2)] \tag{29}$$

A number of properties of the (unknown) function $h_{XC}(\boldsymbol{r}_1,\boldsymbol{r}_2)$ are known and can be put to good use in the construction of density functionals. However, a thorough description of these properties is outside the scope of this article [20,46,47].

4. Realization of DFT

The large majority of approximations to $E_{XC}[\rho]$ are derived on the basis of physical reasoning, intuition, reference to model systems or fitting to experimental data. It is customary to neglect the kinetic energy contribution to $E_{XC}[\rho]$.

4.1. Ab initio DFT

One obvious suggestion that, unfortunately, does not work is to simply calculate the exchange energy as in Hartree–Fock theory (but from the Kohn–Sham orbitals) and simply add a correlation functional. First, the KS construction shows that the exchange potential must be local while the HF exchange is nonlocal. In fact, the construction of the *exact*, *local* exchange functional is surprisingly difficult but much progress has been made over the years. The most important approaches carry the acronyms OEP (optimized effective potential [48]) and LHF (localized Hartree–Fock [49]). Unfortunately, these exact exchange treatments are not compatible with the known correlation functionals and consequently, the results obtained for energetic quantities such like atomization or reaction energies are not good. The procedures required to obtain the exact exchange functional are also still not economical in terms of computational requirements and consequently some of the advantages of DFT over wavefunction-based theories are lost. Nevertheless, more progress along the lines of combining exact, local exchange with suitable correlation functionals is to be expected in the future.

A suitable route to "*ab initio*" DFT that systematically converges to the exact solution (as wavefunction theory) has been pursued in recent years by Bartlett and co-workers. As a result correlation functionals and potentials are available that are consistent with many body perturbation and coupled cluster theories [50–55]. Comparison of these potentials with the ones that are in present use reveals that the widely used potentials do not agree well with the *ab initio* ones. One example is shown in Fig. 3 where it is evident that *minus* the correlation potential predicted by the PBE functional for the Argon atom agrees better with the *ab initio* derived potential than the one that is actually used. The PBE exchange potential on the other hand follows the exact potential reasonably well except for the structure at the shell boundaries where the PBE potential is too smooth and at long distance from the nucleus where it falls off too quickly [511,512]. This may serve as a reminder that the success of the standard functionals to be discussed below largely rests on the compensation of large errors.

A second promising route for the construction of new XC potentials is to reconstruct them from accurate densities, for example obtained for small model systems from elaborate wavefunction based approaches. Several such methods have been devised and as a consequence the shape of the XC-potential is known for several systems [56,57]. However, despite significant trials [58–66] these fittings have not yet led to functionals that are systematically more accurate than the standard approaches described below.

4.2. Self-interaction

The immediate consequence of departing from exact exchange is one of the important features of DFT (which is perhaps to a significant part responsible for its successes and its failures): self-interaction. In HF theory, the diagonal exchange terms K_{ii} cancel the self-interaction terms J_{ii}. The same must hold for the exact exchange potential, though in a less obvious way. It does not, however, hold for non-exact approximations to the exchange such as the ones that are currently used. Since the self-interaction is unphysical, methods have been devised to remove it [67,68]. However, they have met with mixed success [69–74] and it is often argued that the self-interaction actually simulates to some extent long-range (so called 'static') correlation effects [72,73,75,76].

[7] This is most easily seen if one considers the orbitals to be the natural orbitals of the density. See Parr and Yang, chapter 7, p. 143.

[8] The functional derivative may be defined by expanding the functional in $\rho + \delta\rho$ and keeping only linear terms in $\delta\rho$. See Parr and Yang, Appendix A.

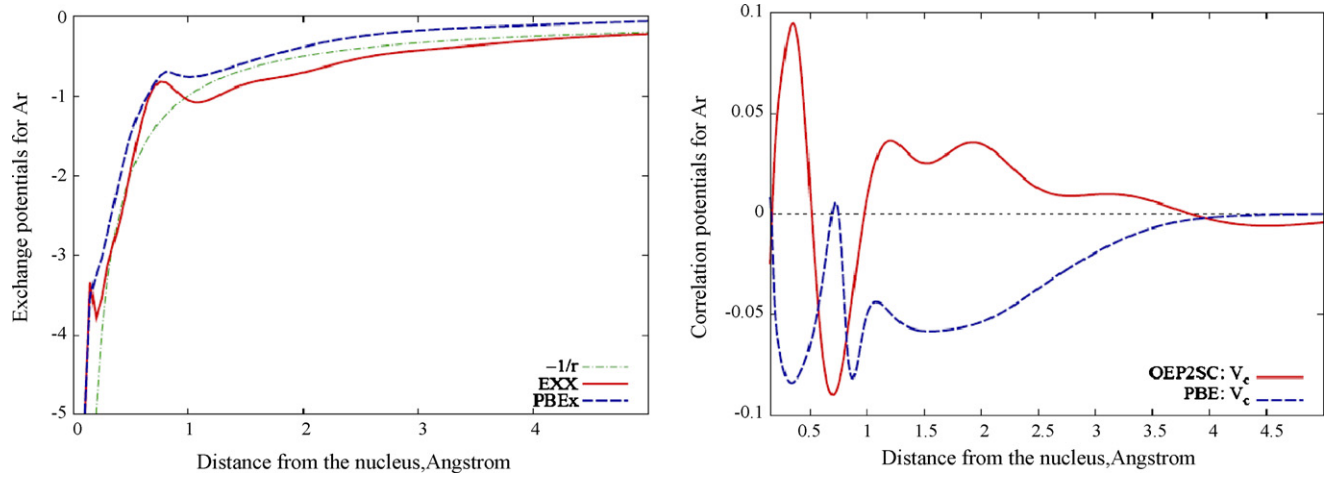

Fig. 3. Comparison of *ab initio* derived exchange potentials (red) with the commonly used PBE potential for the Ar atom. Left: exchange potential. The *y*-axis is in atomic units. Reproduced with permission from [508].

4.3. Standard functionals

The most common part of departure of most approximations in current use is the uniform electron gas. This is a model system of finite volume with a smeared out positive background charge that renders the entire system electrically neutral and that features a constant electron density $\rho = N/V$ (V is the volume into which the electrons are confined). Since this system is a cornerstone of present day DFT, we briefly summarize how one obtains the leading term in the exchange functional.

Assuming periodic boundary conditions, the Hartree–Fock orbitals for this artificial system are plane waves $\psi_{\boldsymbol{k}}(\boldsymbol{r}) = V^{-1/2}\,\mathrm{e}^{i\boldsymbol{k}\boldsymbol{r}}$ with the 'wave-vector' $\boldsymbol{k} = 2\pi/(V^{1/3})\boldsymbol{n}$, where $\boldsymbol{n}$ is a collection of three integer quantum numbers. In the limit of large N, $\boldsymbol{k}$ may be treated as a continuous variable. The calculation of the exchange potential then proceeds as follows:

$$\begin{aligned}\hat{K}\psi_{\boldsymbol{k}}(\boldsymbol{r}_1) &= \sum_{\boldsymbol{q}}\int \psi^*_{\boldsymbol{q}}(\boldsymbol{r}_2)\psi_{\boldsymbol{k}}\boldsymbol{r}_2 r_{12}^{-1}\,\mathrm{d}\boldsymbol{r}_2\psi_{\boldsymbol{q}}\boldsymbol{r}_1 \\ &= V^{-3/2}\sum_{\boldsymbol{q}}\int \mathrm{e}^{i(\boldsymbol{k}-\boldsymbol{q})\boldsymbol{r}_2} r_{12}^{-1}\,\mathrm{d}\boldsymbol{r}_2\,\mathrm{e}^{i\boldsymbol{q}\boldsymbol{r}_1} \\ &= V^{-3/2}\sum_{\boldsymbol{q}}\int \mathrm{e}^{i(\boldsymbol{k}-\boldsymbol{q})(\boldsymbol{r}_2-\boldsymbol{r}_1)} r_{12}^{-1}\,\mathrm{d}\boldsymbol{r}_2\,\mathrm{e}^{i\boldsymbol{k}\boldsymbol{r}_1} \\ &= \frac{\psi_{\boldsymbol{k}}(\boldsymbol{r}_1)4\pi}{V}\sum_{\boldsymbol{q}}(\boldsymbol{k}-\boldsymbol{q})^{-2}\end{aligned} \tag{30}$$

where the crucial third line follows by inserting $e^{-i(\boldsymbol{k}-\boldsymbol{q})\boldsymbol{r}_1}e^{i(\boldsymbol{k}-\boldsymbol{q})\boldsymbol{r}_1} = 1$. What remains is to sum (integrate) over all $\boldsymbol{q}$ which is achieved by using the volume element in $\boldsymbol{k}$-space $V/8\pi^3\,\mathrm{d}\boldsymbol{k}$. Integration in spherical coordinates then yields:

$$\hat{K}\psi_{\boldsymbol{k}}(\boldsymbol{r}_1) = \left(\frac{k_\mathrm{F}}{\pi}\right) S\left(\frac{|\boldsymbol{k}|}{k_\mathrm{F}}\right)\psi_{\boldsymbol{k}}(\boldsymbol{r}_1) \tag{31}$$

with $S(x) = 1 + (1-x^2)/2x\ln((1+x)/(1-x))$ and k_F is the highest occupied ψ_q (Fermi-level). The total exchange energy evaluates to:

$$\begin{aligned}E_\mathrm{X} &= -\frac{1}{2}\int \tfrac{k_\mathrm{F}}{\pi} S\left(\tfrac{|\boldsymbol{k}|}{k_\mathrm{F}}\right)\mathrm{d}\boldsymbol{k} \\ &= -\tfrac{V}{4\pi^3}k_\mathrm{F}^4\end{aligned} \tag{32}$$

This result needs to be re-expressed in terms of the density. Since exchange only works for electrons of like spin, we have:

$$\begin{aligned}\rho_\alpha(\boldsymbol{r}) &= \sum_{\boldsymbol{k}}\psi^*_{\boldsymbol{k}}(\boldsymbol{r})\psi_{\boldsymbol{k}}(\boldsymbol{r}) = \sum_{\boldsymbol{k}}V^{-1} \\ &= \frac{1}{V}\frac{V}{8\pi^3}\frac{4\pi}{3}k_\mathrm{F}^3 = \frac{1}{6\pi^2}k_\mathrm{F}^3\end{aligned} \tag{33}$$

One finds that $k_\mathrm{F} = (6\pi^2\rho_\alpha)^{1/3}$ and hence the exchange energy per electron is:

$$\frac{E_\mathrm{X}}{N} = -\frac{3}{4}\left(\frac{6}{\pi}\right)^{1/3}(\rho_\alpha^{1/3} + \rho_\beta^{1/3}) \tag{34}$$

This is how the famous $\rho^{1/3}$ law for the exchange functional may be formally derived. Of course, a molecule does not at all resemble a homogenous electron gas (unlike a metal) and consequently, it is not at all clear that a method based on such an oversimplified model system should work—but fortunately it does.

The bold suggestion is to now apply the inhomogeneous electron gas exchange equation *locally*. Thus it is assumed that in an inhomogeneous system (where the electron density is *not* homogeneous) the same equation still holds at each point in space and therefore one finds the exchange energy by integrating over all space. This leads to the definition of the *local exchange functional*:

$$E_\mathrm{X}[\rho] = \int \rho(\boldsymbol{r})\varepsilon_x(\rho)\,\mathrm{d}\boldsymbol{r} = -\frac{3}{4}\left(\frac{6}{\pi}\right)^{1/3}\int(\rho_\alpha^{4/3}(\boldsymbol{r}) + \rho_\beta^{4/3}(\boldsymbol{r}))\,\mathrm{d}\boldsymbol{r} \tag{35}$$

Which means that the *local exchange potential* becomes[9]:

$$V_\mathrm{X}^\alpha(\boldsymbol{r}) = \frac{\delta E_\mathrm{X}}{\delta\rho_\alpha(\boldsymbol{r})} = -\left(\frac{6}{\pi}\right)^{1/3}\rho_\alpha^{1/3}(\boldsymbol{r}) \tag{36}$$

and analogously for the spin-down (β)-potential. This famous result carries the names of Dirac [41] and Slater [77] who derived it long before the Hohenberg–Kohn theorems were known. Slater's reasoning has been that the exchange term in the HF equations for orbital ψ_i ($\left\{\sum_j\int\psi^*_j(\boldsymbol{x}_2)\psi_i(\boldsymbol{x}_2)\,\mathrm{d}\boldsymbol{x}_2\right\}\psi_j(\boldsymbol{x}_1)$) could to a good approximation be replaced by a local potential $V_\mathrm{X}(\boldsymbol{r}_1)\psi_i(\boldsymbol{r}_1)$ if one

[9] The local exchange functional like almost all other functionals in common use are of the form $E_X[\rho] = \int f(\rho)\,\mathrm{d}\boldsymbol{r}$ where f is some function of ρ. For such functionals $\delta E_X/\delta\rho(\boldsymbol{r}) = \partial f/\partial\rho$ and similarly if f contains gradients of the density. See Yang and Parr, Appendix A.

averages the potentials for the individual orbitals ψ_i which leads to:

$$V_X(\boldsymbol{r}_1) = \frac{1}{\gamma(\boldsymbol{r}_1,\boldsymbol{r}_1)} \int \gamma(\boldsymbol{r}_1,\boldsymbol{r}_2)\gamma(\boldsymbol{r}_2,\boldsymbol{r}_1) r_{12}^{-1}\, \mathrm{d}\boldsymbol{r}_2 \tag{37}$$

Slater then applied this much more general equation to the homogeneous electron gas for which $\gamma(\boldsymbol{r}_1,\boldsymbol{r}_1) = (1/6\pi^2)k_F^3$ and $\gamma(\boldsymbol{r}_1,\boldsymbol{r}_2) = V^{-1}\sum_{\boldsymbol{q}} e^{i\boldsymbol{q}(\boldsymbol{r}_2-\boldsymbol{r}_1)}$ to arrive at Eq. (36).

Simplistic as this local density approach is, it is surprising that it gives exchange energies that are only underestimated by ~10% compared to their HF values. However, this 10% still presents a large error in the total energies. Hence, early workers multiplied this local exchange by an empirical constant α which defined the so-called Xα-method—an approximation to Hartree–Fock theory that existed before the Hohenberg–Kohn theorems had been derived.

However, there would be little point in stopping the development at the Xα-approximation since the ultimate goal is to proceed beyond the HF method. Thus, one needs to incorporate correlation into the model. Following the same logics as before, the correlation energy of the uniform electron gas can be studied. There is no analytic solution but accurate numerical results that can be expressed through parametric equations. As pointed out by Kohn in his Nobel lecture [39], the first such expression was proposed by Wigner and reads:

$$E_C^W[\rho] = \int \rho(\boldsymbol{r})\varepsilon_C^W[\rho]\,\mathrm{d}\boldsymbol{r} = -\int \rho(\boldsymbol{r})\frac{0.44}{r_S+7.8}\,\mathrm{d}\boldsymbol{r} \tag{38}$$

With $r_S = (3/(4\pi\rho))^{1/3}$ is the Wigner–Seitz-radius and ε denotes the correlation (or exchange) energy per particle. A more accurate parameterization must take into account that the correlation between electrons of the same spin and of opposite spin is drastically different. This arises, because of the exchange—electrons of identical spins avoid each other already because of the antisymmetry of the wavefunction (Fermi hole), while the same is not true for electrons of opposite spin. Hence, opposite spin-pairs contribute more strongly to the correlation energy than parallel spin-pairs. This is a very important effect that, for example, has considerable consequences for the spin-state energetics in transition metal complexes as will be pointed out in Section 7.10.9.

For example, the parameterization of the uniform electron gas exchange and correlation energies due to Gunnarson and Lundqvist [78] is:

$$\varepsilon_{XC}^{GL}[\rho_\alpha,\rho_\beta] \equiv \varepsilon_{XC}^{GL}[r_S,\zeta] = \varepsilon_{XC}^{GL}[r_S,0] + \{\varepsilon_{XC}^{GL}[r_S,1] - \varepsilon_{XC}^{GL}[r_S,0]\} f(\zeta) \tag{39}$$

$$f(\zeta) = \frac{1}{2^{4/3}-2}((1+\zeta)^{4/3} + (1-\zeta)^{4/3} - 2) \tag{40}$$

$$\varepsilon_{XC}^{GL}[r_S,0] = -\frac{3}{4\pi}\left(\frac{9\pi}{4}\right)^{1/3}\frac{1}{r_S} - c_0 G(r_S/r_0) \tag{41}$$

$$\varepsilon_{XC}^{GL}[r_S,1] = -\frac{3}{4\pi}\left(\frac{9\pi}{2}\right)^{1/3}\frac{1}{r_S} - c_1 G\left(\frac{r_S}{r_1}\right) \tag{42}$$

$$G(x) = (1+x^3)\ln\left(1+\frac{1}{x}\right) - x^2 + \frac{1}{2}x - \frac{1}{3} \tag{43}$$

where $\zeta = (\rho_\alpha - \rho_\beta)\rho^{-1}$ is the spin-polarization and $c_0 = 0.0333$, $c_1 = 0.0203$, $r_0 = 11.4$, $r_1 = 15.9$. These expressions are only written down here in order to provide a flavor of how typical density functional expressions look like. Many other parameterizations have been proposed in the literature with the most popular local density expressions being due to Perdew and Wang [79–82] and Vosko et al. [83].

Experience shows that correlation energies for molecules predicted by the local density approximation (LDA) in its spin-polarized form (LSD) are overestimated by about a factor of two compared to accurate wavefunction based values. Since the absolute values for exchange energies are much larger than correlation energies (*vide infra*), the errors for exchange and correlation tend to cancel to a certain extent. Nevertheless, the LSD method is only moderately successful in chemistry since it has a distinct tendency for overbinding while it still predicts surprisingly good geometries [36].

The next logical step after the LSD approximation is to take further terms into account that take care of the inhomogeneity in the electronic distribution. Such terms depend on the derivatives of the electron density. The initial attempts to incorporate them met with little success. However, following the development of the so-called 'generalized gradient approximation' (GGA), DFT became highly popular in chemistry [510]. For GGA's the exchange correlation functional is written as:

$$E_{XC}^{GGA}[\rho_\alpha,\rho_\beta,\nabla\rho_\alpha,\nabla\rho_\beta] = E_{XC}^{LSD}[\rho_\alpha,\rho_\beta] + \Delta E_{XC}[\rho_\alpha,\rho_\beta,\nabla\rho_\alpha,\nabla\rho_\beta] \tag{44}$$

where, for example, the gradient correction for the exchange functional proposed by Becke is [84]:

$$\Delta E_{XC}[\rho_\alpha,\rho_\beta,\nabla\rho_\alpha,\nabla\rho_\beta] = -\rho^{1/3}(\boldsymbol{r})\frac{\beta x(\boldsymbol{r})^2}{1+6\beta x(\boldsymbol{r})\sinh^{-1}x(\boldsymbol{r})} \tag{45}$$

With $x = |\nabla|/\rho^{4/3}$ being a 'reduced gradient variable' and β is an empirical constant that takes the value 0.0042 from fitting to the exchange energies of rare gas atoms.

A number of similar approaches based on modifications of the GGA approach have been derived, implemented and tested. A noticeable exception is the correlation functional of Lee, Yang and Parr (LYP) [85] that has been derived from a parameterization of the correlation energy of the Helium atom by Colle and Salvetti [86]. The functional takes a rather involved form that will not be written down. It has the nice feature of being self-interaction free for one-electron densities and it produces correlation energies that are among the best currently available from DFT [87].

The foregoing discussion exemplifies the route that the mainstream of DFT has followed: start from the uniform electron gas and try to incorporate the effects of density inhomogeneity by a mixture of derivation, physical reasoning and data fitting. The resulting expressions are often rather complicated and reveal their physical content only to experts. Some workers prefer 'non-empirical' functionals over those that contain fitted parameters. Non-empirical means in this context, that these functionals have been derived with reference to a model system without introducing empirical parameters—namely the slowly varying, inhomogenous electron gas. How relevant this model is for chemistry is, however, open to debate. It is not even obvious that a perfect modeling of the slowly varying electron gas would produce results that are superior to those of the standard functionals.

It has been extensively tried to produce better functionals by fitting more and more parameters to more and more experimental data points [63–66,88–91]. These attempts have been, subject to debate, only moderately successful and there has not yet emerged a highly parameterized functional that has found widespread use in the chemical community and that has proven to be uniformly superior to the standard functionals. It appears that the maximum accuracy that is achievable within the GGA framework has probably been reached.

Further corrections based on higher derivatives have only recently gained more popularity and have been termed meta-GGA's. Perhaps the most successful attempt is the TPSS functional

that incorporates the kinetic energy density [92–96]:

$$\tau(\boldsymbol{r}) = \frac{1}{2}\sum_i |\nabla\psi_i(\boldsymbol{r})|^2 \quad (46)$$

The TPSS functional has been implemented into several major codes now and has been shown to perform well for transition metal containing systems [97].

A significant boost in the application of DFT to chemistry has been achieved in 1993 by Becke who proposed the use of so-called hybrid functionals [98,99] that incorporate a fraction of the non-local HF exchange. While this admixture has been motivated by the so-called 'adiabatic-connection' method, it remains largely empirical in character and many workers have chosen to adjust the fraction of exact exchange to fit their needs and whishes. By far the most popular of these hybrid functionals is the B3LYP method, that can be written as [100]:

$$E_{XC}^{B3LYP} = aE_X^{HF} + (1-a)E_X^{LSD} + bE_X^{B88} + E_C^{LSD} + c(E_C^{LYP} - E_C^{LSD}) \quad (47)$$

where the empirical constants a, b, c have the values 0.20, 0.72 and 0.81, respectively. The accuracy of energetic predictions with the B3LYP functional for small molecules has been really astonishing and is competitive with correlated wavefunction approaches. Since the B3LYP functional also proved to be one of the best functionals for property predictions it rapidly became the 'workhorse' of applied quantum chemistry. However, some points must be made: (a) the high accuracy pertains to the basis set limit and does not carry over to the small double-ζ type basis sets that are often used in application studies; (b) the benchmarks are usually done on collections of small molecules that do not contain open-shell transition metals. The results of such studies are not necessarily representative of real life chemistry applications.

In fact, more recently detailed benchmark studies have revealed significant points of concern about the application of the B3LYP functional.

Several authors found that the errors of the B3LYP predictions increase disproportionately with increasing molecular size. In particular, Grimme, who reported a detailed comparison of wavefunction and DFT methods for atomization energies (Table 2) and used large basis sets, found many errors in his test set that exceed 20 kcal/mol [101]. This did not occur for other functionals and the study concluded that of the investigated functionals PBE0 [102,103] performed the best and very similarly to a hybrid version of TPSS with 25% HF exchange (which may be called TPSS0).

Table 2
Performance of different standard functionals in extensive thermochemical tests (in kcal/mol)

	Density functional					
	BP86	PBE	TPSS	TPSSH	B3LYP	PBE0
G2/97′ test set (N = 156)						
Mean deviation	0.39	0.17	0.73	0.39	0.33	−0.25
Mean absolute deviation	2.79	2.87	3.06	2.74	2.12	2.28
Maximum deviation	24.2	25.9	21.7	19.8	14.5	14.7
Second test set (N = 67)						
Mean deviation	−4.6	−2.66	−4.52	−3.55	−6.91	−0.88
Mean absolute deviation	8.77	7.74	8.45	7.02	8.46	4.63
Maximum deviation	87.4	79.0	70.3	52.9	77.9	36.9

Numbers taken from Grimme [101] (N denotes the number of molecules in the test sets).

Several authors found discouragingly large errors (exceeding 10 kcal/mol) even in seemingly simple systems – for example for the isomerisation energies of hydrocarbons (Fig. 4). This disconcerting situation was interpreted in a paper by Grimme [104]. In comparing wavefunction and DFT results, he concluded that the errors of the DFT methods arise from correlation effects at medium electron–electron distances, i.e. from electrons occupying adjacent bonds. Such correlation effects are not included in the standard DFT models since the correlation energy is calculated from the values of the densities and gradients at a given point in space. Thus, the DFT correlation effects are too short-sighted and hence the stability of branched structures is significantly underestimated (Fig. 4).

It is readily anticipated that similar situations must be prevalent throughout chemistry and hence one is well advised to view the theoretical results always with much care and seek feedback from experiment wherever possible.

A small collection of standard functionals that find frequent use in chemistry is shown below in Table 3 together with some comments.

We finally wish to mention a last class of density functionals for which some promising results have been obtained. They have been

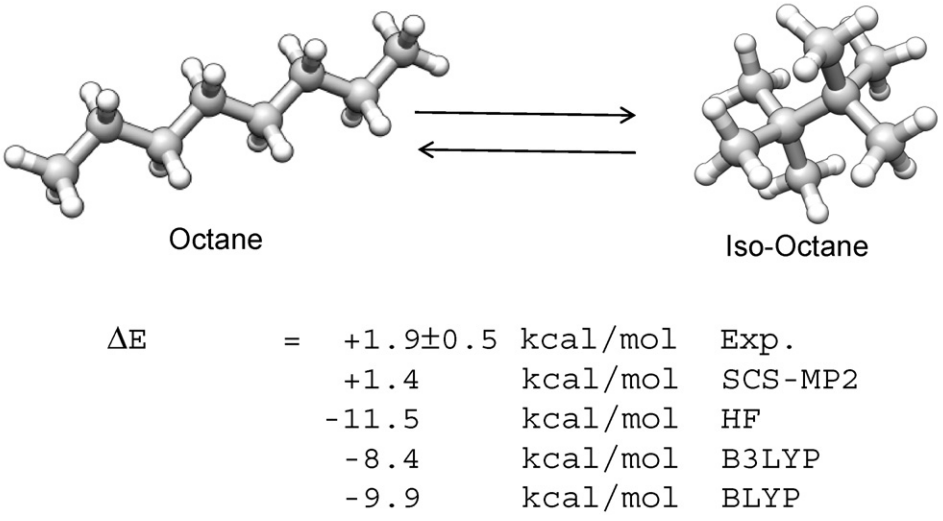

Fig. 4. Unexpectedly large errors from standard DFT calculations for the isomerization energy from octane (left) to *iso*-octane (right). The sign of the experimental isomerization energy is dominated by correlation effects since the HF method predicts the wrong sign but already a modest correlated wavefunction-based method (SCS-MP2) gives good agreement with experiment. DFT misses on the medium range "bond/bond" electron correlation effects and hence underestimates the stability of the branched isomer (taken from [509]).

Table 3
Some standard functionals

Name	Type	Comments
BLYP	GGA	One of the earliest GGA functionals. Usually inferior to BP86 and PBE. Predicts too long bonds
BP86	GGA	Excellent geometries and vibrational frequencies. Energetics is usually not highly accurate but performs often well in spectroscopic investigations
PW91	GGA	One of the older GGA functionals with excellent accuracy for exchange couplings
PBE	GGA	A GGA version designed to replace PW91. Very popular in physics. Often similar to BP86
OLYP	GGA	Violates the uniform electron gas limit but gives improved results for molecules
B3LYP	Hybrid	De facto standard in chemistry for structures, energies and properties. See discussion in the text
PBE0	Hybrid	Excellent accuracy; competitive with B3LYP
TPSS	Meta-GGA	Improvement over PBE
TPSSh	Hybrid meta-GGA	Probably improvement over PBE0; perhaps increase fraction of HF to 25% (TPSS0)

proposed in 2006 by Grimme and contain – in addition to a fraction of exact exchange – also a fraction of wavefunction based correlation energy calculated from second-order many-body perturbation theory (MP2) [105–109]. Thus, this class of functionals has been called 'double hybrid' functionals [108]. The energetic benchmarks reported by Grimme have demonstrated outstanding accuracy with an average error for the so-called G2 set of molecules of <2 kcal/mol which is usually only achieved with the best wavefunction based methods. The method contains two adjustable parameters for the fraction of HF exchange (53%) and the fraction of MP2 correlation (27%) [105,106,108,110,111]. Analytic gradients have recently been reported for this new class of functionals [108] and excellent accuracy was obtained for structures of main group molecules and transition metal complexes, although at somewhat elevated computational cost relative to standard DFT methods (see Section 5). Most recently, excited states have also been treated with this methodology [109]. Further improvements to this method (as well as for standard functionals) are obtained by adding an empirical van der Waals correction to the DFT energies which compensates for the poor behavior of the functionals in the long range regime [110,112–114]. Owing to the large amount of HF exchange and the perturbative estimate of the correlation contribution it might be expected that open-shell transition metal containing systems may be more challenging to treat with these functionals. These questions clearly warrant more detailed studies.

In order to put these results into perspective some numbers for exchange and correlation energies are collected for the ground state of the neutral neon atom (^{1}S) in Table 4. As reference serves an accurate wavefunction based calculation with the CCSD(T) (coupled-cluster theory with single- and double excitations together with a perturbative estimate for triple excitations) method and a very large basis set. This calculation yields a Hartree–Fock exchange energy of $-12.098\,E_h$ which is close to the Hartree–Fock limit. The calculated correlation energy of $-0.379\,E_h$ is quite close to Clementi's experimental estimate of $-0.393\,E_h$ [115]. In fact, adding a relativistic correction using the Douglas–Kroll–Hess method [116], the CCSD(T) total energy of $-129.064\,E_h$ is close the experimental total energy of $-129.056\,E_h$ obtained by summing the first ten ionization potentials. Compared to the CCSD(T) values, the DFT results show a rather large scatter. Some functionals (like PBE) underestimate both the correlation and the exchange energy while others (like TPSS) underestimate correlation and overestimate exchange. The best individual exchange and correlation energies are predicted by the BLYP functional. The significant error in the BLYP total energy must then stem from the shortcomings in the kinetic energy—the difference between T and T_S is nowhere explicitly accounted for in any of the investigated functionals. These numbers are merely shown in order to provide some feeling of how variable the DFT results with different functionals are and how large the individual contributions become. No conclusions about the performance of these functionals in chemical applications should be drawn from this data.

Table 4
Total, correlation and exchange energies of the Neon atom using the *ab initio* CCSD(T) method and various density functionals (deviations from the wavefunction results in mE_h)

	E_{tot}	E_{corr}	E_x
CCSD(T)	−128.9260	−0.379	−12.098
BP86	−128.9776 (−52)	−0.388 (− 9)	−12.104 (−6)
PBE	−128.8664 (+60)	−0.347 (+32)	−12.028 (+70)
BLYP	−128.9730 (−47)	−0.383 (− 4)	−12.099 (−1)
TPSS	−128.9811 (−55)	−0.351 (+28)	−12.152 (−54)
B3LYP	−128.9426 (−17)	−0.452 (−73)	−12.134 (−36)
B2PLYP	−128.9555 (−30)	−0.392 (−13)	−12.103 (−5)

All calculations with uncontracted Partridge-3 basis set together with polarization functions from aug-pw-pCV5Z(-h) basis set (−67 mE_h core-correlation contribution). All DFT results are from self-consistent Kohn–Sham densities.

5. The computational machinery of DFT

Since the Kohn–Sham orbitals (unlike the density) assumes a complicated shape they are almost always expanded in terms of a set of pre-fixed basis functions φ[10]:

$$\psi_i(\boldsymbol{x}) = \sum_\mu c_{\mu i}\varphi_\mu(\boldsymbol{x}) \tag{48}$$

As a consequence, the solutions of the Kohn–Sham equations only become equivalent to the true Kohn–Sham orbitals if the set of φ approaches mathematical completeness. We will not enter a detailed discussion of basis sets at this stage but only make a few (subjective) remarks.

Most present day calculations are performed with Gaussian basis functions for which computational techniques are very well developed. Alternatives involve Slater type orbitals (ADF code), plane waves (CPMD or PQS codes) or numerical basis functions (DMol code) which have certain advantages. However, the Hartree–Fock exchange term or the MP2 contribution to the double hybrid functionals can presently only be efficiently calculated with Gaussian basis functions.

Experience indicates that the results converge relatively quickly towards the basis set limit [120]. By present day standards calculations should be performed with basis sets of at least triple-ζ quality with at least one set of polarization functions. For accurate results three sets of polarization functions[11] and perhaps one set of diffuse functions should be employed. If basis sets of this size are used, the results reflect the properties of the functional and not the properties of the basis set.

Specific properties [for example isotropic hyperfine couplings in EPR spectroscopy, NMR chemical shifts, excitations of Rydberg

[10] However, basis set free methods have been developed as well [117–119].

[11] These are typically two 2p1d for hydrogens and 2d1f for main group elements. For transition metals one should add at least 2p1f. The def2-TZVP and def2-TZVPP basis sets developed by Ahlrichs and co-workers [121] can be recommended for all electron calculations. Smaller basis sets of polarized double-ζ quality (def2-SVP) are also available for less accurate calculations.

character or weak interactions] require special basis set with added flexibility in the core or outer regions of the molecule. Basis sets for such calculations have only partially been standardized.

Inserting the basis function expansion into the Kohn–Sham Eq. (26) yields a matrix pseudo-eigenvalue equation:

$$\boldsymbol{F}(\boldsymbol{c})\boldsymbol{c}_i = \varepsilon_i \boldsymbol{S}\boldsymbol{c}_i \tag{49}$$

where $\boldsymbol{c}_i$ is a vector with elements $c_{\mu i}$, $\boldsymbol{S}$ is the overlap matrix with elements $S_{\mu\nu} = \langle\varphi_\mu|\varphi_\nu\rangle$ and $\boldsymbol{F}$ is the Kohn–Sham matrix. It will be written in a general form that includes pure Kohn–Sham and Hartree–Fock theory as special cases:

$$F_{\mu\nu} = h_{\mu\nu} + J_{\mu\nu}(P) - c_{\mathrm{HF}}K_{\mu\nu}(P) + c_{\mathrm{DF}}V_{\mu\nu}^{\mathrm{XC}}[\rho] \tag{50}$$

where c_{HF} is the fraction of HF exchange possibly included in the functional and $c_{\mathrm{DF}} = 0$ for Hartree–Fock theory. In this equation $\boldsymbol{h}$ is the one-electron matrix, $\boldsymbol{P}$ the density matrix and $\boldsymbol{V}^{\mathrm{XC}}$ the exchange-correlation matrix with elements:

$$h_{\mu\nu} = \left\langle \varphi_\mu \left| -\frac{1}{2}\nabla^2 - \sum\nolimits_A Z_A r_A^{-1} \right| \varphi_\nu \right\rangle \tag{51}$$

$$J_{\mu\nu}(\boldsymbol{P}) = \sum_{\kappa\tau} P_{\kappa\tau}\langle\mu\kappa|\nu\tau\rangle \tag{52}$$

$$K_{\mu\nu}(\boldsymbol{P}) = \sum_{\kappa\tau} P_{\kappa\tau}\langle\mu\kappa|\tau\nu\rangle \tag{53}$$

$$P_{\mu\nu} = \sum_i c_{\mu i}c_{\nu i} \tag{54}$$

$$V_{\mu\nu}^{\mathrm{XC};\sigma} = \int \varphi_\mu(\boldsymbol{r}\sigma)\frac{\delta E_{\mathrm{XC}}[\rho_\alpha, \rho_\beta]}{\delta\rho_\sigma(\boldsymbol{r})}\varphi_\nu(\boldsymbol{r}\sigma)\,\mathrm{d}\boldsymbol{r} \tag{55}$$

$\sigma = \alpha, \beta$. These terms represent rather different computational requirements. The one-electron integrals are not very numerous and present no computational challenge.

As is obvious from Section 4.3, the exchange-correlation terms are of a complicated form and to find closed-form solutions of the associated integrals is next to hopeless. Hence, these terms are best handled by numerical integration. Thus, the integral is approximated by a finite sum over grid points $\boldsymbol{r}_{\mathrm{g}}$ with weights w_{g} that are chosen according to some prescription:

$$V_{\mu\nu}^{\mathrm{XC};\sigma} \approx \sum_{\mathrm{g}} w_{\mathrm{g}}\varphi_\mu(\boldsymbol{r}_{\mathrm{g}}\sigma)\frac{\delta E_{\mathrm{XC}}[\rho_\alpha, \rho_\beta]}{\delta\rho_\sigma(\boldsymbol{r}_{\mathrm{g}})}\varphi_\nu(\boldsymbol{r}_{\mathrm{g}}\sigma) \tag{56}$$

Fortunately, the numerical integration problem did not turn out to be a difficult one [122] and most schemes are modifications of the original proposal by Becke [123], see for example Ref. [124]. If properly coded, the computational effort for the quadrature scales only linearly with the size of the molecular system [125] but the prefactor varies considerably between different implementations. Experience shows that the error in the calculated exchange correlation energies is of the same order as the error in the numerically integrated electron density. Hence, a useful target accuracy is to integrate the electron density to an accuracy of at least 10^{-3} electrons which is readily achieved with about 1000–2000 integration points per atom.

The Coulomb matrix is

$$J_{\mu\nu}(\boldsymbol{P}) = \sum_{\kappa\tau} P_{\kappa\tau}\langle\mu\kappa|\nu\tau\rangle \tag{57}$$

$$J_{\mu\nu}(\boldsymbol{P}) = \int \varphi_\mu(\boldsymbol{x}_1)\varphi_\nu(\boldsymbol{x}_1)\sum_{\kappa\tau} P_{\kappa\tau}\int \varphi_\kappa(\boldsymbol{x}_2)\varphi_\tau(\boldsymbol{x}_2)r_{12}^{-1}\,\mathrm{d}\boldsymbol{x}_2 \tag{58}$$

$$J_{\mu\nu}(\boldsymbol{P}) = \int \varphi_\mu(\boldsymbol{x}_1)\varphi_\nu(\boldsymbol{x}_1)\sum_i \int |\psi_i(\boldsymbol{x}_2)|^2 r_{12}^{-1}\,\mathrm{d}\boldsymbol{x}_2 \tag{59}$$

$$J_{\mu\nu}(\boldsymbol{P}) = \int \varphi_\mu(\boldsymbol{x}_1)\varphi_\nu(\boldsymbol{x}_1)\int \rho(\boldsymbol{r}_2)r_{12}^{-1}d\boldsymbol{x}_2 \tag{60}$$

$$J_{\mu\nu}(\boldsymbol{P}) \equiv \int \varphi_\mu(\boldsymbol{x}_1)\varphi_\nu(\boldsymbol{x}_1)V_C[\rho](\boldsymbol{x}_1)\mathrm{d}\boldsymbol{x}_1 \tag{61}$$

This equation emphasizes that this term represents the interaction of the charge density $\varphi_\mu(\boldsymbol{x})\varphi_\nu(\boldsymbol{x})$ with the Coulomb potential created by the total charge density distribution. The first line implies an exact analytic integration involving four-index, four-center electron–electron repulsion integrals. While these integrals can be efficiently computed over Gaussian basis functions, the number of integrals is very large and grows with the fourth power of the molecular size. Fortunately, negligible charge distributions $\varphi_\mu(\boldsymbol{x})\varphi_\nu(\boldsymbol{x})$ can be efficiently recognized and screened out before the actual computation of the integrals (it is readily shown that $|\langle\mu\kappa|\nu\tau\rangle| \le \sqrt{\langle\mu\nu|\nu\mu\rangle}\sqrt{\langle\kappa\tau|\tau\kappa\rangle}$) [126,127]. Due to the fast decaying nature of the basis functions the product $\varphi_\mu(\boldsymbol{x})\varphi_\nu(\boldsymbol{x})$ is only significant for $\varphi_\nu(\boldsymbol{x})$ being located close to $\varphi_\mu(\boldsymbol{x})$ thus leading to an overall linearly increasing number of significant charge distributions with increasing molecular size. Since the Coulomb operator is of long range, it appears that the effort to evaluate the Coulomb term is asymptotically quadratically scaling with molecular size. However, following the introduction of multipole expansions, the fast-multipole method (FMM) allows for the linear scaling evaluation of the Coulomb term [128–131]. Unfortunately, however, irrespective whether one uses a linear scaling formulation or not, the prefactor for the computation of the Coulomb term by exact analytic integration is high and usually dominates the computational effort for a DFT or HF calculation. Consequently many techniques have been developed in order to speed this part of the computation up. These include pseudo-spectral techniques [132] or the solution of Poisson's equation [119]. However, one of the earliest techniques that has been employed also turns out to be the most efficient one. It has first been applied in the DFT context by Baerends, Ellis and Ros [133], elaborated by Dunlap [134,135], brought to its current form by Vahtras and Almlöf [136] and efficiently standardized for general chemistry applications by Ahlrichs and co-workers [137,138]. The technique is called 'density fitting' (DF) or 'resolution of the identity' (RI) approximation. The idea is to fit the charge distributions $\varphi_\mu(\boldsymbol{x})\varphi_\nu(\boldsymbol{x})$ to an auxiliary basis set $\eta_{\mathrm{P}}(\boldsymbol{x})$ like:

$$\varphi_\mu(\boldsymbol{x})\varphi_\nu(\boldsymbol{x}) \approx \sum_P c_{\mu\nu}^{\mathrm{P}}\eta_{\mathrm{P}}(\boldsymbol{x}) \tag{62}$$

As shown by Vahtras and Almlöf [136], the coefficients $c_{\mu\nu}^{\mathrm{P}}$ are best determined by minimizing the residual self-repulsion[12]:

$$R_{\mu\nu} = \int \left(\varphi_\mu(\boldsymbol{x})\varphi_\nu(\boldsymbol{x}) - \sum_P c_{\mu\nu}^P\eta_P(\boldsymbol{x})\right) r_{12}^{-1} \times \left(\varphi_\mu(\boldsymbol{x})\varphi_\nu(\boldsymbol{x}) - \sum_Q c_{\mu\nu}^Q\eta_Q(\boldsymbol{x})\right)\mathrm{d}\boldsymbol{x}_1\,\mathrm{d}\boldsymbol{x}_2 \tag{63}$$

[12] The original work used three-center overlap integrals instead of three-center repulsion integrals. The work of Vahtras et al. [136]. showed that this approximation is an order of magnitude less accurate than the method described here and consequently larger and more accurate expansion bases have to be used. This was rationalized by Dunlap [139] who pointed out that the minimization of the self-repulsion is equivalent to fitting the electric field generated by the charge distribution.

which immediately leads to a linear equation system:

$$\sum_{PQ} V_{PQ} c^{Q}_{\mu\nu} = (\varphi_\mu \varphi_\nu | \eta_P) \tag{64}$$

With the two- and three-index electron–electron repulsion integrals:

$$V_{PQ} = \int \eta_P(\boldsymbol{x}_1) r_{12}^{-1} \eta_Q(\boldsymbol{x}_2)\, \mathrm{d}\boldsymbol{x}_1\, \mathrm{d}\boldsymbol{x}_2 \tag{65}$$

$$(\varphi_\mu \varphi_\nu | \eta_P) = \int \varphi_\mu(\boldsymbol{x}_1)\varphi_\nu(\boldsymbol{x}_1) r_{12}^{-1} \eta_P(\boldsymbol{x}_2)\, \mathrm{d}\boldsymbol{x}_1\, \mathrm{d}\boldsymbol{x}_2 \tag{66}$$

Inserting this approximation into the expression for the Coulomb matrix yields:

$$J_{\mu\nu} \approx \sum_P (\varphi_\mu \varphi_\nu | \eta_P) \sum_Q V^{-1}_{PQ} \sum_{\kappa\tau} P_{\kappa\tau} (\varphi_\kappa \varphi_\tau | \eta_Q) \tag{67}$$

The evaluation involves the three steps: (a) calculation of density in the auxiliary basis ($P_Q = \sum_{\kappa\tau} P_{\kappa\tau}(\varphi_\kappa\varphi_\tau|\eta_Q)$), (b) solution of the linear equation system $\boldsymbol{g} = \boldsymbol{V}^{-1}\boldsymbol{P}$ and (c) contraction with the three index integrals to give the Coulomb matrix $J_{\mu\nu} = \sum_P (\varphi_\mu\varphi_\nu|\eta_P) g_P$.

Comments: (1) the calculation of the three index repulsion integrals is much more economical than the calculation of the four-index integrals and there is an order of magnitude fewer of them.[13] (2) As shown by Ahlrichs and co-workers [137,138], the solution of the linear equation system is best approached via the Cholesky decomposition of $\boldsymbol{V}$, (3) experience shows that if the auxiliary basis sets are well designed[14] the error of the fitted Coulomb energy is only $\sim 10^{-5}\, E_h$/atom. (4) The fitted Coulomb energy is an upper bound to the true Coulomb energy and the fitting is 'robust' in the sense of Dunlap [140]. (5) The advantages of the RI approximation increase with increasing size of the orbital expansion basis. (6) Without any pre-screening the computational effort for the construction of the Coulomb matrix is reduced from $O(N^4)$ to $O(N^3)$ and using straightforward pre-screening techniques to $O(N^2)$. (7) The error of the approximation is very smooth and the errors for structural parameters and energy differences is negligible 8) the most efficient implementations of this concept [138,141–143] lead to a reduction of the computational cost for the Coulomb problem of the factor 10–100.[15] Quite large systems can be treated with present day DFT programs such as the one shown in Fig. 5.

The contributions by the Hartree–Fock exchange terms that enter into hybrid density functionals are more difficult to approximate with high accuracy. One of the possibilities that is exploited in the Jaguar code are pseudo-spectral techniques that lead to efficient calculations [132,144–147]. Fortunately, however, the analytic calculation of the exchange term scales almost linearly with system size (or can be relatively easily designed to scale perfectly linearly [148]). This is readily seen from Eq. (53) if one assumes that the density matrix element connecting $\varphi_\mu(\boldsymbol{x})$ and $\varphi_\nu(\boldsymbol{x})$ decays exponentially with distance as it appears to do for 'insulators' (systems with sufficiently large HOMO–LUMO gap; Kohn's conjecture [149]).

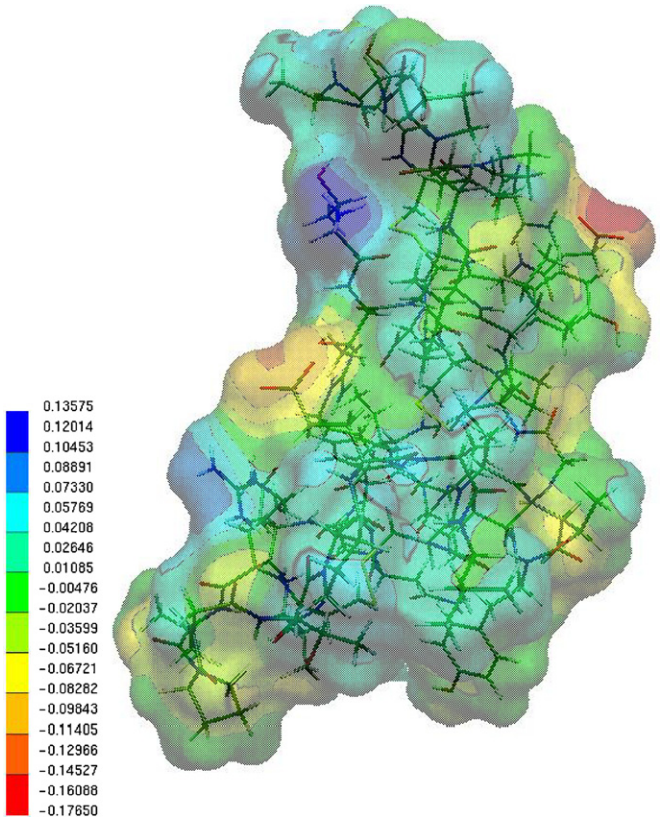

Fig. 5. Example of a large DFT calculation. A BP86 single point calculation of the entire Crambin protein with 642 atoms and more than 4000 basis functions can be completed on a standard personal computer in less than 14 h elapsed time using modern algorithms (calculations done with the ORCA program on a 2.0 GHz Opteron CPU). Superimposed is the electrostatic potential of this system derived from the calculation.

Given the developments in computational hard- and software, DFT calculations with several thousand basis functions (several hundred atoms) can now be routinely carried out on standard personal computers or in parallel fashion on computer clusters. This enormously widens the range of systems are amenable to study by DFT methods. Since the diagonalization of the Kohn–Sham matrix becomes a computationally significant step in large calculations (scaling as $O(N^3)$), techniques have been devised to avoid it. The specialist literature must be consulted for a thorough exposition of such linear-scaling approaches [125,128–131,148,150–157].

6. Theory of molecular property calculations with DFT

We are now in a position to present the calculation of properties of interest of (bio)inorganic chemistry by means of DFT methods. The theory will be presented in the coherent framework of analytic derivative/linear response language which turns out to be the most systematic framework for property calculations.

We assume that we have solved the Kohn–Sham problem already in some of the approximate ways that were described in the previous sections using some molecular coordinates as input. Next, we wish to predict the equilibrium geometry or spectroscopic properties or we want to refine our results by including some smaller terms in the Hamiltonian. Each of these situations can be considered as a small perturbation of the system which will want to adapt to the new situation in the presence of the perturbation. Thus, we have to study the immediate vicinity of the solution of the Kohn–Sham problem and have to examine the restoring forces that

[13] The leading term is $4N_{aux}/N^2_{bas}$ where N_{aux} is the number of auxiliary functions and N_{bas} the number of basis functions. For a reasonably large calculation $N_{aux} \sim 3000$ and $N \sim 1000$ such that there is roughly a factor of 100 fewer three-index integrals than four index integrals.

[14] Particularly good and accurate auxiliary basis sets have been designed by Ahlrichs and co-workers [137,138]. They are typically only 2–3 times larger than the orbital expansion basis set.

[15] A multipole accelerated versions for very large systems has been developed by Sierka et al. [142].

act on the system in the presence of the perturbation. Specifically, the perturbation might be the change of the nuclear coordinates, an external electric field, an external magnetic field or the sudden 'turn-on' of relativistic corrections to the Hamiltonian. In addition, the perturbation may or may not be time dependent.

Based on the foregoing discussion it is evident that the 'immediate vicinity' of the solution is best explored by performing a Taylor expansion in the neighborhood of the initial Kohn–Sham solution which in turn implies that we have to calculate the derivatives (or partial derivatives) $\partial E/\partial\lambda$ of the total Kohn–Sham energy where λ denotes the perturbation. We will first treat the time-independent case and then turn to the more general (and more complicated) time-dependent case in Section 6.4.

6.1. First derivatives

The point of departure is the energy functional:

$$L = V_{\mathrm{NN}} + T_s + V_{\mathrm{eN}} + J - c_{\mathrm{HF}}K + E_{\mathrm{XC}} + \mathrm{OC} \tag{68}$$

$$L = V_{\mathrm{NN}} + \sum_{\mu\nu} P_{\mu\nu}h_{\mu\nu} + \frac{1}{2}\sum_{\mu\nu\kappa\tau} P_{\mu\nu}P_{\kappa\tau}(\langle\mu\kappa|\nu\tau\rangle - c_{\mathrm{HF}}\langle\mu\kappa|\tau\nu\rangle) + E_{\mathrm{XC}}[\rho] - \sum_{i,j\mu\nu}\varepsilon_{ij}(c_{\mu i}S_{\mu\nu}c_{\nu j} - \delta_{ij}) \tag{69}$$

The last term represents the orthogonality constraint (OC) that was forced upon the orbitals in the variation process and the matrix ε_{ij} represent the Lagrange multipliers that turned out be the orbital energies in the canonical representation that diagonalizes $\boldsymbol{\varepsilon}$. Each of the terms may depend on the perturbation λ. However, there is one important simplification: since we have determined the total energy by variation of the MO coefficients $c_{\mu i}$ that enter into the matrix $\boldsymbol{P}$ it is known that $\partial L/\partial P_{\mu\nu} = 0$. Hence, since the derivative with respect to λ certainly contains a term $(\partial L/\partial P_{\mu\nu})(\partial P_{\mu\nu}/\partial\lambda)$ we know that we can ignore the λ dependence of the density matrix, or, expressed differently, the fluctuations in the density matrix due to the perturbation. Hence, the derivative of the total energy becomes [158]:

$$\frac{\partial L}{\partial\lambda} = \frac{\partial V_{NN}}{\partial\lambda} + \sum_{\mu\nu} P_{\mu\nu}\frac{\partial h_{\mu\nu}}{\partial\lambda} + \frac{1}{2}\sum_{\mu\nu\kappa\tau} P_{\mu\nu}P_{\kappa\tau}\frac{\partial(\langle\mu\kappa|\nu\tau\rangle - c_{\mathrm{HF}}\langle\mu\kappa|\tau\nu\rangle)}{\partial\lambda} + \int\frac{\delta E_{\mathrm{XC}}[\rho]}{\delta\rho(\boldsymbol{r})}\frac{\partial\rho(\boldsymbol{r})}{\partial\lambda}\,\mathrm{d}\boldsymbol{r} + \sum_{\mu\nu} W_{\mu\nu}\frac{\partial S_{\mu\nu}}{\partial\lambda} \tag{70}$$

With the 'energy weighted density matrix':

$$W_{\mu\nu} = -\sum_i \varepsilon_i c_{\mu i}c_{\nu i} \tag{71}$$

The derivatives of the one-electron matrix elements contain contributions from the basis function and from the operator derivatives:

$$\frac{\partial h_{\mu\nu}}{\partial\lambda} = \left\langle\frac{\partial\varphi_\mu}{\partial\lambda}|h|\varphi_\nu\right\rangle + \left\langle\varphi_\mu|h|\frac{\partial\varphi_\nu}{\partial\lambda}\right\rangle + \left\langle\varphi_\mu|\frac{\partial h}{\partial\lambda}|\varphi_\nu\right\rangle \tag{72}$$

In taking the derivative of the density, it is sufficient to take the perturbation dependence of the basis functions into account:

$$\frac{\partial\rho(\boldsymbol{r})}{\partial\lambda} = \sum_{\mu\nu} P_{\mu\nu}\left\{\varphi_\nu\frac{\partial\varphi_\mu^*}{\partial\lambda} + \varphi_\mu^*\frac{\partial\varphi_\nu}{\partial\lambda}\right\} \tag{73}$$

Which means that the exchange correlation contribution to the derivative becomes simply $\sum_{\mu\nu}P_{\mu\nu}\int V_{\mathrm{XC}}(\boldsymbol{r})\partial/\partial\lambda(\varphi_\mu^*\varphi_\nu)\,\mathrm{d}\boldsymbol{r}$.

This is the complete expression for the gradient of the Kohn–Sham energy with respect to an arbitrary perturbation. It contains the derivatives of the one- and two-electron integrals and the nuclear-nuclear repulsion energy. The dependence of the integrals arises from the (possible) dependence of the basis set on the perturbation. The basis functions certainly depend on the perturbation in the case that the perturbation represents the movement of a nucleus since the basis functions are 'glued' to their parent nuclei.[16]

Hence, in the special case that the perturbation is simply the addition of a term λh_λ to the Hamiltonian and the basis functions do not depend on the perturbation, the derivative simplifies enormously to:

$$\frac{\partial L}{\partial\lambda} = \sum_{\mu\nu} P_{\mu\nu}\langle\varphi_\mu|h_\lambda|\varphi_\nu\rangle \tag{74}$$

Thus, in this particular case, the Hellmann–Feynman theorem holds. It also holds in the limit of a complete basis set. This simple expression is for example valid for the calculation of electric multipole moments, the electric field gradient at a given nucleus, as well as the spin-dipolar and Fermi contact contributions to the hyperfine coupling tensor. The appropriate matrix elements for these properties have been reviewed in detail recently [11].

6.2. Second derivatives

The second derivatives with respect to the perturbations λ and θ are found by differentiation of Eq. (69) [159]:

$$\begin{aligned}\frac{\partial^2 L}{\partial\lambda\,\partial\theta} &= \frac{\partial^2 V_{NN}}{\partial\lambda\,\partial\theta} + \sum_{\mu\nu}\left(P_{\mu\nu}\frac{\partial^2 h_{\mu\nu}}{\partial\lambda\,\partial\theta} + W_{\mu\nu}\frac{\partial^2 S_{\mu\nu}}{\partial\lambda\,\partial\theta}\right) + \frac{1}{2}\sum_{\mu\nu\kappa\tau} P_{\mu\nu}P_{\kappa\tau}\frac{\partial^2(\langle\mu\kappa|\nu\tau\rangle - c_{\mathrm{HF}}\langle\mu\kappa|\tau\nu\rangle)}{\partial\lambda\,\partial\theta}\\ &+\sum_{\mu\nu}\left(\frac{\partial P_{\mu\nu}}{\partial\theta}\frac{\partial h_{\mu\nu}}{\partial\lambda} + \frac{\partial W_{\mu\nu}}{\partial\theta}\frac{\partial S_{\mu\nu}}{\partial\lambda}\right) + \frac{1}{2}\sum_{\mu\nu\kappa\tau}\frac{\partial(P_{\mu\nu}P_{\kappa\tau})}{\partial\theta}\left(\frac{\partial(\langle\mu\kappa|\nu\tau\rangle - c_{\mathrm{HF}}\langle\mu\kappa|\tau\nu\rangle)}{\partial\lambda}\right)\\ &+\int\frac{\delta E[\rho]}{\delta\rho(\boldsymbol{r})}\frac{\partial^2\rho(\boldsymbol{r})}{\partial\lambda\,\partial\theta}\,\mathrm{d}\boldsymbol{r} + \int\frac{\delta^2 E[\rho]}{\delta\rho(\boldsymbol{r}_1)\,\delta\rho(\boldsymbol{r}_2)}\frac{\partial\rho(\boldsymbol{r}_1)}{\partial\lambda}\frac{\partial\rho(\boldsymbol{r}_2)}{\partial\theta}\,\mathrm{d}\boldsymbol{r}_1\,\mathrm{d}\boldsymbol{r}_2\end{aligned} \tag{75}$$

This expression appears somewhat formidable but has clearly recognizable parts: the first line contains simply second derivative integrals which involves the second derivatives of the basis functions as well as the first- and second derivatives of the one- (and two-) electron operators. The second line contains the derivative of the density matrix – that can no longer be avoided – and the third line contains the second derivative of the exchange correlation contribution. The latter consists of two parts. The first part is straightforward and simply involves the second derivative of the

[16] This is not the case if the basis set consists of plane waves. In this special case all contributions from the basis set derivatives are absent from the gradients which means that it can be computed with very high efficiency. Thus, forces are very cheap and plane wave approaches lend themselves very well to molecular dynamics approaches.

density:

$$\frac{\partial^2 \rho(\boldsymbol{r})}{\partial\lambda\,\partial\theta} = \sum_{\mu\nu}\left(P_{\mu\nu}\frac{\partial^2(\varphi_\mu^*\varphi_\nu)}{\partial\lambda\,\partial\theta} + \frac{\partial P_{\mu\nu}}{\partial\theta}\frac{\partial(\varphi_\mu^*\varphi_\nu)}{\partial\lambda}\right) \tag{76}$$

While the second part involves the second functional derivative of the exchange correlation potential. This quantity is known as the 'exchange-correlation kernel'. Since the XC potential measures the rate of the change of the energy with respect to a change of the density at position $\boldsymbol{r}_1$, the kernel measures the rate of change of the potential at $\boldsymbol{r}_1$ with a change of density at position $\boldsymbol{r}_2$. For the standard functionals described in this review, the second functional derivative always leads to a δ function $\delta(\boldsymbol{r}_1 - \boldsymbol{r}_2)$ and hence only a three-dimensional integral is to be evaluated by numerical quadrature. It is readily appreciated from the complicated expressions for the XC-energy, that the expressions for the XC potential and even more so for the XC kernel become rather involved. However, they are easily handled by widely available computer algebra programs (e.g. MAPLE V: http://www.maplesoft.com/; Mathematica: http://www.wolfram.com/) that are also able to generate computer code for the explicit evaluation of these terms.

Assuming that all technical difficulties in the evaluation of the integral derivatives have been overcome, the remaining difficulty is the calculation of the derivatives of the density matrix elements which comes down to the calculation of the derivatives of the MO coefficients. This concerns the important problem of how the Kohn–Sham orbitals of the system change if a perturbation is applied. This subject is of fundamental importance and will be studied in the next section. In fact, if the basis functions do not depend on the perturbation, the second derivative assumes a rather simple form:

$$\frac{\partial^2 L}{\partial\lambda\,\partial\theta} = \sum_{\mu\nu}\left(P_{\mu\nu}\frac{\partial^2 h_{\mu\nu}}{\partial\lambda\,\partial\theta} + \frac{\partial P_{\mu\nu}}{\partial\theta}\frac{\partial h_{\mu\nu}}{\partial\lambda}\right) \tag{77}$$

This equation covers most of the so-called 'static-response properties'. One says that the first term is of 'first-order' and the second-term of 'second-order'. This nomenclature arises since in sum-over-states based pictures the equivalent of the first term arises as an expectation value over the ground state wavefunction while the second term involves the first-order wavefunction that is represented by an infinite sum over electronically excited states.

6.3. The coupled perturbed SCF equations

It became apparent in the previous section that the derivatives of the density matrix elements are an indispensable ingredient in the calculation of molecular properties. It is thus important to find out how such derivatives can be obtained efficiently.

The point of departure are the Kohn–Sham equations in their basis set form:

$$\sum_\nu F_{\mu\nu}(\boldsymbol{c})c_{\nu i} = \varepsilon_i \sum_\nu S_{\mu\nu}c_{\nu i} \tag{78}$$

This expression is differentiated and re-arranged to obtain:

$$\sum_\nu\left(\frac{\partial F_{\mu\nu}(\boldsymbol{c})}{\partial\lambda}c_{\nu i} + (F_{\mu\nu}(\boldsymbol{c}) - \varepsilon_i S_{\mu\nu})\frac{\partial c(\nu i)}{\partial\lambda}\right) = \frac{\partial\varepsilon_i}{\partial\lambda}\sum_\nu S_{\mu\nu}c_{\nu i} + \varepsilon_i\sum_\nu\frac{\partial S_{\mu\nu}}{\partial\lambda}c_{\nu i} \tag{79}$$

The next step is to make an Ansatz for the perturbed MO coefficients. Since the entire set of unperturbed molecular orbitals spans the same space as the original orbitals but forms an orthonormal set it is convenient to expand the perturbed MOs in terms of the unperturbed ones:

$$\frac{\partial c_{\mu i}}{\partial\lambda} = \sum_p U_{pi}^\lambda c_{\mu p} \tag{80}$$

where the indices p, q, r, s run over *all* molecular orbitals (occupied and unoccupied), the indices i, j refer to occupied orbitals and the indices a, b to unoccupied ones. The condition that the perturbed MOs remain orthonormal leads to an important condition on the matrix elements of the matrix $\boldsymbol{U}$. This is seen by differentiating the orthonormality condition:

$$\sum_{\mu\nu} c_{\mu p}^* S_{\mu\nu}c_{\nu q} = \delta_{\mathrm{pq}} \tag{81}$$

That leads to:

$$U_{qp}^{\lambda *} + U_{pq}^\lambda + S_{pq}^{(\lambda)} = 0 \tag{82}$$

Since the energy is invariant with respect to unitary transformations between orbital pairs within the occupied space and within the virtual space respectively, the corresponding blocks of the $\boldsymbol{U}$-matrix can be fixed from the conditions:

$$U_{ij}^\lambda = -\frac{1}{2}S_{ij}^{(\lambda)} \tag{83}$$

$$U_{ab}^\lambda = -\frac{1}{2}S_{ab}^{(\lambda)} \tag{84}$$

While

$$U_{ia}^\lambda = -U_{ai}^* - S_{ia}^{(\lambda)} \tag{85}$$

Which shows that only the U_{ai} block of the $\boldsymbol{U}$-matrix is to be determined. The perturbed overlap integrals are:

$$S_{pq}^\lambda = \sum_{\mu\nu} c_{\mu p}^* \frac{\partial S_{\mu\nu}}{\partial\lambda}c_{\nu q} \tag{86}$$

The derivative of the Kohn–Sham matrix takes a somewhat involved form:

$$\begin{aligned}\frac{\partial F_{\mu\nu}(\boldsymbol{c})}{\partial\lambda} &= \frac{\partial h_{\mu\nu}}{\partial\lambda} + \sum_{\kappa\tau}P_{\kappa\tau}\left(\frac{\partial(\langle\mu\kappa|\nu\tau\rangle - c_{\mathrm{HF}}\langle\mu\kappa|\tau\nu\rangle)}{\partial\lambda}\right) + \int V_{\mathrm{XC}}[\rho]\frac{\partial(\varphi_\mu^*\varphi_\nu)}{\partial\lambda} + \varphi_\mu^*\varphi_\nu f_{\mathrm{XC}}[\rho]\sum_{\kappa\tau}P_{\kappa\tau}\frac{\partial(\varphi_\kappa^*\varphi_\tau)}{\partial\lambda}\,\mathrm{d}\boldsymbol{r} \\ &+ \sum_{jp\kappa\tau}(U_{pj}^{*\lambda}c_{\kappa p}^* c_{\tau j} + U_{pj}^\lambda c_{\kappa j}^* c_{\tau p})(\langle\mu\kappa|\nu\tau\rangle - c_{\mathrm{HF}}\langle\mu\kappa|\tau\nu\rangle) + \int\left(f_{\mathrm{XC}}[\rho]\sum_{pj\kappa\tau}(U_{pj}^{*\lambda}c_{\kappa p}^* c_{\tau j} + U_{pj}^{*\lambda}c_{\kappa p}^* c_{\tau j})\right)\varphi_\mu^*\varphi_\nu\,\mathrm{d}\boldsymbol{r}\end{aligned} \tag{87}$$

However, the first line involves nothing but the derivative of the one-electron operator and the derivatives of the basis functions. It can be abbreviated as $F_{\mu\nu}^{(\lambda)}$ and shifted to the right-hand side. The second line contains the response of the Kohn–Sham operator with respect to the perturbation. It is this dependence on its own solutions which renders perturbation theory with self-consistent field wavefunctions more complicated than standard perturbation

theory. The perturbed KS equations are further simplified by multiplying them from the left by $c^*_{\mu a}$ and summing over all μ. The result is:

$$\begin{aligned} &U^{\lambda}_{ai}(\varepsilon_a-\varepsilon_i)+\sum_{bj}U^{\lambda *}_{bj}\{\langle ab|ij\rangle+\langle ab|f_{\mathrm{XC}}|ij\rangle-c_{\mathrm{HF}}\langle ab|ji\rangle\}\\ &+\sum_{bj}U^{\lambda}_{bj}\{\langle aj|ib\rangle+\langle aj|f_{\mathrm{XC}}|ib\rangle-c_{\mathrm{HF}}\langle aj|bi\rangle\}\\ &=-F^{(\lambda)}_{ai}+\varepsilon_i S^{(\lambda)}_{ai}+\frac{1}{2}\sum_{kj}S^{(\lambda)*}_{kj}\{\langle ak|ij\rangle+\langle ak|f_{\mathrm{XC}}|ij\rangle-c_{\mathrm{HF}}\langle ak|ji\rangle\}\\ &+\frac{1}{2}\sum_{kj}S^{(\lambda)}_{pj}\{\langle aj|ik\rangle+\langle aj|f_{XC}|ik\rangle-c_{HF}\langle aj|ki\rangle\} \end{aligned} \tag{88}$$

At this point it is advantageous to split the U-coefficients explicitly into a real and an imaginary part:

$$U_{ai}=x_{ai}+iy_{ai} \tag{89}$$

Assuming that the perturbation is either purely real or purely imaginary leads to the final response equations:

$$x^{\lambda}_{ai}(\varepsilon_a-\varepsilon_i)+R^{(re)}_{ai}(\boldsymbol{x}^{\lambda})=-b^{\lambda(re)}_{ai} \tag{90}$$

$$y^{\lambda}_{ai}(\varepsilon_a-\varepsilon_i)+R^{(im)}_{ai}(\boldsymbol{y}^{\lambda})=-b^{\lambda(im)}_{ai} \tag{91}$$

The right-hand sides are defined by

$$b^{\lambda(re)}_{ai}=\mathrm{Re}(F^{(\lambda)}_{ai}-\varepsilon_i S^{(\lambda)}_{ai})-\frac{1}{2}R^{(re)}_{ai}(\boldsymbol{s}^{(re;\lambda)}) \tag{92}$$

$$b^{\lambda(im)}_{ai}=Im(F^{(\lambda)}_{ai}-\varepsilon_i S^{(\lambda)}_{ai})-\frac{1}{2}R^{(im)}_{ai}(\boldsymbol{s}^{(im;\lambda)}) \tag{93}$$

Here $\boldsymbol{s}$ denotes the real and imaginary part of the (ij) block of the perturbed overlap integrals. If the basis functions do not depend on the perturbation, the right-hand sides simplify considerably: the last two terms are zero and $F^{(\lambda)}_{ai}=\langle a|h_\lambda|i\rangle$. The 'response operators' are defined by

$$R^{(re)}_{pq}(\boldsymbol{x}^{\lambda})=\sum_{rs}x^{\lambda}_{rs}\{2\langle pr|qs\rangle+2\langle pr|f_{XC}|qs\rangle-c_{HF}(\langle pr|sq\rangle+\langle ps|rq\rangle)\} \tag{94}$$

$$R^{(im)}_{pq}(\boldsymbol{y}^{\lambda})=c_{\mathrm{HF}}\sum_{rs}y^{\lambda}_{rs}\{(\langle pr|sq\rangle-\langle ps|rq\rangle)\} \tag{95}$$

It is clear from inspection that the real-response operator is symmetric while the imaginary response operator is antisymmetric. Importantly, the imaginary response operator only contains contributions from the Hartree–Fock exchange. Thus, if no HF exchange is present, the linear equation system for a purely imaginary perturbation has the simple solution $y_{\mathrm{ai}}=-b^{(im)}_{ai}/(\varepsilon_a-\varepsilon_i)$ as would have been expected if the Kohn–Sham operator would not be a self-consistent operator.

The perturbed density matrix finally becomes:

$$\frac{\partial P_{\mu\nu}}{\partial\lambda}=\sum_{ip}U^{*}_{pi}c^{*}_{\mu p}c_{\nu i}+U_{pi}c^{*}_{\mu i}c_{\nu p} \tag{96}$$

Thus, for a purely imaginary perturbation:

$$\frac{\partial P_{\mu\nu}}{\partial\lambda}=i\sum_{ia}y_{ai}(c^{*}_{\mu i}c_{\nu a}-c^{*}_{\mu a}c_{\nu i}) \tag{97}$$

And hence:

$$\frac{\partial\rho(\boldsymbol{r})^{\text{density-matrix}}}{\partial\lambda}=\sum_{\mu\nu}\frac{\partial P_{\mu\nu}}{\partial\lambda}\varphi_\mu(\boldsymbol{r})\varphi_\nu(\boldsymbol{r})=0 \tag{98}$$

This shows that a purely imaginary perturbation does not lead to a first order change in the electron density which explains why all local potentials (like the Coulomb and exchange-correlation potentials) do not contribute to the response of the system with respect to an imaginary perturbation. This would be different in extensions of DFT that introduce a dependence of the XC potential on the current density [160–166]. However, such methods have not yet found their way into chemistry.

Since the number of orbitals pairs is usually so large that the linear equation system can not be solved directly, iterative techniques are employed in practice [167]. To this end, the response operators are usually calculated in the AO basis and are transformed back to the MO basis.[17] Since the computational effort that is involved is similar to a single SCF iteration, the solution of the coupled-perturbed Kohn–Sham equations is typically as expensive as one SCF calculation.[18]

6.4. Time-dependent perturbations

If the perturbation is time dependent the formalism is quite a bit more complicated. We will concern ourselves here with only the most straightforward treatment in which the basis functions do not depend on the perturbation and the exchange correlation potential is assumed to be time-independent (adiabatic approximation). The foundations of time-dependent density functional theory have been laid out by Runge and Gross [170] and have recently spawned a detailed dispute that we will not enter into [171].

Just like there is a time-dependent HF treatment, there also is a time-dependent KS treatment. The best way is to start from the following form of the TD–KS equations [172]:

$$\hat{F}\hat{P}-\hat{P}\hat{F}=i\frac{\partial\hat{P}}{\partial t} \tag{99}$$

where $\hat{P}(t)=\sum_i|\psi_i(t)\rangle\langle\psi_i(t)|$ is the idempotent KS density operator and $\hat{F}$ is the Kohn–Sham operator. The static KS equations are readily recovered if the right-hand side is set to zero. Let us assume that we have solved the static KS problem and now turn on a time-dependent perturbation. Such a perturbation can always be written as a sum over its Fourier components. Thus, it is sufficient to investigate a perturbation that oscillates at a single frequency ω:

$$\hat{V}^{(1)}(t)=\frac{1}{2}(\hat{A}\,\mathrm{e}^{-i\omega t}+\hat{A}^{+}\,\mathrm{e}^{i\omega t}) \tag{100}$$

Here $\hat{A}$ is some operator that describes the nature of the perturbation (for example the electric dipole operator if one is interested in the interaction of the molecule with the electric vector of a light wave). We now need to expand the TD–KS equations to first order in the perturbation. However, in the time-dependent case, we need to make an Ansatz for the U-coefficients that reflects the time-dependence. A suitable one takes the form:

$$U^{\lambda}_{bj}(t)=\frac{1}{2}\{X^{\omega;\lambda}_{bj}\,\mathrm{e}^{-i\omega t}+Y^{\omega;\lambda *}_{bj}\,\mathrm{e}^{+i\omega t}\} \tag{101}$$

where the $\boldsymbol{X}$ and $\boldsymbol{Y}$ coefficients have now to be determined. The static case discussed above is readily recovered if the frequency of the perturbation is set to zero.

[17] However, this is not necessary. There are variants of CP-SCF theory that avoid orbitals altogether and directly solve for the perturbed densities. In this case no transformations to the MO basis are necessary [168,169].

[18] However, the CP-SCF equations are linear while the SCF equations are nonlinear. Thus, often the CP-SCF equations converge in fewer iterations than the SCF equations.

The right-hand side of the perturbed TD-KS equation then becomes:

$$i\left\langle b\left|\frac{\partial\hat{P}^{(1)}}{\partial t}\right|j\right\rangle = \frac{\omega}{2}X_{bj}^{\omega;x}\,\mathrm{e}^{-i\omega t} - \frac{\omega}{2}Y_{bj}^{\omega;x*}\,\mathrm{e}^{+i\omega t} \tag{102}$$

While the left hand side is readily obtained from the discussion for the static case. We will not perform the algebra in detail but simply quote the result that reads:

$$(\varepsilon_b-\varepsilon_j)X_{bj}^{\omega;\lambda} + V_{bj}^{\lambda} + \sum_{kc}X_{kc}^{\omega;\lambda}[\langle kj|cb\rangle + \langle kj|f_{\mathrm{XC}}|cb\rangle - c_{\mathrm{HF}}\langle jc|kb\rangle] + \sum_{kc}Y_{kc}^{\omega;\lambda}\{\langle kj|cb\rangle + \langle kj|f_{\mathrm{XC}}|cb\rangle - c_{\mathrm{HF}}\langle jk|cb\rangle\} = \omega X_{bj}^{\omega;\lambda} \tag{103}$$

$$(\varepsilon_b-\varepsilon_j)Y_{bj}^{\omega;\lambda} + V_{bj}^{\lambda*} + \sum_{kc}X_{kc}^{\omega;\lambda}[\langle kj|cb\rangle + \langle kj|f_{\mathrm{XC}}|cb\rangle - c_{\mathrm{HF}}\langle jk|cb\rangle] + \sum_{kc}Y_{kc}^{\omega;\lambda}[\langle kj|cb\rangle + \langle kj|f_{\mathrm{XC}}|cb\rangle - c_{\mathrm{HF}}\langle jc|kb\rangle] = -\omega Y_{bj}^{\omega;\lambda} \tag{104}$$

Here (V_{bj} denotes a matrix element of the time-independent part of the perturbation. It is customary to write these equation in a more neat form by defining the "super-matrices":

$$A_{bj,ck} = (\varepsilon_b-\varepsilon_j)\delta_{bj,ck} + \langle kj|cb\rangle + \langle kj|f_{\mathrm{XC}}|cb\rangle - c_{\mathrm{HF}}\langle jc|kb\rangle \tag{105}$$

$$B_{bj,ck} = \langle kj|cb\rangle + \langle kj|f_{\mathrm{XC}}|cb\rangle - c_{\mathrm{HF}}\langle jk|cb\rangle \tag{106}$$

Note that $\boldsymbol{A}+\boldsymbol{B}$ is related to the real response matrix while $\boldsymbol{A}-\boldsymbol{B}$ is related to the imaginary response matrix. Since in this formalism, $\boldsymbol{X}$ and $\boldsymbol{Y}$ become "vectors" (compound label bj), the TD–KS response equations can be written:

$$\left(\begin{pmatrix}\boldsymbol{A} & \boldsymbol{B}\\ \boldsymbol{B} & \boldsymbol{A}\end{pmatrix} - \omega\begin{pmatrix}\mathbf{1} & \mathbf{0}\\ \mathbf{0} & -\mathbf{1}\end{pmatrix}\right)\begin{pmatrix}\boldsymbol{X}^{\omega;\lambda}\\ \boldsymbol{Y}^{\omega;\lambda}\end{pmatrix} = -\begin{pmatrix}\boldsymbol{V}^{\lambda}\\ \boldsymbol{V}^{\lambda*}\end{pmatrix} \tag{107}$$

These equations are of the form: $\boldsymbol{R}(\omega)\boldsymbol{U}=-\boldsymbol{V}$. It is interesting to ask at which frequencies these equations lead to an infinite solution. This must happen if ω is adjusted such that an eigenvalue of $\boldsymbol{R}(\omega)$ becomes zero. This 'resonance' then implies that ω equals an excitation frequency of the system. Hence, one has *directly* calculated the difference in energy between the ground- and an excited state without ever calculating the excited state itself! Obviously, such a resonance occurs if the equation:

$$\begin{pmatrix}\boldsymbol{A} & \boldsymbol{B}\\ \boldsymbol{B} & \boldsymbol{A}\end{pmatrix}\begin{pmatrix}\boldsymbol{X}^{\omega;\lambda}\\ \boldsymbol{Y}^{\omega;\lambda}\end{pmatrix} = \omega\begin{pmatrix}\mathbf{1} & \mathbf{0}\\ \mathbf{0} & -\mathbf{1}\end{pmatrix}\begin{pmatrix}\boldsymbol{X}^{\omega;\lambda}\\ \boldsymbol{Y}^{\omega;\lambda}\end{pmatrix} \tag{108}$$

is satisfied. Hence, the 'critical' ω's are obtained as the solution of a large non-standard eigenvalue problem. They can be solved by non-standard iterative techniques that are of no concern in the present context [173]. However, there are two special cases that deserve mentioning. The first special case is met when the perturbation is real (e.g. an electric field type perturbation) and there is no HF exchange (or any other non-local potential) in the functional. Then one can re-arrange the equations to a standard eigenvalue problem:

$$\boldsymbol{H}_{\mathrm{eff}}\boldsymbol{Z}_{\mathrm{eff}} = \omega^2\boldsymbol{Z}_{\mathrm{eff}} \tag{109}$$

With:

$$\boldsymbol{H}_{\mathrm{eff}} = (\boldsymbol{A}-\boldsymbol{B})^{1/2}(\boldsymbol{A}+\boldsymbol{B})(\boldsymbol{A}-\boldsymbol{B})^{1/2} \tag{110}$$

$$\boldsymbol{Z}_{\mathrm{eff}} = (\boldsymbol{A}-\boldsymbol{B})^{-1/2}(\boldsymbol{X}^{\omega;\lambda}+\boldsymbol{Y}^{\omega;\lambda}) \tag{111}$$

The matrix square roots present no problem, since $(\boldsymbol{A}-\boldsymbol{B})^{1/2}_{bj,ck} = \delta_{kc,bj}\sqrt{\varepsilon_b-\varepsilon_j}$.

The second special case is met if the $\boldsymbol{B}$ matrix is simply neglected. This leads to $\boldsymbol{Y}=0$ and the resulting standard eigenvalue problem:

$$\boldsymbol{A}\boldsymbol{X}^{\omega;\lambda} = \omega\boldsymbol{X}^{\omega;\lambda} \tag{112}$$

nicely resembles the configuration-interaction with single-excitations (CIS) method that is well known from wavefunction theory [174]. It is often referred to as Tamm-Dancoff approximation (TDA) [175]. Newer developments of TD-DFT can be found in the works of Ziegler, Autschbach and co-workers [176–192] and by Rinkevicius and Vahtras [193].

7. Applications of molecular property calculations with DFT

Thousands of papers have been published that describe applications of DFT to transition metal chemistry including (bio)inorganic chemistry. The majority of these papers focus on structural, energetic and kinetic quantities. Authoritative reviews of these approaches have been provided by Siegbahn and co-workers [1,2] and an excellent introduction is provided by the book of Koch and Holthausen [43]. Consequently, no attempt will be made to describe these important applications. Rather this section will be mainly concerned with the application of the formalism outlined in the previous sections to the calculation of molecular spectra and related properties. The calculation of molecular properties other than the total energy allows the close connection of theory and experiment and often leads to important clues about the geometric and electronic structure of the systems being studied. In many instances, spectroscopic features react much more sensitively to subtle structural variations than the total energies themselves (for an example see [14,194]). Consequently, the calculation of spectroscopic properties is an important area of investigation that is described below.

7.1. Geometries and transition states

Almost every DFT investigation starts by optimizing the geometry of the species under investigation. All algorithms to find stationary points on the potential energy surface require the availability of analytic first derivatives to be effective. These are calculated from Eq. (69) with the perturbation λ being taken as the movement of a given nuclear coordinate. In order to be efficient, all $3M$ derivatives are calculated simultaneously which typically requires less time than the preceding SCF calculation.

Usually all structural parameters are relaxed in searching for stationary points on the potential energy surfaces. However, sometimes it is advantageous to freeze selected structural parameters: (a) if the structure used is part of a much larger structure (e.g. a model for a protein active site) and there are constraints provided by the part that is not included in the model; (b) if the optimizations lead to a qualitative wrong structure; (c) if a 'relaxed surface scan' is performed. Such scans are utilized to obtain insight into the shape of potential energy surfaces or to determine an initial guess for a transition state. Algorithms to find minima (to be confirmed by a frequency calculation) are well established in quantum chemistry while optimization of transition states (characterized by a single negative frequency) requires considerable experience and insight into the system being studied [195,196].

The accuracy of optimized structures with DFT is usually excellent to good when compared with accurate X-ray diffraction data. For some recent benchmark results see, for example Refs. [108,197] and Table 5. The most extensive transition metal benchmark calculations for 3d, 4d and 5d metals that also compare ECP and scalar relativistic all electron approaches is found in Ref. [198]. Scalar relativistic all-electron Gaussian basis sets for third-row transition metal complexes have been developed in Ref. [199].

In applications to 3d transition metal complexes experience indicates that the weaker metal–ligand bonds (e.g. neutral amines, phosphines, thioethers or pyridines) are typically overestimated

Table 5
Statistical assessment of the performance of some common density functionals for the bond distances of the light (31 molecules made of H–Ne) and heavy element test sets (33 molecules containing atoms from Na–Ar), respectively

	BLYP	BP86	PBE	TPSS	B3LYP	B2PLYP	SCS-MP2
Light element test set							
MD	−1.3	−1.1	−1.0	−0.8	0.1	−0.1	−0.3
MAD	1.3	1.1	1.1	0.9	0.6	0.3	0.6
Min.	−3.2	−3.1	−2.9	−3.1	−2.3	−1.6	−2.5
Max.	0.0	0.5	0.6	0.5	2.9	1.2	2.0
	BLYP	BP86	PBE	TPSS	B3LYP	B2PLYP	CCSD(T)
Heavy element test set							
MD	−2.5	−1.8	−1.7	−1.4	−0.7	−0.5	0.0
MAD	2.5	1.8	1.7	1.4	0.8	0.6	0.1
Min.	−6.7	−3.7	−3.4	−3.9	−3.1	−1.8	−0.9
Max.	−0.4	−0.4	−0.3	−0.2	0.8	0.3	0.3

Given are the mean deviation (MD) and mean absolute deviation (MAD) as well as the minimum (min.) and maximum (max.) errors. All values are in pm (data taken from [108]).

by nonrelativistic all-electron DFT calculations with standard functionals by about 3–5 pm (sometimes more) (Table 6), while the strong bonds to anionic or strongly (back)bonding ligands like (O^{2-}, S^{2-}, OH^-, NO^+, CO, N_3^-, ...) are typically predicted with excellent accuracy (errors of ~1–3 pm) by DFT methods. As an example of how the results depend on functional, basis set and relativistic treatment, consider a geometry optimization on the simple complex $[Cu(en)_2]^{2+}$ (en = ethylenediamine) (Table 6).

The results of this calculation are representative of the typical performance of DFT based optimizations and the significant points may be summarized as follows:

Under the plausible assumption that the large decontracted TZVPP basis set is a suitable reference point, it is seen that double-ζ bases are too small for quantitative results but that one approaches basis set saturation already at the level of a singly polarized triple-ζ basis set such as TZVP.

Table 6
Representative geometry optimization results for $[Cu(en)_2]^{2+}$ using a variety of different basis sets and density functionals

Method	Additions to H_{BO}	Basis set	R(Cu–N) (pm)
BP86	None	SV(P)	207.5
BP86	ECP[a]	LANL2DZ	207.4
BP86	None	TZVP	206.8
BP86	None	TZVPP(decr)[b]	206.7
B3LYP	None	TZVPP(decr)[b]	206.7
TPSS	None	TZVP	206.5
BP86	DKH2[c]	SV(P)	206.4
BP86	ECP[a]	SDD	205.8
BP86	DKH2[c]	TZVP	205.5
BP86	ZORA[d]	TZVPP(decr)[b]	205.4
TPSS	DKH2[c]	TZVP	205.2
B3LYP	DKH2[c]	TZVPP(decr)[b]	205.2
BP86	DKH2[c]	TZVPP(decr)[b]	205.0
BP86	DKH2 + VDW[e]	TZVPP(decr)[b]	204.9
BP86	DKH2 + COSMO[f]	TZVP	202.8
BP86	DKH2 + COSMO[f]	TZVPP(decr)[b]	202.1
BP86	DKH2 + COSMO[f] + VDW[e]	TZVPP(decr)[b]	202.0
Exp [507]			201.5

[a] Effective core potential.
[b] Fully decontracted basis set.
[c] Second-order Douglas–Kroll–Hess all electron calculation.
[d] Zeroth order regular approximation.
[e] Includes a correction for the Van der Waals interaction [112].
[f] Includes a continuum model of the surrounding using the conductor like screening model [200] with an effective dielectric constant of infinity. This provides perfect screening of the net charge of the dication by considering it as a perfect conductor. Results for a finite dielectric constant of 80 resembling water are very similar.

The well-known relativistic bond contraction amounts to about 1–2 pm in the first transition row. Since it can be treated at negligible additional computational cost, it may be recommended for all-electron calculations to include such a correction. Apparently, even the standard, non-relativistically contracted basis sets can be used in such calculations if they are at least of TZVP quality. However, even after the relativistic correction, the overestimation of the metal–ligand bond distances for the weaker bonds is not fully remedied.

Possible compensation by net charges through a continuum solvation model such as the COSMO [200] or PCM [201] models further improves the results while van der Waals corrections that are important for modeling weak interactions appear to play a minor role. The best results are obviously obtained by a simultaneous inclusion of relativistic effects and charge compensation models, both of which can be included in the calculations at very limited extra cost compared to a standard all-electron geometry optimization with a triple-ζ quality basis set. It is noticeable that even for a given functional, the quality of the result is very variable—the worst BP86 calculation with the LANL2DZ ECP/basis set provides a result that is in error by 5.5 pm compared to experiment while the best calculation with the same functional approaches the experimental bond distance to within 0.5 pm.

About two thirds of the relativistic effect (perhaps often more) can be recovered through effective core potentials. The Stuttgart–Dresden potentials [202–206] appear to be quite popular while very small ECP and the associated valence basis sets like LANL2DZ [207–209] – despite their popularity – appear to be too small to deliver reliable results.

The differences between different density functionals are typically not large. Hence, a suitable strategy is to select the most efficient functional for the geometry optimizations and to invest the time that has been saved in a better basis set or a more realistic model of the system that one wants to investigate. As alluded to in Section 5, calculations without HF exchange can be done with outstanding efficiency at essentially no loss of accuracy when the density fitting approximation is employed. Hence, there appears to be little reason to pursue computationally expensive geometry optimizations with hybrid density functionals since equally good and often better results are obtained with GGAs. Since the GGAs like PBE and BP86 also deliver excellent vibrational frequencies it is a computationally attractive and logical route to only switch to the computationally much more expensive hybrid functionals for the final total energy and property calculations where they have clear advantages over GGA functionals.

7.2. Vibrational frequencies and IR spectra

The prediction of harmonic vibrational frequencies on the basis of DFT has been rather extensively pursued [43]. They follow directly from the equations presented in Section 6.2 if the two perturbations are both taken to be nuclear movements.

In fact, harmonic frequencies predicted by GGA functionals such as BP86 and PBE agree surprisingly well with observed fundamentals with errors being usually well below 10% [210–212]. It has been shown that this good agreement arises from a cancellation of errors – the underestimation of harmonic frequencies and the neglect of anharmonicities in these calculations [213]. Harmonic frequencies are better predicted by hybrid functionals but to explicitly calculate anharmonic corrections to harmonics vibrational frequencies is a very difficult task. Consequently, the systematic error cancellation that occurs with GGA functionals appears to be fortunate and such calculations are of great help in the assignment of experimental spectra. Secondly, the zero-point energy contributions to the free energy are quite accurately predicted by DFT methods.

IR intensities are straightforward to calculate from the eigenvectors if the Hessian matrix and the derivative of the electric dipole integrals with respect to nuclear coordinates. A compilation of benchmark results can be found in the book by Koch and Holthausen [43].

7.3. Raman spectroscopy

It is well known that the intensity of Raman active vibrational modes can be calculated from the derivatives of the polarizability tensor with respect to the normal coordinates of the system [214]. However, the polarizability tensor itself is a second derivative property according to Eq. (77) with both perturbations being represented by the electric dipole operator[19] [120]. Consequently, Raman intensities and depolarization ratios are *third* derivative properties. Owing to the '$2n+1$ rule' [20] they can, however, still be calculated from the second derivative data assembled during the frequency calculation and the solution of the first order CP-SCF equations with respect to an external electric field [215–219]. However, Raman spectroscopy itself finds limited use in (bio)inorganic chemistry and consequently the subject will not be further discussed here.

7.4. Optical spectroscopy (UV/vis, CD, MCD)

The calculation of transition energies from time-dependent density functional linear response theory has been described in some detail in Section 6.4. It is emphasized again that the linear response approach *directly* yields the transition energy rather than the total energies of the ground- and excited states. Thus, the excited states themselves are never explicitly calculated. Rather, their energies are deduced from the poles of a frequency dependent ground state property. Thus, one may wonder how one should calculate transition properties such as transition dipole moments and excited state properties such as the dipole moment of the excited states?

The answer to the second question is simply: in the same way as for the ground state. Thus, for the ground state it has been greatly elaborated in Section 6 that all properties can be calculated from the analytic derivatives of the total energy. Thus, the same procedure applies to the excited states as well. The total energy of the excited state is simply the sum of the ground state energy and the transition energy predicted by the TD-DFT procedure. The derivatives of this total energy then define all excited state properties. However, it is evident that the excited state derivatives are more difficult to calculate than the ground state derivatives because the excited state total energy is not fully stationary. By this statement we mean that the ground state total energy is stationary with respect to variations of the MO coefficients and the transition energies are stationary with respect to the variations in the $\boldsymbol{X}$ and $\boldsymbol{Y}$ amplitudes. However, the transition energies are *not* stationary with respect to variations of the MO coefficients. Hence, there are additional CP-SCF equations (so-called Z-vector equations) that need to be solved in order to obtain what is called the excited state *relaxed* densities that take the part of the ground state density in property calculations. A lucid discussion and an impressive implementation of excited state derivatives (first implemented by Amos and co-workers [220]) based on TD-DFT (into the TurboMole program) has been given by Furche [221–223].

[19] Thus, the dipole moment itself is the first derivative of the total energy with respect to the external field strength. The polarizability is the second derivative and therefore represents the change of dipole moment induced by an external electric field.

Thus, the problem remains how to calculate transition properties from TD-DFT. Fortunately, this turns out to be rather straightforward because TD-DFT fully determines *both*, the transition density and the transition *current* density [223]. For a given eigenvector '0n' for a transition from the ground to the nth excited state they are given by:

$$\rho^{0n}(\boldsymbol{x}) = \sum_{ia}(X_{ia}^{0n} + Y_{ia}^{0n})\psi_i(\boldsymbol{x})\psi_a(\boldsymbol{x}) \tag{113}$$

$$\boldsymbol{j}^{0n}(\boldsymbol{x}) = \frac{1}{2}\sum_{ia}(X_{ia}^{0n} - Y_{ia}^{0n})(\psi_a(\boldsymbol{x})\pi\psi_i(\boldsymbol{x}) + \psi_i(\boldsymbol{x})(\pi\psi_a(\boldsymbol{x}))^*) \tag{114}$$

With π being the kinematic momentum operator. From these transition quantities one readily calculates the electric and magnetic transition dipole moments (in atomic units) as:

$$\mu^{\mathrm{el}} = -\int \rho^{0n}(\boldsymbol{x})\boldsymbol{r}\,\mathrm{d}\boldsymbol{x} \tag{115}$$

$$\mu^{\mathrm{mag}} = \frac{\alpha}{2}\int \boldsymbol{r}\times\boldsymbol{j}^{0n}(\boldsymbol{x})\,\mathrm{d}\boldsymbol{x} \tag{116}$$

Since $\boldsymbol{j}$ contains the momentum $\boldsymbol{p}$, the magnetic dipole moment contains the familiar angular momentum operator $\boldsymbol{l}$. Thus, the oscillator strength f^{0n} and the rotary strength R^{0n} are given by:

$$f^{0n} = \frac{2}{3}\omega^{0n}|\mu^{\mathrm{el}}|^2 \tag{117}$$

$$R^{0n} = \mathrm{Im}(\mu^{\mathrm{el}}\,\mu^{\mathrm{mag}}) \tag{118}$$

These quantities are the central ones for the calculation of absorption and CD spectra. The latter has been quite extensively developed for organic molecules and also for inorganic complexes by Ziegler, Autschbach and co-workers [190–192,224,225]. The results for transition energies are typically similar between the full TD-DFT and TD-DFT in the Tamm–Dancoff approximation [175] while the former treatment delivers better transition moments. On the other hand, the full response treatment occasionally leads to instabilities and the predictions for singlet-to-triplet transitions are often not of high accuracy.

MCD spectra have been studied by Ziegler, Seth, Autschbach and co-workers on the basis of TD-DFT [179,189,226]. Their methods have been mainly developed for MCD A- and B-terms and proved to be valuable. C-terms – the most significant for (bio)inorganic chemistry – have been treated as well [179], but based on the general discussion in Ref. [227] these methods are not yet fully general and more development work appears to be necessary. The challenge is substantial since essentially the entire ground state spin-Hamiltonian (see below) needs to be well predicted alongside with the transition energies and the transition properties.

The situation has changed most recently when a general method for the calculation of MCD spectra was introduced on the basis of multireference configuration interaction methods (MRCI-MCD) [228].

The method extends and generalizes earlier semi-empirical work [229,230] as well as the theory of Ref. [227]. While the computational effort of such methods excludes the application to truly large systems, it covers all of the correct physics and is applicable to at least medium sized systems. As an example, the calculated absorption and MCD spectra of $[Fe(CN)_6]^{3-}$ are shown in Fig. 6. The spectra are dominated by ligand-to-metal charge transfer transitions that are not easy to calculate by *ab initio* methods. This may be ascribed to very large electronic excitation and differential electron correlation effects that occur upon increasing (or decreasing) the formal d-electron count on the metal. In particular, the high-negative charge of the cluster was only crudely modeled by con-

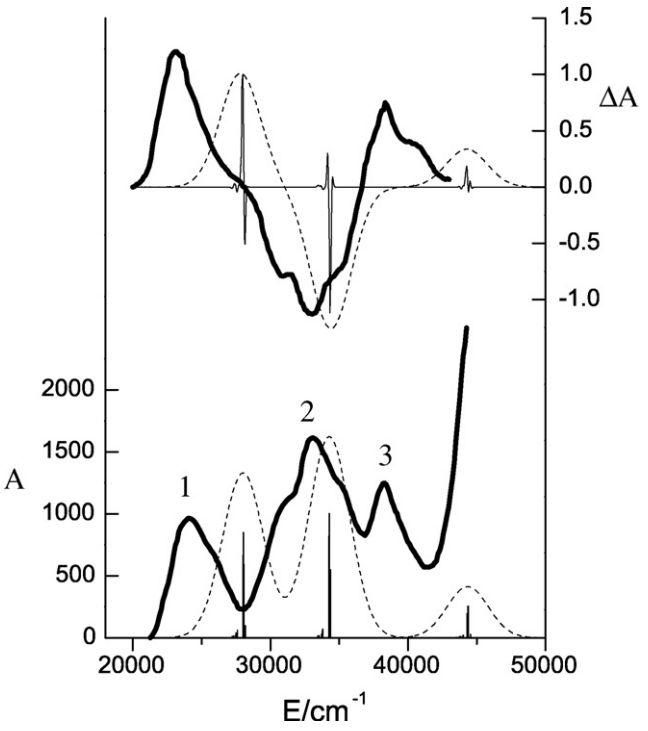

Fig. 6. Calculated (broken line) versus experimental (full lines) absorption (bottom) and MCD spectra of $[Fe(CN)_6]^{3-}$. For theoretical and computational details see Ref. [228].

tinuum solvation models. Given these constraints, the agreement is qualitatively excellent and quantitatively at least reasonable.

Following the first efficient implementations [231–236] TD-DFT has quickly become very popular and is nowadays frequently used (e.g. [109,237–249]). The method is very attractive indeed since its computational cost is at most equal to that of a CIS calculation and is considerably faster for HF exchange free functionals if the density fitting technique is employed [221,236,250–252]. Initially there was much excitement since it looked like as if TD-DFT was an accurate technique for excited state calculations. However, the situation has been found to be more complex and we note below some of the typical problems that have been found with TD-DFT calculations (see also [14]):

(a) TD-DFT linear response calculations in the adiabatic approximations do not include any double excitations. Thus, these will be systematically missing from the spectrum although they appear prominently in the d-d spectra of transition metal spectra. Consequently, single excitations that mix strongly with double excitations are poorly described by TD-DFT. A 1 typical example is the complex $[Ni(H_2O)_6]^{2+}$ shown in Ref. [14] but the problem is omnipresent in transition metal spectroscopy.
(b) Just like DFT ground state calculations fail for orbitally degenerate states, TD-DFT calculations cannot properly resolve the multiplet structure for systems with orbitally degenerate ground states. Some progress has recently be made for spin flip transitions [253].
(c) TD-DFT calculations do not account for electronic relaxation effects (e.g. the change of orbitals in the excited state). This typically leads to overestimation of transition energies. These effects have been fully included in the older DFT based calculations of excited states that were based on Delta-SCF and Slater transition state approaches. Consequently, TD-DFT predicted transition energies are frequently inferior to Delta-SCF or transition state calculations. However, these latter calculations are laborious since a full SCF calculation is needed for each excited state, they may face convergence problems or variational collapse and lead to non-orthogonal wavefunctions which complicates the calculation of transition properties.[20]
(d) The erroneous long-range behaviour of the functionals leads to orbital energies that are much too high (5–6 eV compared to accurate *ab initio* Kohn–Sham calculations) and also to very poor results for Rydberg states. However, such states are of limited importance for spectroscopy in condensed phases.
(e) The self-interaction error of DFT becomes *much* more severe for excited states. In charge transfer transitions or transitions of neutral-to-ionic valence character, the transferred electron does not see the proper +1 charge that is "left behind" but more positive charge. Consequently, such transitions are calculated much too low in energy—sometimes by several electron volts. These problems become less severe with hybrid functionals since the Hartree–Fock exchange removes some of the self-interaction error. However, as pointed out above, at the same time the transitions move to higher energy.

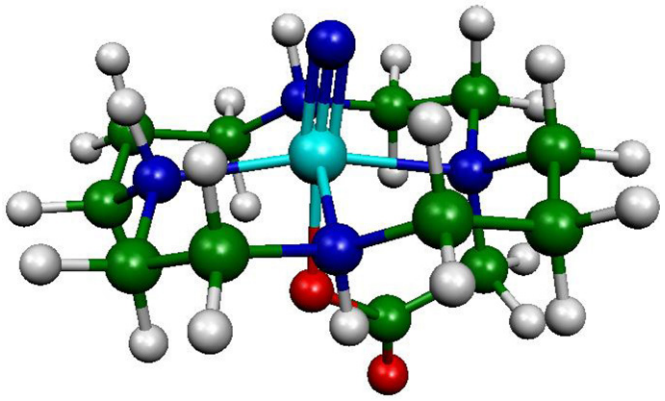

Fig. 7. Structure of the [Mn(N)(cyclam-acetate)]$^+$ cation used in the TD-DFT calculations described in the text.

A typical example for the problems that TD-DFT calculations frequently face has been analyzed several years ago [258] and is shown in Fig. 7. The low-spin d^2 (closed-shell $S=0$ with the ground state electronic configuration $(d_{xy})^2(d_{xz,yz})^0(d_{x2-y2})^0(d_{z2})^0$) complex $[Mn^VN(cyclam\text{-}acetate)]^+$ has been spectroscopically characterized and is known to feature only four electronic transitions in the visible region that are all of the d–d type [258]. A closely related Mn^VN complex has been studied by polarized single-crystal absorption and MCD spectroscopies [259]. The transitions occur experimentally at 11,800 cm^{-1} ($^1A_1 \rightarrow {}^3E(d_{xy} \rightarrow d_{xz,yz})$), 16,700 cm^{-1} ($^1A_1 \rightarrow {}^1E(d_{xy} \rightarrow d_{xz,yz})$), 19,900 cm^{-1} ($^1A_1 \rightarrow {}^3E(d_{xy} \rightarrow d_{x2-y2})$) and 37,700 cm^{-1} ($^1A_1 \rightarrow {}^3E(d_{xy} \rightarrow d_{z2})$). These transition energies are well predicted by TD-DFT calculations using either the BP86 or B3LYP functionals with errors of only ~2000–3000 cm^{-1}.[21] However, the DFT calculations predict in addition a series of

[20] The convergence problems are far less pronounced for transition state calculations in which one-half electron is moved from the donor to the acceptor orbital [254–257]. In these calculations the transition moment is straightforwardly calculated from the matrix elements between the two half-occupied orbitals. From this perspective, transition state calculations may be preferred over Delta-SCF calculations.

[21] For example, the d–d transitions predicted with the B3LYP functional within the Tamm–Dancoff approximation and in combination with the TZVP basis set are 11,500 (^3E), 17,900 (^1E), 19,400 ($^1A_2$) and 34,000 ($^1A_1$) cm^{-1} which is in excellent agreement with experiment.

ligand-to-metal charge transfer transitions arising from the axial carboxylate. This series starts already at 13,000 cm^{-1} in the BP86 calculations and smoothly extends to the far UV with at least 15 such states being calculated below 40,000 cm^{-1}. The nature and energies of these transitions are absurdly low and there is no experimental evidence for them. Such transitions are expected to occur above 35,000–40,000 cm^{-1} [260]. The B3LYP functional is much better in this respect since due to the HF exchange it is less plagued by the self-interaction error. The predicted d-d transition energies are similar to those of the BP86 functional but the LMCT series starts 'only' at 26,500 cm^{-1} which is still much too low and consequently, there are 'only' six artificial states interspersed into the d-d spectrum.

This simple example shows that TD-DFT predicted spectra are often quite good *except* that they are plagued with artifacts like erroneous or missing states. In fact, TD-DFT in the adiabatic approximation and in combination with the standard functionals misses on one of the most important aspects of theoretical electronic spectroscopy—the *balanced* treatment of excited states of different character.

Taken together, the combination of all of these problems lead to predicted optical spectra for open shell transition metals that are not fully reliable and sometimes, as in the example shown, even absurd. The situation is usually but not always better for closed-shell species and for systems with strong metal–ligand bonds such as organometallics. However, in general one has to apply TD-DFT calculations with utmost caution and one is well advised to seek critical feedback from experimental data. Uncritical trust in the results of TD-DFT calculations is not justified.

7.5. Resonance Raman spectroscopy and absorption bandshapes

The resonance Raman (rR) effect arises from a strong enhancement of the Raman intensities if laser excitations occurs within an absorption band [214,261,262]. In this case, the response of the system to the perturbation is highly nonlinear and it is better to step outside the linear response formalism developed above. Several competing formalisms have been developed for the calculation of rR intensities and absorption bandshapes (for a relatively comprehensive list see references in [38,263]) A very convenient technique has been developed by Heller and co-workers who outlined a general time-dependent formalism that allows the calculation of absorption (and fluorescence) bandshapes, rR intensities and rR excitation profiles [264–267]. The formalism has the appealing feature that the computational effort scales only linearly with respect to the number of vibrational modes.[22] For the special case that the vibrational modes are treated in the harmonic approximation and the Franck–Condon approximation is invoked, closed form solutions to the desired integrals are known [271]. Without going into any detail of the somewhat intricate mathematical procedures [38,263] The central quantity that appears in these calculations is the displacement of the equilibrium energy minimum along each vibrational mode in the electronically excited state (Fig. 8).

These quantities are directly related to bonding changes and hence give much insight into the electronic structure of the system. They may be viewed as the optical spectroscopy equivalent of the spin-Hamiltonian parameters mentioned in the next section. They can be determined by fitting experimental data [272,273] or from quantum chemical calculations. Our recent suggestion has been to

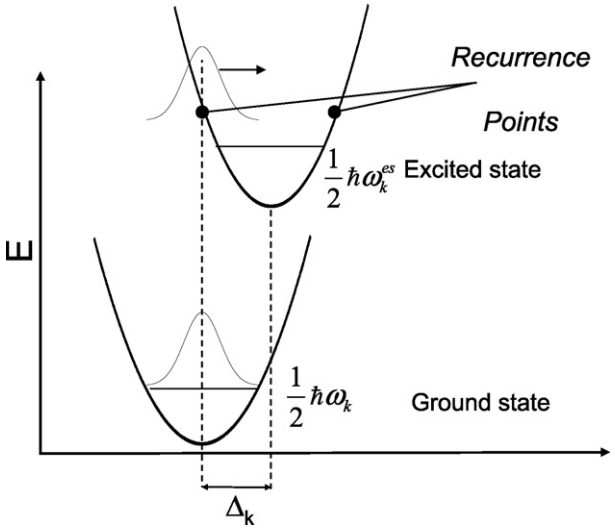

Fig. 8. Schematic description of the most important parameters that enter the calculation of resonance Raman intensities. The ground- and excited state potential energy surfaces are represented by harmonic potentials where the excited PES is shifted by Δ_k along the kth normal mode. Excitation of the ground state wavepacket to the excited state leads to a non-stationary state that evolves with time on the excited PES as described by Heller's theory. The resonance Raman intensity is directly related to Δ_k.

estimate these quantities from ground state force fields and excited state gradients as [263]:

$$\Delta_{Q,k}(n) = -\omega_k^2(n)\left.\frac{\partial E_n}{\partial Q_k}\right|_{Q=0} \tag{119}$$

Where $\omega_k(n)$ is the kth vibrational frequency in the nth electronically excited state (that may to a 0th order approximation be taken from the ground state force-field), E_n is the total energy of the nth electronically excited state and Q_k is the kth normal mode. The derivative is best obtained from the Cartesian derivatives by a simple linear transformation:

$$\frac{\partial E_n}{\partial Q_k} = \sum_p \frac{L_{pk}}{m_p^{1/2}}\frac{\partial E_n}{\partial X_p} \tag{120}$$

where X_p is a Cartesian coordinate of an atom with mass m_p and L_{pk} is an eigenvector of the mass-weighted Hessian matrix that describes the kth normal mode.

If these displacements are fed into the full-dynamics wavepacket equations of Heller and co-workers, it has been our experience that excellent agreement with experimental spectra can be obtained (Fig. 9 [263,274]). The central quantity to be obtained are the first derivatives of the excited state energy as discussed above. In such calculations, TD-DFT methods are moderately successful (somewhat inferior to *ab initio* methods) but if an analytical TD-DFT gradient is available, the spectra can be obtained very efficiently. It is stressed that this way of calculating absorption (and fluorescence) bandshapes, rR intensities and excitation profiles is superior to the short time approximation that has sometimes be used together with excited state gradients to calculate rR intensities. Conversely, the calculated displacements serve as excellent approximations for fitting procedures and also provide the signs of the displacements that are difficult to determine experimentally (Fig. 9).

As a recent example, we quote an extensive resonance-Raman study on transition metal dithiolenes with the formula $[M(L)_2]^-$ [274]. In these complexes, M = Co, Ni, Cu, Pd, Pt and L is a benzene-dithiolate derived ligand. All these complexes have the metal in the

[22] Direct calculation of multi-dimensional Franck–Condon factors on the other hand scales with the number of excited quanta to power $3N_{atoms}$ and quickly become impossible for larger molecules (however, see recent developments by Berger [268] and Grimme [269,270,269]).

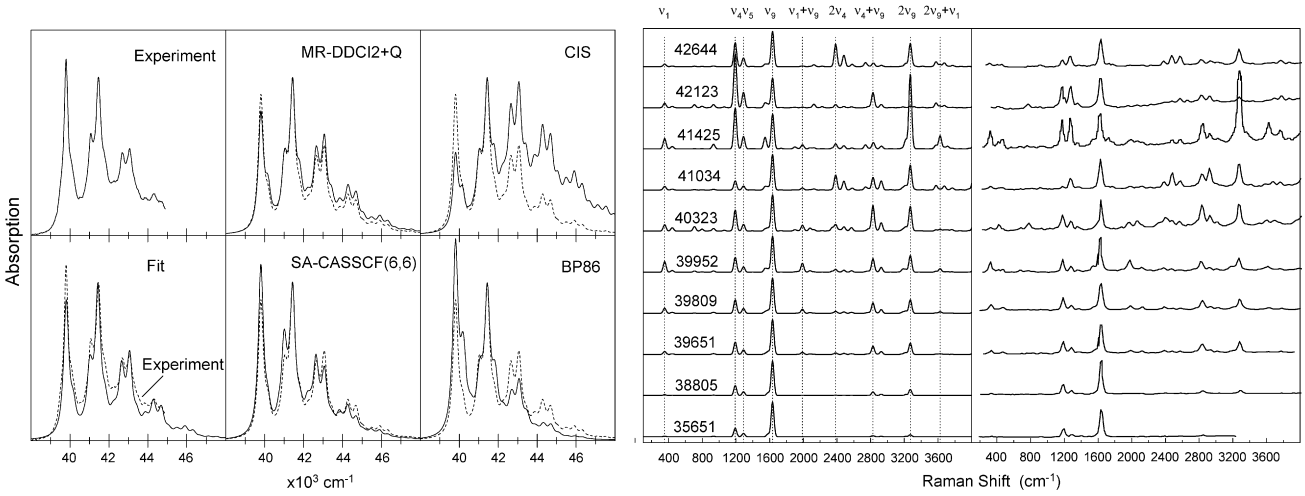

Fig. 9. Comparison of calculated and experimental absorption (left) and resonance Raman (right) spectra for the $^1A_g \rightarrow {}^1B_u$ transition of *trans*-hexatriene. The upper left curve on the left represents the experimental spectrum and the other traces are predictions of different quantum chemical methods compared to the best fit result on the lower left. On the right, the left panel corresponds to calculated (MR-DDCI2 + Q) rR spectra with excitation throughout the absorption band compared to experimental spectra on the right (arbitrary intensity units on the *y*-axis of the right-hand side figure).

formal oxidation state of +3 and show intense absorption bands in the visible and near-infrared region. Since the complexes were suspected to contain dithiolene radicals, the nature of the excitations was of particular interest. If an absorption band could be identified as a ligand-to-ligand charge transfer (LLCT) process, this would be indicative of a ligand-radical in the electronic ground state. Alternatively, if the excitation could be identified as ligand-to-metal charge transfer excitation, the dithiolenes would be seen to behave as innocent ligands. Obviously, the resonance Raman spectra of these complexes are very rich and display complex enhancements patterns. However, on the basis of simplified correlated *ab initio* calculations or TD-DFT calculations, the spectra of all systems could be reproduced with near-quantitative accuracy (Fig. 10). The analysis demonstrated that highly intense rR bands in the low-frequency region (<500 cm^{-1}) are the signature of LMCT transitions that mainly enhance the metal–ligand stretching modes. However, strongly enhanced rR bands in the region around 1000 cm^{-1} are indicative of ligand radicals, since these modes dominantly belong to C–S stretching vibrations that become enhanced upon LLCT excitations.

7.6. X-ray absorption spectroscopy

X-ray absorption spectra may be divided into three regions [17]: (a) the pre-edge region consisting of transitions from core-orbitals into valence orbitals, (b) the edge region consisting of transitions from core-levels into high lying empty orbitals close to the continuum and (c) transitions from the core-levels into the continuum

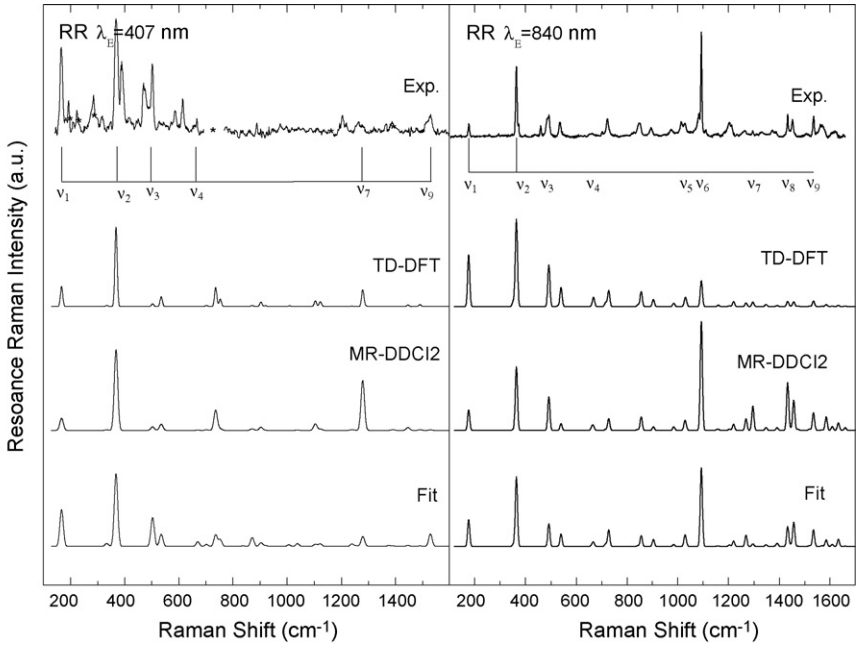

Fig. 10. Resonance Raman spectra of $[Cu(L)_2]^-$ (left) and $[Ni(L)_2]^-$ (right) upon excitation into the strongest absorption band. Experimental spectra are given on top. Predictions by TD-DFT and MR-DDCI2 methods are given underneath. At the bottom, least-squares fits to the spectra are given that result from minor (<10%) adjustments of the quantum chemically predicted excited state displacements.

giving rise to the extended X-ray absorption fine structure. While the analysis of the EXAFS region results in accurate structural information that can be compared with structure optimizations, the analysis of the pre-edge region is most informative with respect to its electronic structure content. More recently, direct DFT calculations of pre-edge spectra have been performed. We will focus here on the calculation of metal- and ligand K-edge spectra which have mostly been pursued.

In principle, these calculations could be done just like an ordinary TD-DFT calculation of the valence-to-valence transitions. However, there are several additional complications:

(a) In the metal K-edge region, the wavelength of the radiation is no longer large compared to the size of the absorbing system and hence the approximation of constant electric field over the size of a single molecule is no longer valid. Thus, higher order transition moments such as the quadrupole transition moment become important. However, a straightforward evaluation of this transition moment leads to problems of gauge-noninvariance that must be overcome.
(b) Excitations of core electrons are subject to significant relativistic effects owing to the low energy of the core orbitals and the associated high momentum of the core electrons.
(c) If one would proceed to calculate the excitation spectrum all the way from the near-infrared and visible regions down to the X-ray region, very many roots would have to be determined and this would lead to unrealistically long computation times. Hence, a way is needed to focus attention on the pre-edge region without having to deal with the valence-to-valence excitations.

There has been a considerable history of pre-edge calculations on light atoms that have been based on the Slater transition state concept [275–281]. In these calculations potentially many individual SCF calculations have to be done in order to construct the spectrum. The benefit is that the electronic relaxation of the core-hole is treated together with the relaxation of the valence shell electronic structure. If relativistic corrections are properly accounted for, such calculations lead to fairly good predicted transition energies and intensities [277–281].

The second type of approach that has been particularly intensely pursued by Solomon and co-workers is to connect the results of ground state DFT calculations to the intensity distribution in the XAS pre-edge peaks. For these analyses standardized effective values for the radial transition moment integrals had to be defined [282–288].

In keeping with the linear response philosophy, recent efforts have been centered around a direct calculation of the entire core-to-valence spectrum without resorting to system dependent calibration procedures. A standard protocol has been worked out that turned out to be simple and effective [289,290]. In these calculations, excitations are only allowed out of localized core-holes into the entire virtual space of MOs. Thus, by construction, the transitions included in the excitation space within the standard TD-DFT treatment fall into the K-edge region of the absorber atom of interest. The initial localization of the core hole is consistent with the sudden approximation [291]. The construction covers the final state effects to the same extent as TD-DFT covers these effects in the valence region but the relaxation of the core–hole is not allowed for in this protocol. It has also been argued that such effects are probably small [292]. The inclusion of relativistic effects and very large and flexible basis sets in the core region has been tried but not found to greatly improve the results. These calculations do not lead to accurate values of *absolute* transition energies—even after relativistic corrections, the erroneous potential of the standard DFT functionals close to the nucleus prevents this anyways. However, *relative* transition energies for series of complexes or different transitions within the same species are usually very well predicted by the calculations with an accuracy of a few tenths of an eV. Thus, a constant shift can be applied for each absorber at a given level of DFT functional and basis set in order to obtain good predicted transition energies. The intensity distributions calculated with this simple minded but effective approach are fairly good and overall the calculations are efficient and successful [243,289,293]. It is readily anticipated that one will see much more use of this approach in the future. Similar studies on the basis of two-component relativistic TD-DFT calculations have been reported by Ziegler and co-workers [177].

As an example the calculation of ligand K-edges for a series of transition metal dithiolenes is quoted [289]. As shown in Fig. 11, excellent agreement between the measured and theoretically calculated pre-edges in terms of the number of features, the energetic shifts and the relative intensities of the bands has been obtained. Similarly good agreement is often obtained in application studies [289,294–302].

7.7. EPR and NMR spectroscopy

EPR and NMR experiments are parameterized by an effective spin-Hamiltonian (SH) that only contains spin-degrees of freedom. For an isolated spin-system with total spin S, the spin-Hamiltonian can be written [303,304]:

$$H_{\mathrm{Spin}} = \hat{\boldsymbol{S}}\boldsymbol{D}\hat{\boldsymbol{S}} + \beta\boldsymbol{B}\boldsymbol{g}\hat{\boldsymbol{S}} + \sum_A \{\hat{\boldsymbol{S}}\boldsymbol{A}^{(A)} + \hat{\boldsymbol{I}}^{(A)}\boldsymbol{Q}^{(A)} - \gamma_N^A\boldsymbol{B}\sigma^{(A)}\}\hat{\boldsymbol{I}}^{(A)} + \cdots \quad (121)$$

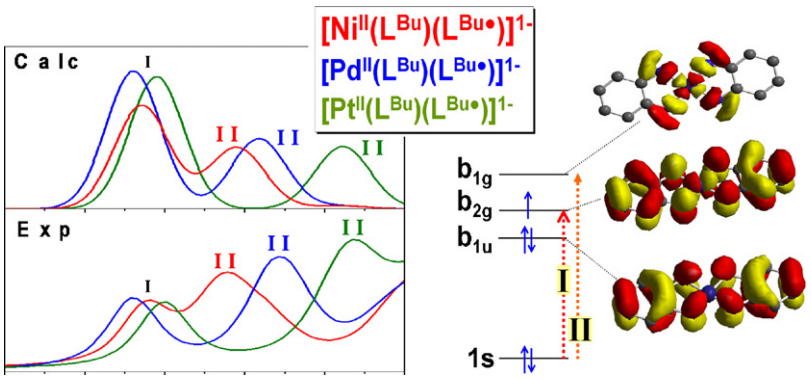

Fig. 11. Comparison of calculated (upper panel) and experimental sulfur K-edge spectra for a series of transition metal dithiolene monoanions with the central metal varying from Ni to Pd to Pt. Adapted from Ref. [289].

The individual terms refer to the zero-field splitting, the electronic Zeeman-effect, the hyperfine coupling, the nuclear quadrupole interaction and the nuclear Zeeman effect respectively. $\hat{\boldsymbol{S}}$ and $\hat{\boldsymbol{I}}^{(A)}$ refer to the spin-operators for the fictitious total spin of the system and $\boldsymbol{D}$, $\boldsymbol{g}$, $\boldsymbol{A}^{(A)}$, $\boldsymbol{Q}^{(A)}$ and $\boldsymbol{\sigma}^{(A)}$ are numerical parameters (SH parameters) that are obtained experimentally from fitting the observed spectra. The spin-Hamiltonian works on a (usually) low dimensional Hilbert space that is spanned by the product functions $|SM_S\rangle \otimes |I^{(1)}M_I^{(1)}\rangle \cdots \otimes |I^{(M)}M_I^{(M)}\rangle$ where S, M_S refer to the total spin of the electronic system and its projection quantum number ($M_S = S$, $S-1, \ldots, -S$) and analogously $I^{(1)}$, $M_I^{(1)}$ denotes the nuclear spin and its projection. Fortunately, (almost) all magnetic resonance experiments can be completely described by the spin-Hamiltonian since exact or at least accurate approximate solutions to the (time dependent) Schrödinger equation are readily obtained. The contribution of quantum chemistry is to relate the spin-Hamiltonian parameters to the microscopic interactions that occur in the full (relativistic) molecular Hamiltonian.

While there has been a longstanding tradition to interpret the spin-Hamiltonian parameters by sum-over-states type treatments based on ligand field theory [305–307], modern quantum chemistry employs the language of analytic derivative theory as outlined in Section 6. This is not to say that the ligand field treatments are not extremely useful as qualitative guides. It is, however, of utmost importance to not "mix up" the levels of argumentation between the spin-Hamiltonian, ligand field arguments and numerical quantum chemical calculations. It should be remembered that, when taken literally, systematically accurate predictions can not be delivered by ligand field type calculations even when they are "interspersed" with elements of DFT calculations. Perhaps the most convincing marriage of ligand-field and DFT methods has been developed by Atanasov and Daul and has proven to be very useful in the interpretation of molecular spectra [308–317].

The linear response treatment of SH parameters appears now to be reasonably well understood for all of the parameters that occur in the SH. We will briefly summarize the results in order to show the application of the methods described in Section 6. One complication that had to be overcome in the derivation of the equations presented below is that DFT based quantum chemical calculations always (and only approximately so) only deliver one particular M_S component of an S, M_S multiplet (invariably the 'principal' component with $M_S = S$). The properties of the remaining components and their interrelationship must then be deduced from application of the Wigner–Eckart theorem [20,227,318–325]. As becomes evident from the form of the SH, all of the SH parameters can be related to *second* derivatives of the total energy after supplementing the BO Hamiltonian with the appropriate terms that describe the interactions of the various spins with the magnetic field, with the orbital motions of the electrons and amongst each other. Full details of the relevant operators have been collected in various places [11,12,323,326].

7.7.1. Zero-field splitting

The ZFS is the least well developed SH parameter in EPR spectroscopy. From quantum chemistry, this term has two contributions that arise from the direct magnetic spin–spin dipole–dipole interaction (to first order in perturbation theory) and from the spin–orbit coupling (to second-order in perturbation theory).

For the SS contribution McWeeny and Mizuno have shown [46]:

$$D_{kl}^{(SS)} = -\frac{g_e^2}{16}\frac{\alpha^2}{S(2S-1)}\sum_{\mu\nu}\sum_{\kappa\tau}\{P_{\mu\nu}^{\alpha-\beta}P_{\kappa\tau}^{\alpha-\beta} - P_{\mu\kappa}^{\alpha-\beta}P_{\nu\tau}^{\alpha-\beta}\} \times \langle\mu\nu|r_{12}^{-5}\{3\boldsymbol{r}_{12,k}\boldsymbol{r}_{12,l} - \delta_{kl}r_{12}^2\}|\kappa\tau\rangle \quad (122)$$

The integrals appearing in Eq. (122) look complicated at first glance but are readily calculated and owing to the factorization of the two-particle spin-density matrix, Eq. (122) can be implemented for large scale application without creating storage or computation time bottlenecks. However, generally applicable programs have only appeared recently [327–333]. The importance of the spin–spin terms has been clearly recognized for the ZFS of organic triplets and biradicals but it has been essentially discarded as an important contribution to the ZFS of transition metals. However, recent results show that the SS terms also contributes a non-negligible fraction to the ZFSs of transition metal complexes (up to $\sim$1–2 cm^{-1}) and needs to be taken into account for quantitative results [328].

The formalism to achieve an analytic derivative formulation of the spin–orbit coupling part of the SH has been worked out only most recently and is somewhat more involved than the treatment presented in Section 6 [325]. The complications arise from the fact that the SOC mixes states of different total spin and hence the derivatives of the density matrices with respect to the total spin become more involved. Since the formalism and the associated arguments are somewhat lengthy [325,318], this contribution will not be covered in detail here. For alternative approaches see [330–333,334–342].

7.7.2. g-Tensor

The g-tensor is well studied by now with a number of implementations and applications available (for reviews see Refs. [11,14,16,343–345]). One obtains the following expressions for the four contributions:

$$g_{kl} = g_e\delta_{kl} + \Delta g^{\mathrm{RMC}}\delta_{kl} + \Delta g_{kl}^{\mathrm{GC}} + \Delta g_{kl}^{\mathrm{OZ/SOC}} \quad (123)$$

$$\Delta g^{\mathrm{RMC}} = -\frac{\alpha^2}{S}\sum_{\mu,\nu}P_{\mu\nu}^{\alpha-\beta}\left\langle\varphi_\mu\left|-\frac{1}{2}\nabla^2\right|\varphi_\nu\right\rangle \quad (124)$$

$$\Delta g_{\mathrm{kl}}^{\mathrm{GC}} = \frac{\alpha^2}{4S}\sum_{\mu,\nu}P_{\mu\nu}^{\alpha-\beta}\left\langle\varphi_\mu\left|\sum_A Z_A r_A^{-3}[\boldsymbol{r}_A\boldsymbol{r} - \boldsymbol{r}_{A,k}\boldsymbol{r}_l]\right|\varphi_\nu\right\rangle \quad (125)$$

$$\Delta g_{kl}^{(\mathrm{OZ/SOC})} = \frac{1}{2S}\sum_{\mu\nu}\frac{\partial P_{\mu\nu}^{\alpha-\beta}}{\partial B_k}\langle\varphi_\mu|\hat{z}_l^{\mathrm{SOMF}}|\varphi_\nu\rangle \quad (126)$$

The first three terms represent first-order contributions while the – usually dominant – contribution is provided by the second-order contribution in the fourth term. This term involves the derivative of the spin-density matrix with respect to a component of the magnetic field (thus the CP-SCF equations are solved for a purely imaginary perturbation represented by the orbital Zeeman operator $\beta\sum_k(-i\nabla_k \times \boldsymbol{r}_k)\boldsymbol{B}$) and the SOC coupling operator that is represented by various approximations to the full two-electron Breit–Pauli SOC operator (spin–orbit mean-field approximation, SOMF; Refs. [346–349]).

7.7.3. Hyperfine coupling

One finds for the three parts of the HFC the following expressions:

$$A_{kl}^{(A;c)} = \delta_{kl}\frac{8\pi}{3}\frac{P_A}{2S}\rho^{\alpha-\beta}(\boldsymbol{R}_A) \quad (127)$$

$$A_{kl}^{(A;d)} = \frac{P_A}{2S}\sum_{\mu\nu}P_{\mu\nu}^{\alpha-\beta}\langle\varphi_\kappa|r_A^{-5}(r_A^2\delta_{\mu\nu} - 3r_{A;\mu}r_{A;\nu})|\varphi_\tau\rangle \quad (128)$$

$$A_{kl}^{(A;\mathrm{SO})} = -\frac{P_A}{S}\sum_{\mu\nu}\frac{\partial P_{\mu\nu}^{\alpha-\beta}}{\partial\hat{I}_k^{(A)}}\langle\varphi_\mu|z_l^{\mathrm{SOMF}}|\varphi_\nu\rangle \quad (129)$$

With $P_A = g_e g_N \beta_e \beta_N$. Thus, the first two terms are straightforward expectation values that represent the Fermi contact interaction and the electron-spin-nuclear spin dipolar interactions while the SOC contribution is a response property [321]. In this case, one has to solve a set of coupled-perturbed equations with the three spatial components of the nucleus-orbit interaction operator $(P_A \sum_k (-i\nabla_k \times (\boldsymbol{r}_k - \boldsymbol{R}_A)) r_{kA}^{-3})$ taken as the perturbation. Since, the solution of the coupled-perturbed equations becomes time consuming for larger molecules this should only be done for a few selected heavier nuclei. For light nuclei, the SOC correction is usually negligible [350].

7.7.4. Electric field gradient

The EFG tensor is straightforwardly calculated from:

$$V_{\mu\nu}^{(A)} = \sum_{\kappa,\tau} P_{\kappa\tau} \langle \varphi_\kappa | r_A^{-5} (r_A^2 \delta_{\mu\nu} - 3 r_{A;\mu} r_{A;\nu}) | \varphi_\tau \rangle \tag{130}$$

Once available and supplemented by the nuclear contribution, the EFG tensor can be diagonalized. The numerically largest element $V_{\max}$ (in atomic units) defines the value of q which is in turn used to calculate the quadrupole splitting parameter as $e^2qQ = 235.28 V_{\max} Q$ where Q is the quadrupole moment of the nucleus in barn. Transformed to its eigensystem, the quadrupole splitting enters the SH in the following form: [351,352]:

$$\hat{H}_Q = \hat{I}\boldsymbol{Q}\hat{I} = \frac{e^2qQ}{4I(2I-1)} \hat{I} \begin{pmatrix} -(1-\eta) & 0 & 0 \\ 0 & -(1+\eta) & 0 \\ 0 & 0 & 2 \end{pmatrix} \hat{I} \tag{131}$$

The asymmetry parameter η is defined as:

$$\eta = \frac{|V_{\mathrm{mid}} - V_{\min}|}{V_{\max}} \tag{132}$$

It is to be noted that this is the only term which involves the total electron density rather than the spin density. The field gradient tensor is consequently of a quite different nature than the hyperfine coupling which depends on the same dipolar interaction integrals but in the case of the HFC they are contracted with the spin density instead of the electron density.

7.7.5. Chemical shift tensor

The chemical shift tensor is closely analogous to the theory of the g-tensor and consists of a first- and a second-order part. However, instead of the derivative of the spin-density, it involves the derivative of the total electron density since the *spin*–orbit operator is replaced by the *nucleus*-orbit operator (see reviews in [353]):

$$\sigma_{kl} = \sigma_{kl}^{(d)} + \sigma_{kl}^{(p)} \tag{133}$$

$$\sigma_{kl}^{(d)} = \frac{\alpha^2}{2} \sum_{\mu,\nu} P_{\mu\nu} \langle \varphi_\mu | r_A^{-3} [\boldsymbol{r}_A \boldsymbol{r} - \boldsymbol{r}_{A,k} \boldsymbol{r}_l] | \varphi_\nu \rangle \tag{134}$$

$$\sigma_{kl}^{(p)} = \frac{\alpha^2}{2} \sum_{\mu\nu} \frac{\partial P_{\mu\nu}}{\partial B_k} \langle \varphi_\mu | (-i\nabla \times (\boldsymbol{r} - \boldsymbol{R}_A))_l r_A^{-3} \varphi_\nu \rangle \tag{135}$$

All the one-electron integrals that appear in this section are straightforward to calculate if Gaussian basis functions are used. A complication is met in taking the first derivatives of the electron density matrix with respect to a magnetic field because the angular momentum operator occurring in the orbital-Zeeman perturbation is referred to the global origin of the coordinate system. Hence, the results depend on the choice of origin which is undesirable and unphysical. While this dependence is known to vanish in the limit of a complete basis set, care has to be taken in practice where a complete basis set cannot be used. The most satisfactory solution is to employ magnetic field dependent basis functions (GIAO's, Ref. [354–356] that are of the form $\tilde{\varphi}_\mu^A(\boldsymbol{x}, \boldsymbol{B}) = \varphi_\mu^A(\boldsymbol{x}) \exp(i(\alpha/2)(\boldsymbol{B} \times \boldsymbol{R}_A)\boldsymbol{r})$. As a consequence of this Ansatz, the basis set depends on the perturbation and the more general form of the CP-SCF equations (Eq. (93)) must be employed.

7.7.6. Performance of DFT

The accuracy of EPR parameter calculations with DFT is somewhat variable. For organic radicals and biradicals including amino acid radicals, usually very good results are obtained for g-tensors, hyperfine and quadrupole couplings and also for zero-field splittings. In such investigations, the EPR II or EPR III basis sets appear to be adequate. Hybrid functionals such as B3LYP and PBE0 have been found to be somewhat more accurate than GGA functionals, in particular for hyperfine couplings. A recent calibration study has shown that the meta-GGA hybrid TPSSh (and possibly also TPSS0) leads to competitive performance [357].

For transition metals, the situation is more involved. The g-shifts, being a response property, are usually significantly underestimated by the standard functionals [320,358,359]. However, this underestimation depends somewhat on the metal and the oxidation state. The worst results are usually obtained for Cu(II) complexes while other configurations such as Ni(III) or V(IV) appear to work much better. The underestimation of the g-shift has been attributed to a combination of too covalent bonding and too high d–d transition energies (that essentially determine the stiffness of the system with respect to external perturbations). In these calculations hybrid functionals like B3LYP are certainly to be preferred [320]. However, as pointed out by Kaupp and co-workers [358], elevated levels of HF exchange are dangerous since they lead to strong spin contamination and bring with it all of the disastrous failures of HF theory for transition metals.

For zero-field splittings very little data exists and most of it is based on theoretical approaches that are significantly inferior to the linear response treatment mentioned above. There is evidence that the new method leads to better results than the previous calculations and are comparable to the results obtained for g-tensors [325,360]. However, much more work is certainly necessary in this area. Nevertheless, reasonable results have been obtained for Mn(II) [245,361] and Mn(III) [328] complexes while the very large zero-field splittings in Fe(IV)-oxo compounds that arise from very low-lying excited states of different multiplicity than the ground state [362–364] cannot be predicted to high accuracy by standard DFT methods.

For hyperfine couplings to the metal nucleus the additional problem is the significant contribution of the SOC part (that is negligible for most ligand nuclei with the exception of sulfur, selenium and other heavier ligands). The SOC contribution to the hyperfine coupling is closely related to the g-tensor and hence a similar underestimation is evident by present day DFT methods. On the other hand, the Fermi contact term is particularly pathological since it depends on the indirect core level spin polarization arising from the unpaired spin density in the metal d-orbitals. This spin-polarization is difficult to calculate to high accuracy and so far DFT calculations significantly underestimate it [321,365,366]. Again, increasing the fraction of HF exchange helps but the same comments as for the g-tensor above apply. Also, relativistic effects on the isotropic hyperfine coupling can no longer be neglected in the first, and of course also in the second- and third transition rows [513–515]. Since the three contributions to the hyperfine coupling feature very different physical mechanisms (core-polarization for the contact term, the valence shell spin-density distribution for the dipolar term and the linear response for the SOC part) it is difficult to arrive at highly

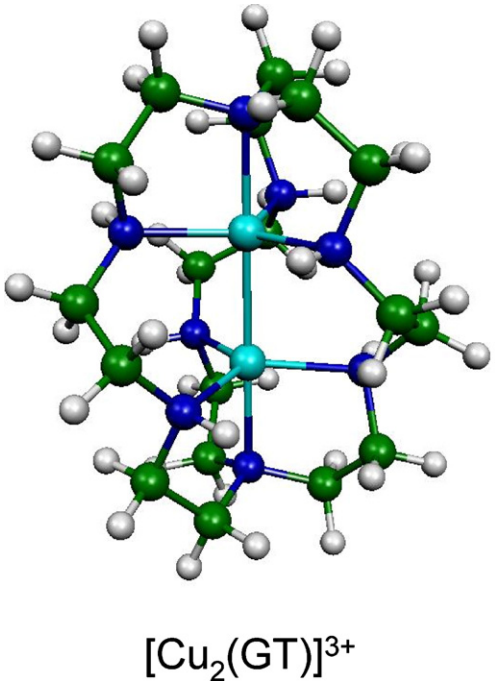

Fig. 12. Comparison of calculated and experimental EPR parameters for the delocalized mixed-valence Cu(1.5)···Cu(1.5) complex $[Cu_2(GT)]^{3+}$ shown in the right. Data adapted from Ref. [367].

accurate predictions. Again, results depend somewhat on the metal and oxidation state.

As a recent example for EPR calculations, a study is quoted were very detailed experimental information has been obtained (Fig. 12, Ref. [367]). The complication in such studies is that the high-resolution (2D, high-field) EPR spectra are very rich owing to the many magnetic nuclei that contribute to them. The simulation of the spectra was only achieved in a consistent way through a combination of the quantum chemically calculated parameters with the experimental measurements. In particular, the orientations of the many hyperfine tensors were best established from the theoretical calculations. Overall, the agreement between theory and experiment should be considered as satisfactory (Fig. 13).

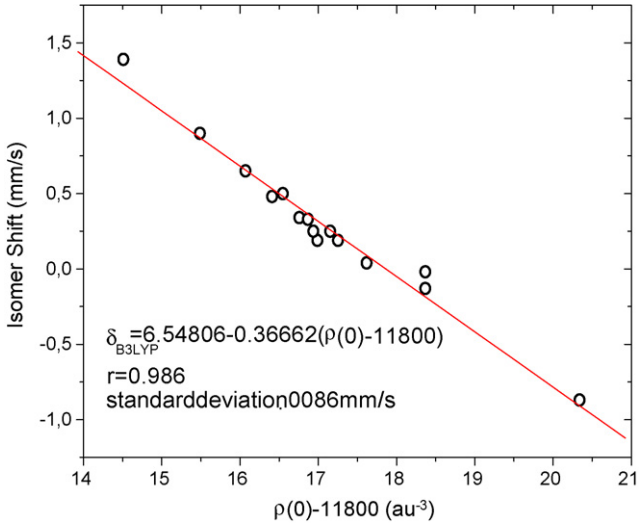

Fig. 13. Calibration curve for the prediction of Mössbauer isomer shifts from non-relativistic B3LYP calculations with the CP(PPP) basis set. Adapted from Ref. [384].

7.7.7. Quadrupole splitting and NMR chemical shifts

Not much systematic work appears to have been done on the quadrupole couplings of the metal nuclei, except for ^{57}Fe that is described below. Transition metal complex NMR properties have been extensively investigated by Bühl et al. [368–375]. More recently, several groups have begun to calculate paramagnetic NMR spectra which is relatively straightforward once the EPR property calculations have been accomplished [376–378].

Overall, it may be concluded that DFT approaches are already quite useful for the interpretation of magnetic resonance parameters but further development is required before fully quantitative accuracy has been achieved. Whether or not this is possible along the lines of the standard functionals is an open question.

7.8. Mössbauer spectroscopy

The combination of DFT calculations with ^{57}Fe-Mössbauer spectroscopy [379,380] has been found to be a particularly fruitful combination in the study of iron enzymes and has quickly been taken up by a number of groups [16,381–389]. In zero-magnetic field the two main quantities that are extracted for a given iron site are the quadrupole-splitting ΔE_q and the isomer shift δ that is referred to a suitable standard (metallic iron foil).

7.8.1. Quadrupole splitting

From a theoretical point of view the calculation of the quadrupole splitting is relatively simple since it can be calculated directly from the elements of the electric field gradient (EFG) tensor at the iron nucleus as:

$$\Delta E_Q = \frac{1}{2} eQ\, V_z \sqrt{1 + \frac{1}{3}\eta^2} \tag{136}$$

V_x, V_y and V_z are the principal components of the electric field gradient tensors in a coordinate system with $|V_z| \geq |V_y| \geq |V_x|$, e is the

positive elementary charge and $Q(^{57}Fe)$ is the nuclear quadrupole moment (measured in barn).

The EFG tensor itself is readily calculated as an expectation value over the ground state electron density. One point of concern, owing to the r^{-3} dependence of the field gradient operator, is the influence of relativistic effects on the results. However, it has been found to be very limited in a systematic study of iron complexes together with the ZORA treatment for relativistic effects [385]. Several groups have performed calibration studies in order to arrive at a suitable value for the quadrupole moment of the ^{57}Fe nucleus and a value of 0.16 barn now largely appears to be consensus. The performance of DFT for the prediction of ^{57}Fe quadrupole splittings is somewhat variable. Depending on the series of complexes studied, errors may range from 0.3 mm/s up to 1.0 mm/s. Unfortunately, it has been found in several studies (e.g. [390]) that the computed quadrupole splittings react fairly sensitively to details of the surrounding such as counter-ions. The sign of the computed quadrupole splittings is usually in agreement with experiment unless η approaches unity where the sign itself becomes essentially meaningless.

Quadrupole splittings are often interpreted from ligand field models with simple rules for the contributions from each occupied d-orbital. However, these models fail even qualitatively in the case of more covalent metal–ligand bonds. A worked out example has been provided for the quadrupole splittings of Fe(IV)-oxo sites in their $S = 1$ or 2 spin states. Here, ligand field considerations do not even provide the correct sign of the quadrupole splitting [391].

7.8.2. Isomer shift

While the complications that are met in the computation of quadrupole splittings are severe enough that full quantitative accuracy is seldom met, the situation is different for isomer shifts. From theoretical considerations [380], the isomer shift is linearly related to the electron density at the nucleus:

$$\delta_{MB} = a + b[\rho(0) - c] \quad (137)$$

Where a and b are fit parameters to be determined by linear regression and c is a number that is merely introduced for convenience Consequently, several workers have provided plots of the calculated electron density at the iron nucleus versus the experimentally obtained isomer shift for a range of complexes [16,381–389]. More recently Filatov has developed a linear response theory for the isomer shift and used it in conjunction with DFT or *ab initio* methods [392]. All of these plots show that very good linearity is obtained that allows the prediction if isomer shifts with an uncertainty that is smaller than 0.1 mm/s. Some workers have preferred to construct plots for a limited set of iron oxidation states and coordination environments while others have argued in favor of a single, unique calibration.

These calibration curves have already seen dozens if not hundreds of successful applications (e.g. [8,12,13,243,246,295,363,381–387,389–391,393–421,16,422]). Importantly, the experience gained in these applications indicates that the quality of the calibration does not depend on the charge-state of the iron centers, not on their spin state, not on their coordination number or the nature of ligands or whether the iron is involved in spin-coupling or not. Thus, these calculations, despite their simplicity, are successful and robust.

Nevertheless, some statements must be made:

(a) Since the electron density shows a cusp at the nucleus, it appears to be necessary to carry out calculations with basis functions that show the correct behavior at the nuclei. This is not the case for the typically employed Gaussian basis sets that decay too slowly for small distances (and too fast for large distances). Consequently, the basis set limit, known from numerical Hartree–Fock calculations to be ~11,900 a.u.$^{-3}$, is difficult to reach with Gaussian basis sets. With good bases (say 19 uncontracted s-primitives) one reaches electron densities at the nucleus that are around 11,820 a.u.$^{-3}$. Obviously, the percentage error is small but the absolute error of several dozen a.u.$^{-3}$ is large compared to the limited variation of the electron density over the chemical range of Fe(VI) to Fe(I) compounds that amount to only ~10 a.u.$^{-3}$.

(b) Secondly, the relativistic effects on the electron density at the nucleus are already very large for iron. Proper account for relativistic effects shifts $\rho(0)$ to around 15703.951 a.u.$^{-3}$ [423]. Thus, if one pursues a non-relativistic treatment, the electron densities one calculations are off by thousands of a.u.$^{-3}$ while one interprets changes on the order of a fraction of 1 a.u.$^{-3}$. The situation is even worse, since with a point nucleus, the relativistic orbitals (and also the quasi-relativistic one- or two-component orbitals) diverge in the basis limit. Thus, in order to obtain a systematically correct relativistic electron density at the iron nucleus one needs to resort to a finite nucleus model.

Based on these two comments one could conclude that the calculation of Mössbauer isomer shifts is a very involved subject where accuracy is difficult to achieve. The reason why this is not the case is revealed in Fig. 14 which analyzes the contributions of the iron 1s, 2s, 3s and 4s (valence shell) to the *variation* in the electron density at the nucleus from non-relativistic calculations. It is clear that by far the largest contributions to the electron density of ~11,800 comes from the Fe 1s and Fe 2s orbitals. However, these contributions are to a brilliant approximation constant in molecules and practically all variation occurs in the semi-core 3s and valence 4s shells. These shells are mainly influenced by the effects of bonding and these in turn are well described by DFT. Consequently, even the non-relativistically calculated $\rho(0)$ values accurately follow the chemical variations and provide a reliable tool for Mössbauer property predictions.

If one pursues such an approach, one has to stick to a given combination of density functional and basis set since the calibration will change for each such combination. The important points to realize are:

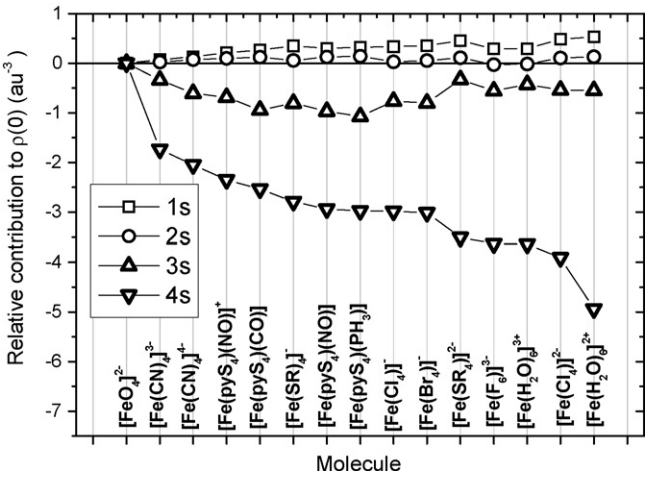

Fig. 14. Origin of the observed variation in the electron density at the iron nucleus according to B3LYP DFT calculations on a series of iron complexes. It is evident that practically all the variation that lead to the observed isomer shifts stems from the valence (4s) and semi-core (3s) orbitals. Adapted from Ref. [384].

The DFT potential provided by the standard functionals is not only wrong in the long range but is also in error close to the nucleus. Since the different functionals differ in this respect the absolute values of the electron density differ strongly.

Different basis sets approach the basis set limit to a different extent and consequently, the calibration only holds for the special basis set with which the calibration was performed. While it was originally thought, that it might be important to provide additional flexibility in the s-part of the basis set in order to allow the core-orbitals to properly distort in the molecular environment [384], subsequent studies showed that this is not the case and one obtains almost equally good results with the standard basis sets that offer only limited flexibility in the core region [383].

The slope one obtains from the linear regression varies with functional and basis set. However, in reality there is a definitive and known slope with an absolute value $-0.1573\,\mathrm{mm\,s^{-1}}$ a.u.$^{-3}$ [424]. This underlines the semi-empirical character of this simple minded approach to the theory of the isomer shift.

7.8.3. Magnetic hyperfine structure

Since Mössbauer spectroscopy is sensitive to all SH parameters, they can also be obtained from an analysis of the spectra and the same comments as in Section 7.7 apply A detailed study of the magnetic hyperfine structure in Mössbauer spectra and the performance of DFT methods is available [385]. As pointed out above, the accuracy is moderate but can be improved by scaling procedures. A scaling factor of 1.8 is suggested for the isotropic ^{57}Fe hyperfine coupling calculated with the B3LYP functional and the CP(PPP) basis set [384].

7.8.4. Nuclear resonance vibrational spectroscopy (NRVS)

A modern development in Mössbauer spectroscopy that has been fuelled by the progress in synchrotron techniques is the measurement of vibrational spectra via Mössbauer transitions. The inelastically scattered radiation (resembling the resonance Raman effect), contains vibrational side bands the intensity of which correlates with the involvement of iron motion into the normal modes that are probed. The details of the theory are slightly more involved and will not be discussed here [412,425–432]. However, the major contributor to the NRVS intensity are the normal mode composition factors $\boldsymbol{e}_{Ak}$. In terms of these factors, the kth normal mode can be written as:

$$Q_k = \sum_{A=1}^{M} \boldsymbol{e}_{Ak} \boldsymbol{R}_A \sqrt{m_A} \tag{138}$$

Which implies that $\boldsymbol{e}_{Ak}$ is simply the Cartesian part of the kth eigenvector $\boldsymbol{L}_k$ of the mass weighted Hessian matrix that refers to atom A with mass m_A. Thus, the $\boldsymbol{e}_{Ak}$ referred to the iron nuclei in the molecule are readily obtained from the second-derivatives of the total energy. The construction of the theoretical spectrum at a given temperature from these quantities is discussed for example in Refs. [412,432].

Since the force fields delivered by DFT calculations are usually quite good, excellent agreement with experiment can be obtain in such calculations [412]. Recently, a general program package has been developed and attached to the ORCA electronic structure program that not only allows the direct calculation of NRVS spectra from DFT calculations but also allows for least square fitting of the experimental data starting from the vibrational modes and NRVS intensities predicted by quantum chemistry [432].

As an example, consider the NRVS spectrum of the low-spin Fe(III) complex [Fe^{III}(cyclam-acetate)(N$_3$)]$^+$ from Ref. [412] (Fig. 15).

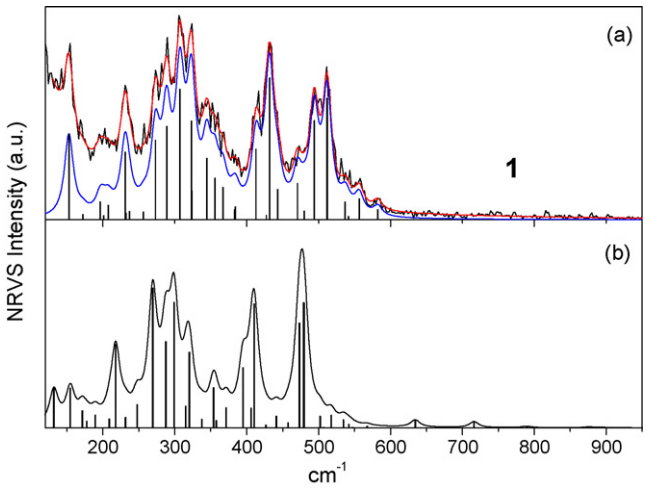

Fig. 15. Comparison of calculated and measured NRVS spectra for [Fe^{III}(cyclam-acetate)(N$_3$)]$^+$. The upper panel shows the experimental spectra together with the best fit and the individual transitions corresponding ot it. The lower panel shows the spectrum that has been predicted by BP86 DFT calculations together with the TZVP basis set. Adapted from Ref. [412].

7.9. Spin state energetics

A characteristic feature of open-shell transition metal ions is that several electronic configurations are accessible that may give rise to a number of different spin-states. These spin states are often close enough in energy such that their correct prediction becomes challenging for theory. However, since it has been found that the reactivity of different spin states of the same compound may be very different and that a reaction might as well proceed on two (or more) potential surfaces (the important 'two-state' reactivity concept [10]), the accurate description of such states is of obvious importance. Furthermore, the field of 'spin-crossover' complexes where two spin states are in thermal equilibrium or there may be a thermally or optically induced transition from one spin-state to the other has found considerable attention in the inorganic chemistry community [433].

The case is perhaps best illustrated with Fe(II) complexes that have also been extensively studied theoretically [434–447] In these complexes, the low-spin state ($^1A_{1g}$) corresponds to the electronic configuration $(t_{2g})^6(e_g)^0$ in an idealized octahedral notation while the high spin state ($^5T_{2g}$) corresponds to $((t_{2g})^4(e_g)^2)$. Note that the HS state is orbitally degenerate and hence Jahn–Teller active which is a nontrivial complication that will, however, be ignored for the purpose of the present discussion. Already ligand-field theory is able to indicate the nature of the challenge: The electronic energy difference E_{HS}–E_{LS} is given by $20Dq - 5B - 8C$ where $10Dq$ is the ligand field splitting parameter and B and C are the Racah parameters. Thus, a large ligand-field splitting favors the LS state while strong interelectronic repulsion and a weak ligand field favors the high-spin state. The considerable increase in interelectronic repulsion in the LS state arises from the fact that the electrons are 'more crowded' in the t_{2g} subshell and more importantly that there are more antiparallel spin pairs than in the HS state. Owing to the existence of the Fermi correlation, electrons of like spin repel each other less strongly than electrons of opposite spin. Obviously, a theoretical method that aims at a quantitative prediction of the HS/LS energy gap must be very well balanced in order to correctly predict the interplay between 10Dq (being dominated by metal–ligand bonding) and interelectronic repulsion (being dominated by dynamic correlation effects within the d-subshell).

From this discussion it becomes evident that wavefunction based *ab initio* methods face a severe problem: a lack of balance. In the HF method only exchange is covered but no correlation. Therefore, the HF method itself is *strongly* biased in favor of high-spin states. For example, HF theory even predicts $[Co(NH_3)_6]^{3+}$ to have a high-spin ground state [448]. The enormous bias for this state must be corrected for by the inclusion of dynamic correlation. However, it is known that the correlation energy calculated with standard wavefunction methods converges only very slowly with increasing size of the basis set for the correlation of antiparallel spin pairs (and only slightly better for parallel spin pairs). Thus, humungous basis sets must be used in wavefunction based calculations of spin state energetics in order to obtain quantitative results. For example, a recent study of Pierloot and co-workers on $[Fe(NH_3)_6]^{2+}$ [449] following up on earlier *ab initio* work [450], has used up to h-functions ($L = 5$) in the basis set. Clearly, such calculations on larger complexes will not become routine in the near future.

Unfortunately, experience has shown that standard DFT methods have an opposite bias in favor of the LS states [436]. This behavior may to some extent be related to the characteristic overbinding that still frequently occurs also for GGA functionals and also to the self-interaction error. It is not at all surprising that hybrid functionals greatly profit from error compensation and yield better predictions than either HF or 'pure' DFT methods.[23] However, also the B3LYP functional fails in certain instances to predict the correct ground state. Reiher and co-workers have proposed to decrease the amount of HF exchange in B3LYP to 0.15 in order to arrive at better predictions for Fe(II) systems. Later it was shown that this B3LYP* functional yields other properties with similar quality as the original B3LYP. However, the optimum amount of HF exchange appears to depend on the metal-, oxidation-state and property one is interested in and countless examples of similar reparameterizations of hybrid functionals can be found in the literature (e.g. [451]). It is therefore probably fair to state that a 'universal' solution to the spin-state problems with DFT has not yet been found and that a proliferation of purpose specific functionals does not aid in increasing the comparability of results among different studies.

7.10. Exchange coupling constants and the 'broken-symmetry' approach

A subject that has caused extended and ongoing controversies is how to best calculate the electronic structure and properties of two (or more) interacting open-shell magnetic ions. This presents no problem if the spins on the two sites (fictitious 'site spins' S_A and S_B)[24] are ferromagnetically aligned to produce the maximum total spin $S_{max} = S_A + S_B$ since in this case a single Kohn–Sham determinant is readily constructed that describes the system as good (or as bad) as a corresponding open-shell monomeric species.

The problems start in the much more frequently met case, when the local spins are antiferromagnetically aligned to produce the minimum total spin $S_{min} = |S_A - S_B|$. Even in the case that one whishes to describe such a system with a single electronic *configuration*, several *determinants* are necessary in wavefunction theory to construct a *configuration state function* (CSF) that is an eigenfunction of the total spin squared $S^2 = (\boldsymbol{S}_A + \boldsymbol{S}_B)^2$ operator with an eigenvalue of $S_{min}(S_{min} + 1)$. Examples of such CSFs for one and two unpaired electrons on sites '*A*' and '*B*' are:

$$\Psi_{AF}^{(1)} = \frac{1}{\sqrt{2}}(|a_1\bar{b}_1| - |\bar{a}_1 b_1|) \tag{139}$$

$$\Psi_{AF}^{(2)} = \frac{\sqrt{3}}{6}(2|a_1a_2\bar{b}_1\bar{b}_2| - |\bar{a}_1a_2\bar{b}_1b_2| - |\bar{a}_1a_2b_1\bar{b}_2| - |a_1\bar{a}_2b_1\bar{b}_2| + 2|\bar{a}_1\bar{a}_2b_1b_2|) \tag{140}$$

where (the here unspecified) orbitals a_i and b_i are essentially localized on fragments '*A*' and '*B*', respectively. Note that these wavefunctions are proper eigenfunctions of S^2 with total spin $S = 0$ and parallel coupling of the spins on the '*A*' and '*B*' sites, respectively. The expressions above emphasize the multi-determinantal nature of such wavefunctions and that one should not confuse the total spin S with its projection M_S for which a single determinant $|a_1a_2\ldots a_K\bar{b}_1\bar{b}_2\ldots\bar{b}_K|$ (for K-unpaired electrons on each site) would describe "the antiferromagnetic state". However, this latter determinant is *not* an eigenfunction of S^2 and hence it is not a proper starting point for a proper treatment of spin-coupling.

7.10.1. Spin Hamiltonian

In many cases, the energy differences between the states that are dominated by ferromagnetic alignment and by antiferromagnetic alignment of local spins are close in energy (less than a few hundred wavenumbers). For the dimer case of this section, the possible total spins form the sequence: $S_A + S_B, S_A + S_B - 1, \ldots, -|S_A - S_B|$. To a good approximation they can be represented by a phenomenological spin-Hamiltonian type operator:

$$H_{Spin} = -2J\hat{S}_A\hat{S}_B \tag{141}$$

That works on a basis of direct product spin-functions $|S_AM_A\rangle \otimes |S_BM_B\rangle$. Using the relationship $\hat{S}^2 = (\hat{S}_A + \hat{S}_B)^2 = \hat{S}_A^2 + \hat{S}_B^2 + 2\hat{S}_A\hat{S}_B$ the more useful form of the SH operator is:

$$H_{Spin} = -J(\hat{S}^2 - \hat{S}_A^2 - \hat{S}_B^2) \tag{142}$$

where the effective exchange coupling constant J measures the strength of the "interaction" and is positive for ferromagnetic spin alignment and negative for antiferromagnetic alignment. However, it is important to note that there is no genuine 'exchange interaction' in nature but that the spin-state energy differences arise purely from electrostatic interactions covered by the BO Hamiltonian. It is furthermore very important to clearly distinguish the exchange-coupling type of spin-state energy differences from the spin-crossover type spin-state energy differences. The latter arise from different orbital configurations for the two spin states and, as discussed above, are heavily influenced by differences in dynamic correlation energy of the two spin states. However, for the problem of the exchange coupling type the different spin states arise from the *same* orbital configuration—a problem of an entirely different quality that is influenced by many factors as will be discussed below.

Unfortunately, such multideterminantal wavefunctions such as Eqs. (139) and (140) are unsuitable in combination with the Kohn–Sham construction.[25] An obvious alternative to DFT meth-

[23] The dependence of the spin-state energies on the amount of HF exchange is to a very good approximation linear [442], as expected from the Ansatz for the hybrid functionals if the orbital relaxation effects with increasing HF exchange are not overly large.

[24] It is evident that these site spins are poorly defined in terms of rigorous quantum mechanics since only the total spin-angular momentum can be measured in experiments. The assumption that such site spins are meaningful entities is of course strongly implicated by chemical evidence and it would perhaps not be wise to refute the usefulness of the concept that the interacting system can be composed of magnetically interacting ions that in the majority of cases can be assigned a meaningful site spin S_A or S_B. Problems arise in the case of hetero-metallic clusters and in particular in the highly interesting mixed-valence systems. A thorough discussion of such systems is outside the scope of this chapter.

[25] Restricted open-shell Kohn–Sham treatments have been proposed that would cover such situations but they suffer from a lack of unitary noninvariance for rotations between the partially occupied orbitals [452].

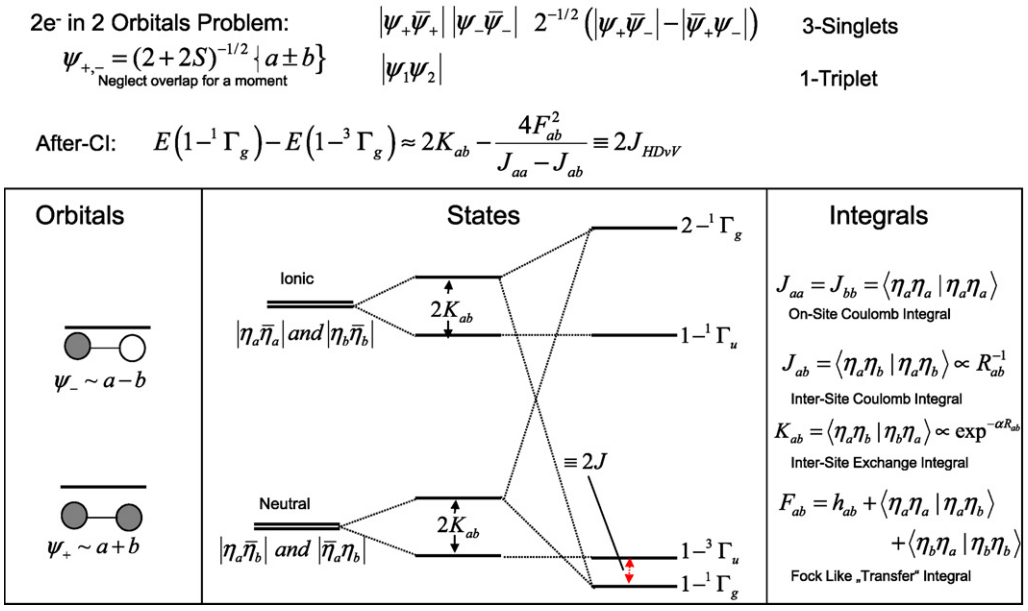

Fig. 16. Interpretation of the origin of antiferromagnetic coupling in wavefunction theory through configuration interaction of neutral and ionic singlet wavefucntions.

ods are correlated multireference *ab initio* approaches. However, these face serious challenges in trying to simultaneously treat static and dynamic correlation in such systems. While excellent calculations can be done for not too many unpaired electrons (e.g. Cu(II) or Ni(II) dimers) [453–464], it is probably fair to state the situation is not fully under control and an accurate *ab initio* calculation on an Fe(III)–Fe(III) dimer has yet to be accomplished (however, see the recent investigation by Marx et al. [465]). Thus, for at least some time to come one is practically obliged to resort to DFT methods in order to treat antiferromagnetically coupled systems. In fact, it is possible to do fairly reasonable calculations on the basis of the so-called 'broken-symmetry' (BS) approach [466–469], the physical contents of which will be discussed below.

7.10.2. Nature and origin of antiferromagnetic coupling

In order to illustrate the principle it is sufficient to study a model dimer with only one unpaired electron on each site (Fig. 16). Assuming for simplicity that the system features a center of inversion and one uses an open-shell spin-restricted formalism to compute the high-spin (triplet) state, the Kohn–Sham determinant will be of the form $\Psi_F = |(\text{core})\psi_+\,\psi_-|$ where (core) denotes all the doubly occupied orbitals. The symmetric and antisymmetric MOs are formed from the singly occupied MOs (SOMOs) on each site $\psi_{+,-} = (a \pm b)/(2 \pm 2S)^{1/2}$ where '*S*' is the overlap integral of the fragment orbitals '*a*' and '*b*'. One can pass from the delocalized MOs to essentially localized MOs $\eta_{a,b}$ by forming $\eta_{a,b} = (\psi_+ \pm \psi_-)/2^{1/2}$. These 'essentially localized' MOs are not perfectly local since due to the orthogonalization constraint η_a has a tail extending to site *b* and vice versa (an example will be provided below). Obviously, the antiferromagnetic state could initially by represented by the CSF $\Psi_{AF} = (|(\text{core})\eta_a\bar{\eta}_b| - |(\text{core})\bar{\eta}_a\eta_b|)/2^{1/2}$ where the overbar denotes occupation with a spin-down electron. Two points are to be noted: (a) as pointed out above, already this two-determinant Kohn–Sham determinant can not be properly represented in the Kohn–Sham framework; (b) if this was the entire story, the solution would always be *ferro*magnetic behavior since it is an elementary exercise to show that the energy of Ψ_{AF} is always above that of Ψ_F. In fact, in Hartree–Fock theory, the energy difference is simply $2K_{ab} \equiv 2\langle\eta_a\eta_b|\eta_b\eta_a\rangle$. Since K_{ab} is always positive [470], the 'direct' contribution to the exchange coupling constant *J* is always positive (and referred to as 'potential' exchange). In order to see how antiferromagnetism comes about we will once more rely on wavefunction theory and ask for the appropriate translation into the DFT framework later. In fact, in wavefunction theory one can form in addition to the 'neutral' singlet state Ψ_{AF} also the two 'ionic' singlet states $\Psi_{Ia,b} = |(core)\eta_a\bar{\eta}_a|, |(core)\eta_b\bar{\eta}_b|$. The symmetric combination of these two CSFs can interact with Ψ_{AF} through 'configuration interaction' and leads to an energy lowering that is, necessarily, a negative contribution to the exchange coupling constant *J* (and is called 'kinetic exchange'). From second-order perturbation theory, the energy lowering is $-4F_{ab}^2/(J_{aa} - J_{ab})$ where F_{ab} is the suitable Fock-matrix element between η_a and η_b and J_{aa} and J_{ab} are the Coulomb integrals $J_{ab} = \langle\eta_a\eta_b|\eta_a\eta_b\rangle$ and $J_{aa} = \langle\eta_a\eta_a|\eta_a\eta_a\rangle$ (Fig. 16).

In order to illustrate this principle consider a model calculation on a simple, hypothetical Cu(II) dimer ($[Cu_2(\mu\text{-}F)(H_2O)_6]^{3+}$) (Figs. 17 and 18).

It is now an elementary task for a quantum chemical program to rigorously evaluate the integrals that contribute to the exchange coupling constant. One finds that the 'direct' ferromagnetic term is small and accounts for only +17 cm^{-1} while the 'kinetic' antiferromagnetic contribution yields −57 cm^{-1}. Thus, the total predicted *J* is only −40 cm^{-1}. This value is *much* too small compared to reasonable values for compounds of this kind that typically amount to more than −100 cm^{-1}. The reason for this underestimation has been deeply discussed by Malrieu and co-workers [457–459] and Staemmler and co-workers [471–476]. At the heart of the problem is that the ionic configurations are much too high in energy in such a simple picture. Their energies are greatly lowered if they are allowed to 'relax' in an extensive dynamic correlation treatment. Consequently, in such calculations they will mix much more strongly with the neutral singlet configurations and hence increase the antiferromagnetic coupling. Inclusion of these effects via the so-called difference dedicated configuration interaction (DDCI) [477,478] approach yields a *J* of −206 cm^{-1} and the fraction of ionic character in the singlet ground state has increased from 0.06% to 3.3%—more than a factor of five.

7.10.3. The broken symmetry Ansatz

The very clever idea to simulate the effects of this configuration interaction without resorting to actual CI calculations is

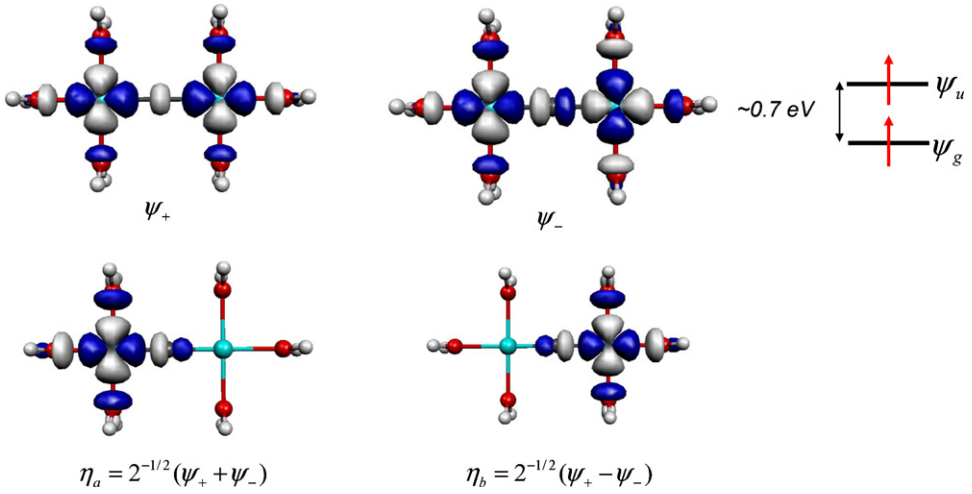

Fig. 17. The 'magnetic orbitals' of the model complex $[Cu_2(\mu\text{-}F)(H_2O)_6]^{3+}$.

to start from a single determinant wavefunction that reflects the antiferromagnetic state but is of the 'wrong' spin symmetry. This wavefunction is written:

$$\Psi_{BS}^{guess} = |(core)\eta_a\bar{\eta}_b| \quad (143)$$

Contrary to common belief, this determinant is *not* the broken symmetry determinant. It has the following three properties: (a) its energy is always higher than that of Ψ_F, (b) it is a 50:50 mixture of Ψ_F and Ψ_{AF} and (c) it has the same charge density as Ψ_{AF} (and Ψ_F) but a qualitatively wrong spin-density. In fact, one observes for a wavefunction of this type, that there are regions of positive- (around site '*A*') and regions of negative (around site '*B*') spin-density with the integral over all space being zero. It is crucial to understand that this is qualitatively wrong since a proper singlet wavefunction has zero spin density at each point in space.

From this discussion, it is clear, that a wavefunction of the type Ψ_{BS}^{guess} could never describe antiferromagnetic coupling properly. The crucial point, that appears to be widely underappreciated in discussions of the broken-symmetry method, is that after deciding on the form of Ψ_{BS}^{guess}, *one applies the variational principle to re-optimize the orbitals* [479]. Thus, after having found a stationary point, the true broken-symmetry wavefunction is of the form:

$$\Psi_{BS} = |(core')\tau_a\bar{\tau}_b| \quad (144)$$

Where τ_a and τ_b have relaxed to their final form under the action of the variational principle. They are typically *less* localized than η_a and η_b. Importantly, while η_a and η_b are orthogonal in their space part, the same is *not* true for τ_a and τ_b. Since these two spin–orbitals are always orthogonal by their spin-parts there is no further orthogonality restriction on their space parts. Thus, there is additional variational flexibility that the system uses to lower its energy and it is only this additional flexibility that brings about the antiferromagnetism. In fact, it is perfectly permissible and also occurs frequently in practice that – in the limit of very strong subsystem interaction – both, τ_a and τ_b relax back to ψ_+. In this case, the BS determinant is a standard closed-shell determinant and one has to conclude that a standard two-electron bond has been formed between fragments '*A*' and '*B*'.

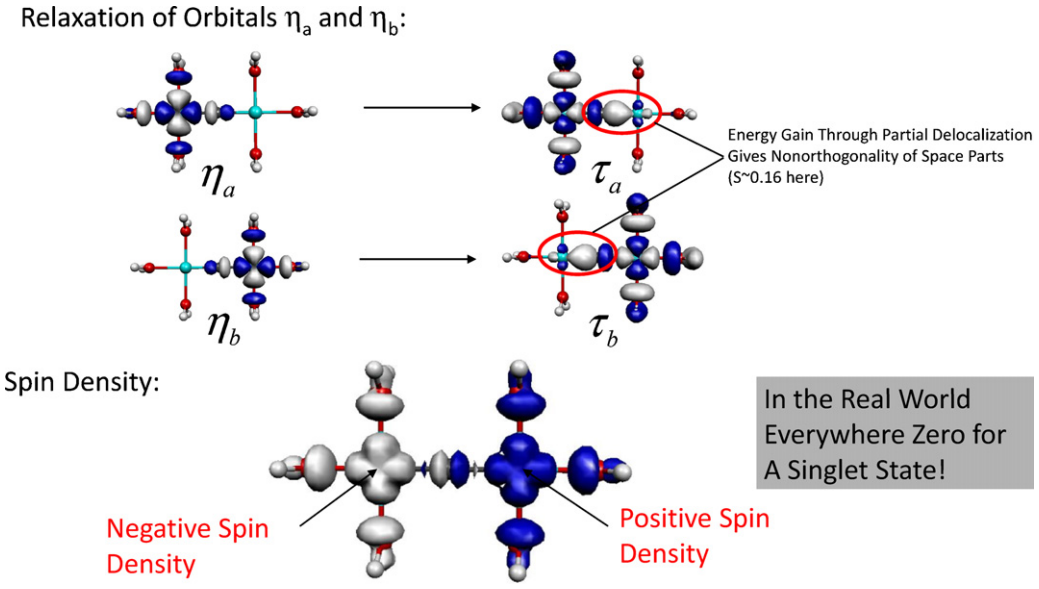

Fig. 18. Relaxation of the initial orthogonal magnetic orbitals η_a and η_b to the final broken-symmetry magnetic orbitals τ_a and τ_b. The bottom shows the erroneous spin-density obtained from a broken-symmetry calculation.

This situation for the model system described above is shown in Fig. 18 where it is obvious that after relaxation of the electronic structure, the tails on the bridging fluoride increase and the final BS orbitals are non-orthogonal by the space parts with an overlap of ~0.16.

Owing to the strong nonlinearity of the SCF equations, it is difficult to foresee when this situation will occur. In fact, different density functionals have very different propensity for symmetry breaking. In general, the more HF exchange is in the functional the more likely is one to remain in a broken-symmetry type solution with τ_a and τ_b being localized fragment MOs. This simply reflects the typical intrinsic bias of HF and DFT—overly delocalized electronic structure for DFT and overly local electronic structure for HF.

7.10.4. Physical interpretation of the BS wavefunction

Since any situation between no relaxation at all and full relaxation to the closed-shell determinant is possible, it is clear that the broken symmetry determinant is *not* an equal mixture of Ψ_{AF} and Ψ_F any longer. The situation has been analyzed in some detail in Ref. [479] where it is shown that Ψ_{BS} is a weighted linear combination of Ψ_F (describing a neutral configuration) and $\Psi_{Ia,b}$ (describing ionic configurations). Thus, what is achieved by the broken symmetry formalism is something that is essentially physically correct: the adjustment of ionic and neutral components to the wavefunction through the variational principle. The physically correct configuration interaction description described above does essentially the same thing: mixing of neutral Ψ_{AF} and ionic $\Psi_{Ia,b}$ in order to minimize the total energy of the system. However, the BS formalism does not have enough flexibility in its Ansatz in order to allow the neutral Ψ_{AF} to enter in the final result. Rather, it is – and incorrectly so – Ψ_F that is mixed into Ψ_{BS}. Qualitatively this is reasonable since both wavefunction describe the neutral situation. Thus, there is every reason to believe that the BS method yields a correct *charge* density (as good as that obtained from standard DFT calculations), but an incorrect *spin* density (Fig. 18). The occurrence of net spin density in certain regions of space is clearly an artefact of the method. It is however, also not entirely unphysical since these plots indicate the distribution of 'effectively unpaired' electrons [480–482] – merely they have an erroneous spin coupling in these broken-symmetry calculations.

Thus, molecular properties that only depend on the charge density of the ground state are expected to be well represented by BS-DFT calculations while properties that depend on the spin density require projection techniques. Note however, that the common practice to discard a calculation on the basis of a spin-expectation value $\langle S^2\rangle > S(S+1)$ as 'badly spin contaminated' is inappropriate in the context of BS-DFT: Rather it is *desired* and *required* that this spin expectation value is substantially higher than the correct value and this simply reflects the variational adjustment of neutral and ionic components that is necessary in order to obtain the correct result.

7.10.5. Energy of the broken-symmetry solution

In order to establish the contact between the SH operator and the broken-symmetry energy several routes have been proposed. Perhaps the most straightforward way is to assume that Ψ_F and Ψ_{BS} are both eigenfunctions of $\hat{S}_A$ and $\hat{S}_B$ and then to equate the expectation values of the effective Hamiltonian with the expectation values of the Born–Oppenheimer Hamiltonian.[26] Thus, from the two relations:

$$\begin{aligned}\langle\Psi_{BS}|H_{Spin}|\Psi_{BS}\rangle &= -J[\langle\hat{S}^2\rangle_{BS} - S_A(S_A+1) - S_B(S_B+1)] \\ &= E_{BS} = \langle\Psi_{BS}|H_{BO}|\Psi_{BS}\rangle\end{aligned} \quad (145)$$

$$\begin{aligned}\langle\Psi_F|H_{Spin}|\Psi_F\rangle &= -J\left[\langle\hat{S}^2\rangle_{HS} - S_A(S_A+1) - S_B(S_B+1)\right] \\ &= E_{HS} = \left\langle\Psi_F|H_{BO}|\Psi_F\right\rangle\end{aligned} \quad (146)$$

One obtains:

$$J = -\frac{E_{HS} - E_{BS}}{\langle\hat{S}^2\rangle_{HS} - \langle\hat{S}^2\rangle_{BS}} \quad (147)$$

Which has been advocated by Yamaguchi and co-workers [483,484]. This equation has some appealing aspects. Let us start with the plausible assumption that Ψ_{HS} is an eigenfunction of the total spin.[27] We then have $\langle\hat{S}^2\rangle_{HS} = S_{max}(S_{max}+1)$. In the cases where, in addition the BS calculation converged back to the closed shell solution we would have $\langle\hat{S}^2\rangle_{BS} = 0$ and obviously $J = -(E_{HS} - E_{BS})/\{S_{max}(S_{max}+1)\}$. This extreme case corresponds to very strong subsystem interaction (i.e. bond formation). The other extreme case is met for *no* subsystem interaction. In this case, the BS wavefunction remains at Ψ_{BS}^{guess} and the expectation value $\langle\hat{S}^2\rangle_{BS} = S_{max}$ thus implying $J = -(E_{HS} - E_{BS})/S_{max}^2$. Obviously, the predictions differ by a factor of two in the two extreme cases. Both extreme cases have been suggested in the literature. The original treatment of Noodleman [255,466–469,485–487] implies the small interaction limit while Alvarez et al. advocate the use of the strong interaction limit ([488] and references therein as well as the associated dispute in [489,490]). While for genuine antiferromagnetic coupling the weak interaction case is certainly more realistic, it may be appreciated that Eq. (147) nicely interpolates between the two limits and includes both of them as special cases.

The calculation of the spin-expectation values that enter Eq. (147) is a somewhat difficult subject since $\hat{S}^2$ is a two-electron operator. Standard practice is to evaluate it like in wavefunction theory as an expectation value over the Kohn–Sham determinant. This is, however, not correct since the expectation values should be taken over the (unknown) many-electron wavefunction of the real system. Since $\langle\hat{S}^2\rangle$ must be a functional of the density as well, expressions have been suggested that allow the calculation the expectation value from the density alone [491,492]. Practically speaking, the differences between the Kohn–Sham expectation value and the real $\langle\hat{S}^2\rangle$ values should be of limited importance for the calculation of exchange coupling constants given all the approximations that are already involved.

7.10.6. Display of broken-symmetry solutions and the corresponding orbital transformation

Given an arbitrary N-electron system and its high-spin and broken symmetry wavefunctions, the question arises of how to properly identify the SOMOs that are involved in the magnetic interaction. Frequently, these are not the highest occupied orbitals due to spin-polarization effects of the type reviewed by Noodleman and co-workers [493]. However, as apparently first discussed in Refs. [479,494] one can put the invariance of the Kohn–Sham determinant with respect to unitary transformations between the spin-up and spin-down orbitals amongst each other to good use. In fact, as shown by Amos et al. long

[26] The assumption that the two states are eigenfunctions of (however defined) local spin-operators is certainly difficult to defend at any level of rigor. For the argument made below it is sufficient if the expectation values of the local operators over Ψ_F and Ψ_{BS} are sufficiently similar. This is, however, not fully realistic. If anything the expectation values of S_A and S_B over Ψ_{BS} must be smaller than those of Ψ_F and hence this equation might be expected to somewhat overestimate the exchange coupling constant.

[27] In practice this is not the case in spin-polarized calculations. However, the deviations from a spin-eigenfunction are usually small.

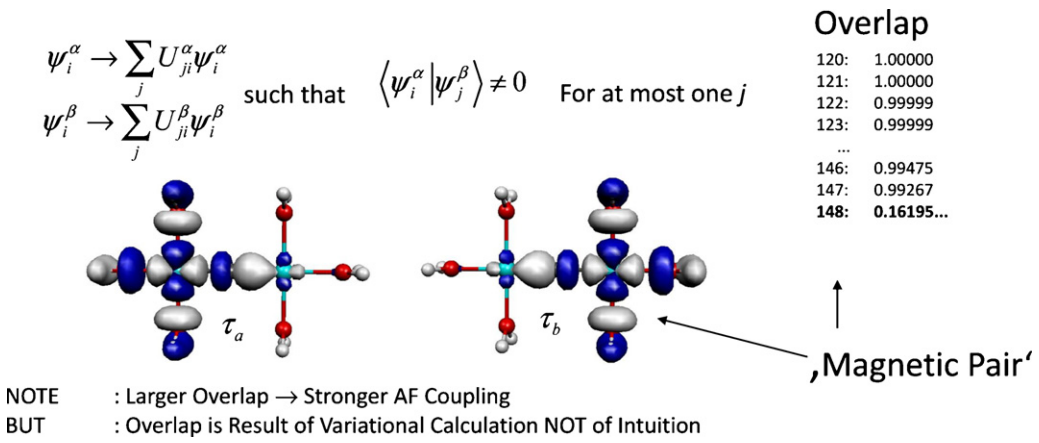

Fig. 19. Determination of the magnetic orbital pairs through the corresponding orbital transformation for the simple model system $[Cu_2(\mu\text{-}F)(H_2O)_6]^{3+}$.

ago [495,496], one can define the transformation such that for the transformed spin-unrestricted orbitals each occupied spin-up orbital has a spatial overlap unequal zero with at most one spin-down orbital. This is known as the corresponding orbital transformation (COT). Thus, the corresponding orbital transformation leads to an ordering of orbitals into three subsets: (a) essentially doubly occupied spin-up/spin-down pairs with a spatial overlap of essentially unity (typically 0.98-0.999); the slight deviations are a consequence of spin-polarization, (b) $2|S_A - S_B|$ non-orthogonal 'singlet coupled' magnetic pairs and (c) unmatched spin-up orbitals.

For the model system discussed above, the situation is shown in Fig. 19.

The non-orthogonal singlet coupled pairs are of course not properly singlet coupled but represent a $\tau_A\bar{\tau}_B$ broken symmetry pair. Thus, the COT leads to an illuminating display of the contents of the broken-symmetry solution. In particular, the spatial overlap of the two orbitals being involved in the magnetic pair is an indicator of the strength of the subsystem interaction. If it approaches zero, the interaction is in the weak limit while values close to unity indicate the strong interaction limit. In fact, using the spatial overlaps of the magnetic pairs, the spin-expectation value of the BS determinant can be conveniently calculated as:

$$\langle S^2\rangle_{BS} = \left(\frac{N^\alpha - N^\beta}{2}\right)\left(\frac{N^\alpha - N^\beta}{2} + 1\right) + N^\beta \leftrightarrows - \sum_i n_i^\alpha n_i^\beta |S_{ii}^{\alpha\beta}|^2 \tag{148}$$

N^α and N^β are the total number of spin-up and spin down electrons and n_i^σ is the occupation number of the corresponding orbital i with spin σ.

We refer to this way of looking at the BS determinant as a 'valence bond reading' of the electronic structure in a similar sense like Malrieu and co-workers have advocated it for looking at the results of CASSCF calculations [497]. The form of the BS determinant revealed by the COT is strongly reminiscent of that used in Goddard's generalized valence bond (GVB) *ab initio* method [498]. In this method and Ansatz of the same type is made but the singlet pairs are properly coupled and configuration interaction between the components of the singlet pairs is allowed [498]. However, while the GVB method is only very moderately correlated and contains essentially no dynamic correlation, the BS energy contains dynamic correlation in the effective way provided by DFT. In his early pioneering applications Noodleman even referred to his BS calculations as being obtained with the 'valence-bond Xα' method [466]. These considerations may help to rationalize the considerable success of the BS approach for 'magnetically interacting' systems.

7.10.7. Performance of DFT

The numbers obtained from BS-DFT calculations are often surprisingly good when compared to experimental measurements. For example, for the model system described above, a B3LYP BS-DFT calculation yields a J of $-215\,cm^{-1}$ based on the Yamaguchi Eq. (147) which is in (fortuitously) close agreement with the more elaborate *ab initio* result. GGA functionals typically suffer from the characteristic overdelocalization and hence tend to overestimate the exchange coupling.[28] For example, a BP86 calculation together with the Yamaguchi equation yields a J of $-517\,cm^{-1}$ which is about a factor of two too large. This result is typical and explains why some workers prefer to invoke the strong interaction limit in their BS-DFT calculations. The physical justification of this error compensation appears to be open to debate.

7.10.8. Comparison with experiment

In closing this section it should be pointed out the comparison of measured and calculated numbers if often not unambiguous. One point of concern is, that the measurement of exchange couplings usually proceeds via thermal depopulation experiments. This means that the system is always in thermal equilibrium and consequently, the measurement is an adiabatic one. Thus, each spin state has relaxed to its own equilibrium geometry during the measurement. This does, however, destroy the regularity of the spin ladder assumed by the Heisenberg Hamiltonian. Most calculations, on the other hand, are performed only at a single geometry which most often is the high spin geometry. In many if not most cases, the energy lowering due to structure relaxation is only on the order of a few or a few dozen wavenumbers. However, the exchange couplings that one tries to predict are also on this order of magnitude and hence some ambiguity arises as to what the best approach is. If the structure is taken from the high-spin calculation, an artificial bias for this state is created and the antiferromagnetism will be overestimated by the calculations. If the structure is relaxed tight convergence criteria have to be used and if the relaxation effects are large the underlying picture of a Heisenberg type situation is lost.

[28] Some workers have reported that the PW91 functional provides better predictions for exchange coupling constants than BP86 [6,393] but the reasons for this behavior are not clear.

7.10.9. Alternative approaches to antiferromagnetic coupling

There has been a multitude of alternative DFT approaches to the evaluation of exchange couplings. Here we only note the promising application of the "spin-flip TD-DFT" concept [253,499–501] as well as a 'constrained DFT' approach [502] both of which appear to provide predictions of similar quality as the BS approach.

7.10.10. More complicated situations

A lucid analysis of more complicated magnetic coupling situations like mixed valence systems with more than one-unpaired electron on each site has recently been provided by Guihery and co-workers. In particular, the crucial role of 'non-Hund' states (local low-spin states) for inducing non-Heisenberg behavior has been analyzed in detail [503–506].

8. Concluding remarks

In this chapter, a relatively comprehensive account has been given of the calculation of molecular spectra on the basis of DFT at the present state of the art. Starting from a brief exposition of the foundations of DFT, the main density functionals in present use have been described. The subject of time-dependent and time-independent linear response theory has been treated in some detail followed by a brief discussion of the computational realization of DFT. These foundations have then been used in order to formulate the linear response theory for a wide variety of spectroscopic techniques that can now all be tackled with DFT methods. The exposition of each individual technique was necessarily brief but it is hoped that the connection to the general theory has become evident. Furthermore, a – certainly partially subjective – discussion of the strengths and weaknesses of DFT for each of the techniques covered in this chapter has also been provided together with selected examples that illustrate the type of agreement or problem that one is likely to encounter in practical applications.

It may be considered pleasing that a common framework – namely DFT in conjunction with analytic derivative/linear response theory – accounts for so many molecular properties. The success of DFT in predicting these properties is also significant. Property calculations of the type indicated here already prove to be enormously useful in many application studies and in conjunction with experimental investigations. In favorable cases, the calculated properties are accurate enough to reliably distinguish structural alternatives for reaction intermediates or other species that are not amenable to experimental structure elucidation. However, in many cases, remaining problems have also been evident and it would be highly desirable to arrive at predictions that are significantly more accurate than the ones that are presently within reach. How to modify DFT in order to achieve this goal is presently not clear since progress towards systematically more accurate functionals than the now well established standard GGA or hybrid functionals has been slow in the past 10–15 years.

Thus, there is renewed interest in wavefunction based methods which are believed to converge systematically towards the correct answer. However, in particular when it comes to open-shell transition metals, these methods have a long way to come before they can be reliably applied to 'real life' problems. First of all, their computational cost is intrinsically still very high. Secondly, they need to be applied in conjunction with very large and flexible basis sets and third, the HF wavefunction is very often a very poor starting point such that very extensive correlation treatments will be necessary. It will be interesting to see whether the development of such methods can be pushed far enough such that they become standard research tools in (bio)inorganic chemistry.

In the context of DFT there are many subjects that warrant much further development. Such challenges include the role, implications and removal of the self-interaction error, functionals that are consistent with exact exchange, that cover medium range electron–electron correlation, weak interactions and that show the correct long range behavior, the treatment of multiplet effects, electronic relaxation and excited states, the treatment of system dynamics, very large systems and the proper treatment of magnetic and relativistic effects as well as their interplay—to name only a few areas where currently much effort is concentrated.

Taken together, the tremendous international efforts in the development and application of new theoretical methods are expected to greatly enhance the impact of theoretical chemistry on the further development of chemistry. Thus, there appears to be every reason to look forward to the future marriage of theory and experiment in (bio)inorganic- and coordination chemistry.

Acknowledgements

I am deeply indebted to the many collaborators who have shared their knowledge, enthusiasm and expertise in chemistry, spectroscopy and theory with me over the years in exciting and fruitful collaborations. This work would not have been possible without the hard work of the students and post docs who are listed in the original citations and to whom I am particularly grateful. Finally, I also gratefully acknowledge the generous financial support by the University of Bonn, the German Science Foundation (SFB 624, SFB 663, SPP 1137) as well as from the Max-Planck Gesellschaft and the German Israeli Foundation.

References

[1] P.E.M. Siegbahn, T. Borowski, Acc. Chem. Res. 39 (2006) 729.
[2] P.E.M. Siegbahn, J. Biol. Inorg. Chem. 11 (2006) 695.
[3] M.R.A. Blomberg, P.E.M. Siegbahn, J. Comput. Chem. 27 (2006) 1373.
[4] A. Bassan, M.R.A. Blomberg, T. Borowski, P.E.M. Siegbahn, J. Inorg. Biochem. 100 (2006) 727.
[5] P.E.M. Siegbahn, M.R.A. Blomberg, Phil. Trans. R. Soc. 363 (2005) 847.
[6] L. Noodleman, W.G. Han, J. Biol. Inorg. Chem. 11 (2006) 674.
[7] L. Noodleman, T. Lovell, W.G. Han, J. Li, F. Himo, Chem. Rev. 104 (2004) 459.
[8] T. Lovell, F. Himo, W.G. Han, L. Noodleman, Coord. Chem. Rev. 238 (2003) 211.
[9] S. Shaik, D. Kumar, S.P. de Visser, A. Altun, W. Thiel, Chem. Rev. 105 (2005) 2279.
[10] D. Schröder, S. Shaik, H. Schwarz, Acc. Chem. Res. 33 (2000) 139.
[11] F. Neese, in: G. Hanson (Ed.), Biol. Magn. Reson. (2008).
[12] S. Sinnecker, F. Neese, in: M. Reiher (Ed.), Atomistic Approaches in Modern Biology from Quantum Chemistry to Molecular Simulations, 2007, p. 47.
[13] B. Kirchner, F. Wennmohs, S.F. Ye, F. Neese, Curr. Opin. Chem. Biol. 11 (2007) 134.
[14] F. Neese, J. Biol. Inorg. Chem. 11 (2006) 702.
[15] F. Neese, in: M. Kaupp, M. Bühl, V. Malkin (Eds.), The Quantum Chemical Calculation of NMR and EPR Properties, Wiley–VCH, Heidelberg, 2004, p. 581.
[16] F. Neese, Curr. Opin. Chem. Biol. 7 (2003) 125.
[17] E.I. Solomon, A.B.P. Lever (Eds.), Inorganic Electronic Structure and Spectroscopy, John Wiley & Sons, New York, 1999.
[18] L. Que Jr. (Ed.), Physical Methods in Bioinorganic Chemistry, Spectroscopy and Magnetism, University Science Books, Sausalito, CA, USA, 2000.
[19] A. Szabo, N.S. Ostlund, Modern Theoretical Chemistry, MacMillan Pub. Inc., New York, 1982.
[20] R. McWeeny, Methods of Molecular Quantum Mechanics, Academic Press, London, 1992.
[21] P. Dahle, T. Helgaker, D. Jonsson, P.R. Taylor, Phys. Chem. Chem. Phys. 9 (2007) 3112.
[22] M. Heckert, M. Kallay, D.P. Tew, W. Klopper, J. Gauss, J. Chem. Phys. 125 (2006).
[23] Y.J. Bomble, J. Vazquez, M. Kallay, C. Michauk, P.G. Szalay, A.G. Csaszar, J. Gauss, J.F. Stanton, J. Chem. Phys. 125 (2006).
[24] J.M.L. Martin, J. Mol. Struct. Theochem 771 (2006) 19.
[25] A. Karton, E. Rabinovich, J.M.L. Martin, B. Ruscic, J. Chem. Phys. 125 (2006).
[26] H. Nakatsuji, J. Chem. Phys. 113 (2000) 2949.
[27] T.D. Crawford, H.F. Schaefer, Rev. Comput. Chem. 14 (2000) 33.
[28] R.J. Bartlett, Rev. Mod. Phys. 79 (2007) 291.
[29] H.-J. Werner, in: K.P. Lawley (Ed.), Ab Initio Methods in Quantum Chemistry, vol. 2, Wiley, New York, Adv. Chem. Phys. LXIX (1987).
[30] C.D. Sherill, H.F. Schaefer III, Adv. Quant. Chem. 34 (1999) 143.

[31] K. Andersson, P.A. Malmqvist, B.O. Roos, A.J. Sadlej, K. Wolinski, J. Phys. Chem. 94 (1990) 5483.
[32] K. Andersson, P.A. Malmqvist, B.O. Roos, J. Chem. Phys. 96 (1992) 1218.
[33] U.S. Mahapatra, B. Datta, D. Mukherjee, J. Chem. Phys. 110 (1999) 6171.
[34] S. Pal, M. Rittby, R.J. Bartlett, D. Sinha, D. Mukherjee, J. Chem. Phys. 88 (1988) 4357.
[35] S. Pal, M. Rittby, R.J. Bartlett, D. Sinha, D. Mukherjee, Chem. Phys. Lett. 137 (1987) 273.
[36] L.A. Eriksson, L.G.M. Pettersson, P.E.M. Siegbahn, U. Wahlgren, J. Chem. Phys. 102 (1995) 872.
[37] P.E.M. Siegbahn, Adv. Chem. Phys. Xciii (1996) 333.
[38] F. Neese, T. Petrenko, D. Ganyushin, G. Olbrich, Coord. Chem. Rev. 251 (2007) 288.
[39] W. Kohn, Rev. Mod. Phys. 71 (1999) 1253.
[40] P. Hohenberg, W. Kohn, Phys. Rev. B 136 (1964) 864.
[41] P.A.M. Dirac, Proc. Cambridge Phil. Soc. 26 (1930) 376.
[42] W. Kutzelnigg, J. Mol. Struct. Theochem 768 (2006) 163.
[43] W. Koch, M.C. Holthausen, A Chemist's Guide to Density Functional Theory, Wiley–VCH, Weinheim, 2000.
[44] R.G. Parr, W. Yang, Density Functional Theory of Atoms and Molecules, Oxford University Press, Oxford, 1989.
[45] W. Kohn, L.J. Sham, Phys. Rev. A 140 (1965) 1133.
[46] R. McWeeny, Y. Mizuno, Proc. R. Soc. (Lond.) A 259 (1961) 554.
[47] E.R. Davidson, Reduced Density Matrices in Quantum Chemistry, Academic Press, New York, 1976.
[48] S. Kummel, J.P. Perdew, Phys. Rev. B 68 (2003).
[49] F. Della Sala, A. Gorling, J. Chem. Phys. 115 (2001) 5718.
[50] R.J. Bartlett, V.F. Lotrich, I.V. Schweigert, J. Chem. Phys. 123 (2005).
[51] R.J. Bartlett, I. Grabowski, S. Hirata, S. Ivanov, J. Chem. Phys. 122 (2005).
[52] S. Ivanov, S. Hirata, I. Grabowski, R.J. Bartlett, J. Chem. Phys. 118 (2003) 461.
[53] S. Hirata, S. Ivanov, I. Grabowski, R.J. Bartlett, J. Chem. Phys. 116 (2002) 6468.
[54] I. Grabowski, S. Hirata, S. Ivanov, R.J. Bartlett, J. Chem. Phys. 116 (2002) 4415.
[55] S. Ivanov, R.J. Bartlett, J. Chem. Phys. 114 (2001) 1952.
[56] Q.S. Zhao, R.C. Morrison, R.G. Parr, Phys. Rev. A 50 (1994) 2138.
[57] J.B. Lucks, A.J. Cohen, N.C. Handy, Phys. Chem. Chem. Phys. 4 (2002) 4612.
[58] D.J. Tozer, V.E. Ingamells, N.C. Handy, J. Chem. Phys. 105 (1996) 9200.
[59] G.K.L. Chan, D.J. Tozer, N.C. Handy, J. Chem. Phys. 107 (1997) 1536.
[60] D.J. Tozer, N.C. Handy, W.H. Green, Chem. Phys. Lett. 273 (1997) 183.
[61] D.J. Tozer, K. Somasundram, N.C. Handy, Chem. Phys. Lett. 265 (1997) 614.
[62] W.H. Green, D.J. Tozer, N.C. Handy, Chem. Phys. Lett. 290 (1998) 465.
[63] F.A. Hamprecht, A.J. Cohen, D.J. Tozer, N.C. Handy, J. Chem. Phys. 109 (1998) 6264.
[64] N.C. Handy, D.J. Tozer, Mol. Phys. 94 (1998) 707.
[65] D.J. Tozer, N.C. Handy, J. Phys. Chem. A 102 (1998) 3162.
[66] D.J. Tozer, N.C. Handy, J. Chem. Phys. 108 (1998) 2545.
[67] J.P. Perdew, A. Zunger, Phys. Rev. B 23 (1981).
[68] S. Kummel, J.P. Perdew, Mol. Phys. 101 (2003) 1363.
[69] A. Ruzsinszky, J.P. Perdew, G.I. Csonka, O.A. Vydrov, G.E. Scuseria, J. Chem. Phys. 126 (2007).
[70] G.I. Csonka, O.A. Vydrov, G.E. Scuseria, A. Ruzsinszky, J.P. Perdew, J. Chem. Phys. 126 (2007).
[71] M. Lundberg, P.E.M. Siegbahn, J. Chem. Phys. 122 (2005).
[72] J. Grafenstein, E. Kraka, D. Cremer, J. Chem. Phys. 120 (2004) 524.
[73] J. Grafenstein, E. Kraka, D. Cremer, Phys. Chem. Chem. Phys. 6 (2004) 1096.
[74] V. Polo, J. Grafenstein, E. Kraka, D. Cremer, Chem. Phys. Lett. 352 (2002) 469.
[75] J. Grafenstein, D. Cremer, Mol. Phys. 103 (2005) 279.
[76] V. Polo, J. Grafenstein, E. Kraka, D. Cremer, Theor. Chem. Acc. 109 (2003) 22.
[77] J.C. Slater, Phys. Rev. B 81 (1951) 385.
[78] O. Gunnarson, B.I. Lundqvist, Phys. Rev. B 13 (1976) 4274.
[79] J.P. Perdew, Y. Wang, Phys. Rev. B 45 (1992) 13244.
[80] Y. Wang, J.P. Perdew, Phys. Rev. B 43 (1991) 8911.
[81] Y. Wang, J.P. Perdew, Phys. Rev. B 44 (1991) 13298.
[82] Y. Wang, J.P. Perdew, J.A. Chevary, L.D. Macdonald, S.H. Vosko, Phys. Rev. A 41 (1990) 78.
[83] S.H. Vosko, L. Wilk, M. Nusair, Can. J. Phys. 58 (1980).
[84] A.D. Becke, Phys. Rev. A 38 (1988) 3098.
[85] C. Lee, W. Yang, R.G. Parr, Phys. Rev. B 37 (1988) 785.
[86] R. Colle, O. Salvetti, Theor. Chim. Acta 37 (1975) 329.
[87] C. Adamo, A. di Matteo, V. Barone, Adv. Quant. Chem. 36 (2000) 45.
[88] H.L. Schmider, A.D. Becke, J. Chem. Phys. 108 (1998) 9624.
[89] H.L. Schmider, A.D. Becke, J. Chem. Phys. 109 (1998) 8188.
[90] A.D. Becke, J. Chem. Phys. 107 (1997) 8554.
[91] J.A. Altmann, N.C. Handy, Phys. Chem. Chem. Phys. 1 (1999) 5529.
[92] J.P. Perdew, A. Ruzsinszky, J.M. Tao, V.N. Staroverov, G.E. Scuseria, G.I. Csonka, J. Chem. Phys. 123 (2005).
[93] V.N. Staroverov, G.E. Scuseria, J.M. Tao, J.P. Perdew, J. Chem. Phys. 121 (2004) 11507.
[94] V.N. Staroverov, G.E. Scuseria, J. Tao, J.P. Perdew, Phys. Rev. B 69 (2004).
[95] J.P. Perdew, J.M. Tao, V.N. Staroverov, G.E. Scuseria, J. Chem. Phys. 120 (2004) 6898.
[96] J.M. Tao, J.P. Perdew, V.N. Staroverov, G.E. Scuseria, Phys. Rev. Lett. 91 (2003).
[97] F. Furche, J.P. Perdew, J. Chem. Phys. 124 (2006).
[98] A.D. Becke, J. Chem. Phys. 98 (1993) 1372.
[99] A.D. Becke, J. Chem. Phys. 98 (1993) 5648.
[100] P.J. Stephens, F.J. Devlin, C.F. Chabalowski, M.J. Frisch, J. Phys. Chem. 98 (1994) 11623.
[101] S. Grimme, J. Chem. Phys. 109 (2003) 3067.
[102] C. Adamo, V. Barone, J. Chem. Phys. 110 (1999) 6158.
[103] C. Adamo, V. Barone, Chem. Phys. Lett. 298 (1998) 113.
[104] S. Grimme, Angew. Chem. Int. Ed. 45 (2006) 4460.
[105] S. Grimme, J. Chem. Phys. 124 (2006) 34108.
[106] T. Schwabe, S. Grimme, Phys. Chem. Chem. Phys. 8 (2006) 4398.
[107] S. Grimme, J. Antony, T. Schwabe, C. Muck-Lichtenfeld, Org. Biomol. Chem. 5 (2007) 741.
[108] F. Neese, T. Schwabe, S. Grimme, J. Chem. Phys. 126 (2007) 124115.
[109] S. Grimme, F. Neese, J. Chem. Phys. 127 (2007) 154116.
[110] T. Schwabe, S. Grimme, Phys. Chem. Chem. Phys. 38 (2006) 4398.
[111] S. Grimme, C. Mück-Lichtenfeld, E.-U. Würthwein, A.W. Ehler, T.P.M. Goumans, K. Lammertsma, J. Phys. Chem. A 110 (2006) 2583.
[112] S. Grimme, J. Comput. Chem. 27 (2006) 1787.
[113] J. Antony, S. Grimme, Phys. Chem. Chem. Phys. 8 (2006) 5287.
[114] M. Piacenza, S. Grimme, ChemPhysChem 6 (2005) 1554.
[115] E. Clementi, J. Chem. Phys. 38 (1963) 2248.
[116] B.A. Hess, C.M. Marian, in: P. Jensen, P.R. Bunker (Eds.), Computational Molecular Spectroscopy, John Wiley & sons, New York, 2000, p. 169ff.
[117] R.M. Dickson, A.D. Becke, J. Chem. Phys. 99 (1993) 3898.
[118] A.D. Becke, R.M. Dickson, J. Chem. Phys. 92 (1990) 3610.
[119] A.D. Becke, R.M. Dickson, J. Chem. Phys. 89 (1988) 2993.
[120] F. Jensen, Introduction to Computational Chemistry, Wiley, New York, 1999.
[121] F. Weigend, R. Ahlrichs, Phys. Chem. Chem. Phys. 7 (2005) 3297.
[122] C.W. Murray, N.C. Handy, G.J. Laming, Mol. Phys. 78 (1993) 997.
[123] A.D. Becke, J. Chem. Phys. 88 (1988) 2547.
[124] O. Treutler, R. Ahlrichs, J. Chem. Phys. 102 (1995) 346.
[125] R.E. Stratmann, G.E. Scuseria, M.J. Frisch, Chem. Phys. Lett. 257 (1996) 213.
[126] J. Almlöf, K. Faegri, K. Korsell, J. Comput. Chem. 3 (1982) 385.
[127] M. Häser, R. Ahlrichs, J. Comput. Chem. 10 (1989) 104.
[128] M.C. Strain, G.E. Scuseria, M.J. Frisch, Science 271 (1996) 51.
[129] C.A. White, B.G. Johnson, P.M.W. Gill, M. HeadGordon, Chem. Phys. Lett. 253 (1996) 268.
[130] G.E. Scuseria, J. Phys. Chem. A 103 (1999) 4782.
[131] A. Sodt, J.E. Subotnik, M. Head-Gordon, J. Chem. Phys. 125 (2006).
[132] R.B. Murphy, Y. Cao, M.D. Beachy, M.N. Ringnalda, R.A. Friesner, J. Chem. Phys. 112 (2000) 10131.
[133] E.J. Baerends, D.E. Ellis, P. Ros, Chem. Phys. 2 (1973) 41.
[134] J.W. Mintmire, B.I. Dunlap, Phys. Rev. A 25 (1982) 88.
[135] B.I. Dunlap, J.W.D. Connolly, J.R. Sabin, J. Chem. Phys. 71 (1979) 3396.
[136] O. Vahtras, J. Almlöf, M.W. Feyereisen, Chem. Phys. Lett. 213 (1993) 514.
[137] K. Eichkorn, O. Treutler, H. Öhm, M. Häser, R. Ahlrichs, Chem. Phys. Lett. 240 (1995) 283.
[138] K. Eichkorn, F. Weigend, O. Treutler, R. Ahlrichs, Theor. Chem. Acc. 97 (1997) 119.
[139] B.I. Dunlap, Phys. Chem. Chem. Phys. 2 (2000) 2113.
[140] B.I. Dunlap, J. Mol. Struct. Theochem 529 (2000) 37.
[141] K. Eichkorn, O. Treutler, H. Ohm, M. Häser, R. Ahlrichs, Chem. Phys. Lett. 242 (1995) 652.
[142] M. Sierka, A. Hogekamp, R. Ahlrichs, J. Chem. Phys. 118 (2003) 9136.
[143] F. Neese, J. Comput. Chem. 24 (2003) 1740.
[144] R.A. Friesner, Chem. Phys. Lett. 116 (1985) 39.
[145] R.A. Friesner, J. Chem. Phys. 85 (1986) 1462.
[146] R.A. Friesner, J. Chem. Phys. 86 (1986) 3522.
[147] R.A. Friesner, R.B. Murphy, M.D. Beachy, M.N. Ringnalda, W.T. Pollard, B.D. Dunietz, Y. Cao, J. Phys. Chem. A 103 (1999) 1913.
[148] J.C. Burant, G.E. Scuseria, M.J. Frisch, J. Chem. Phys. 105 (1996) 8969.
[149] W. Kohn, Int. J. Quant. Chem. 56 (1995) 229.
[150] J.M. Millam, G.E. Scuseria, J. Chem. Phys. 106 (1997) 5569.
[151] E. Schwegler, M. Challacombe, M. HeadGordon, J. Chem. Phys. 106 (1997) 9708.
[152] N. Rega, M. Cossi, V. Barone, Chem. Phys. Lett. 293 (1998) 221.
[153] K. Nemeth, G.E. Scuseria, J. Chem. Phys. 113 (2000) 6035.
[154] M.A. Watson, P. Salek, P. Macak, T. Helgaker, J. Chem. Phys. 121 (2004) 2915.
[155] A.F. Izmaylov, E.N. Brothers, G.E. Scuseria, J. Chem. Phys. 125 (2006).
[156] B. Jansik, S. Host, P. Jorgensen, J. Olsen, T. Helgaker, J. Chem. Phys. 126 (2007).
[157] P. Salek, S. Host, L. Thogersen, P. Jorgensen, P. Manninen, J. Olsen, B. Jansik, S. Reine, F. Pawlowski, E. Tellgren, T. Helgaker, S. Coriani, J. Chem. Phys. 126 (2007).
[158] J.A. Pople, P.M.W. Gill, B.G. Johnson, Chem. Phys. Lett. 199 (1992) 557.
[159] B.G. Johnson, M.J. Frisch, Chem. Phys. Lett. 216 (1993) 133.
[160] A.M. Lee, S.M. Colwell, N.C. Handy, Chem. Phys. Lett. 229 (1994) 225.
[161] J.M. Tao, J.P. Perdew, Phys. Rev. Lett. 95 (2005).
[162] G. Vignale, W. Kohn, Phys. Rev. Lett. 77 (1996) 2037.
[163] J. Juselius, D. Sundholm, J. Gauss, J. Chem. Phys. 121 (2004) 3952.
[164] S. Rohra, A. Gorling, Phys. Rev. Lett. 97 (2006).
[165] A.M. Lee, N.C. Handy, Phys. Rev. A 59 (1999) 209.
[166] A.D. Becke, Can. J. Chem. 74 (1996) 995.
[167] J.A. Pople, R. Krishnan, H.B. Schlegel, J.S. Binkley, Int. J. Quant. Chem., Quant. Chem. Symp. 13 (1979) 225.
[168] G.H.F. Diercksen, R. McWeeny, J. Chem. Phys. 44 (1966) 3554.
[169] C. Ochsenfeld, M. HeadGordon, Chem. Phys. Lett. 270 (1997) 399.
[170] E. Runge, E.K.U. Gross, Phys. Rev. Lett. 52 (1984) 997.
[171] J. Schirmer, A. Dreuw, Phys. Rev. A 75 (2007).

[172] A. Dreuw, M. Head-Gordon, Chem. Rev. 105 (2005) 4009.
[173] J. Olsen, H. Jorgen, A. Jensen, P. Jorgensen, J. Comp. Phys. 74 (1988) 265.
[174] J.B. Foresman, M. Head-Gordon, J.A. Pople, M.J. Frisch, J. Phys. Chem. 96 (1992) 135.
[175] S. Hirata, M. Head-Gordon, Chem. Phys. Lett. 314 (1999) 291.
[176] J. Autschbach, M. Seth, T. Ziegler, J. Chem. Phys. 126 (2007).
[177] M. Casarin, P. Finetti, A. Vittadini, F. Wang, T. Ziegler, J. Phys. Chem. A 111 (2007) 5270.
[178] F. Wang, T. Ziegler, Int. J. Quant. Chem. 106 (2006) 2545.
[179] M. Seth, T. Ziegler, J. Chem. Phys. 124 (2006).
[180] J.G. Guan, F. Wang, T. Ziegler, H. Cox, J. Chem. Phys. 125 (2006).
[181] F. Wang, T. Ziegler, E. van Lenthe, S. van Gisbergen, E.J. Baerends, J. Chem. Phys. 122 (2005).
[182] F. Wang, T. Ziegler, J. Chem. Phys. 122 (2005).
[183] F. Wang, T. Ziegler, J. Chem. Phys. 123 (2005).
[184] M. Krykunov, A. Banerjee, T. Ziegler, J. Autschbach, J. Chem. Phys. 122 (2005).
[185] F.E. Jorge, J. Autschbach, T. Ziegler, J. Am. Chem. Soc. 127 (2005) 975.
[186] G. Fronzoni, M. Stener, P. Decleva, F. Wang, T. Ziegler, E. van Lenthe, E.J. Baerends, Chem. Phys. Lett. 416 (2005) 56.
[187] A. Banerjee, J. Autschbach, T. Ziegler, Int. J. Quant. Chem. 101 (2005) 572.
[188] F. Wang, T. Ziegler, J. Chem. Phys. 121 (2004) 12191.
[189] M. Seth, T. Ziegler, A. Banerjee, J. Autschbach, S.J.A. van Gisbergen, E.J. Baerends, J. Chem. Phys. 120 (2004) 10942.
[190] J. Autschbach, T. Ziegler, S.J.A. van Gisbergen, E.J. Baerends, J. Chem. Phys. 116 (2002) 6930.
[191] J. Autschbach, T. Ziegler, J. Chem. Phys. 116 (2002) 891.
[192] J. Autschbach, S. Patchkovskii, T. Ziegler, S.J.A. van Gisbergen, E.J. Baerends, J. Chem. Phys. 117 (2002) 581.
[193] O. Vahtras, Z. Rinkevicius, J. Chem. Phys. 126 (2007).
[194] L. Benisvy, R. Bittl, E. Bothe, C.D. Garner, J. McMaster, S. Ross, C. Teutloff, F. Neese, Angew. Chem.-Int. Ed. 44 (2005) 5314.
[195] O. Farkas, H.B. Schlegel, J. Mol. Struct. Theochem 666 (2003) 31.
[196] C.Y. Peng, P.Y. Ayala, H.B. Schlegel, M.J. Frisch, J. Comput. Chem. 17 (1996) 49.
[197] M. Bühl, H. Kabrede, J. Chem. Theory Comput. 2 (2006) 1282.
[198] M. Bühl, C. Reimann, D.A. Pantazis, T. Bredow, F. Neese, J. Chem. Theor. Comput., submitted for publication.
[199] D.A. Pantazis, X.-Y. Chen, C.R. Landis, F. Neese, J. Chem. Theor. Comput. 4 (2008), ASAP.
[200] A. Klamt, G. Schüürmann, Perkin Trans. (1993) 799.
[201] M. Cossi, V. Barone, R. Cammi, J. Tomasi, Chem. Phys. Lett. 255 (1996) 327.
[202] D. Andrae, U. Häussermannm, M. Dolg, H. Stoll, H. Preuss, Theor. Chim. Acta 77 (1990) 123.
[203] M. Dolg, Theor. Chim. Acta 93 (1996) 141.
[204] M. Dolg, H. Preuss, in: K.A. Gschneider, L. Eyring (Eds.), Handbook of Physics and Chemistry of Rare Earths, vol. 22, Elsevier, Amsterdam, 1995.
[205] M. Dolg, H. Stoll, H. Preuss, J. Chem. Phys. 90 (1989) 1730.
[206] W. Kuechle, M. Dolg, H. Stoll, H. Preuss, Mol. Phys. 74 (1991) 1245.
[207] P.J. Hay, W.R. Wadt, J. Chem. Phys. 82 (1985) 270.
[208] W.R. Wadt, P.J. Hay, J. Chem. Phys. 82 (1985) 284.
[209] P.J. Hay, W.R. Wadt, J. Chem. Phys. 82 (1985) 299.
[210] C.W. Murray, G.J. Laming, N.C. Handy, R.D. Amos, Chem. Phys. Lett. 199 (1992) 551.
[211] C. Sosa, J. Andzelm, B.C. Elkin, E. Wimmer, K.D. Dobbs, D.A. Dixon, J. Phys. Chem. 96 (1992) 6630.
[212] R.E. Stratmann, J.C. Burant, G.E. Scuseria, M.J. Frisch, J. Chem. Phys. 106 (1997) 10175.
[213] J. Neugebauer, B.A. Hess, J. Chem. Phys 118 (2003) 7215.
[214] T.G. Spiro, R. Czernuszewicz, in: E.i. Solomon, A.B.P. Lever (Eds.), Inorganic Electronic Structure and Spectroscopy, Wiley, New York, 1999, p. 392.
[215] S.J.A. vanGisbergen, J.G. Snijders, E.J. Baerends, Chem. Phys. Lett. 259 (1996) 599.
[216] A.G. Ioannou, R.D. Amos, Chem. Phys. Lett. 279 (1997) 17.
[217] C. Van Caillie, R.D. Amos, Phys. Chem. Chem. Phys. 2 (2000) 2123.
[218] M. Reiher, G. Brehm, S. Schneider, J. Phys. Chem. A 108 (2004) 734.
[219] M. Reiher, V. Liegeois, K. Ruud, J. Phys. Chem. A 109 (2005) 7567.
[220] C. Van Caillie, R.D. Amos, Chem. Phys. Lett. 291 (1998) 71.
[221] F. Furche, R. Ahlrichs, J. Chem. Phys. 117 (2002) 7433.
[222] F. Furche, J. Chem. Phys. 114 (2001) 5982.
[223] F. Furche, R. Ahlrichs, C. Wachsmann, E. Weber, A. Sobanski, R. Vögtle, S. Grimme, J. Am. Chem. Soc. 122 (2000) 1717.
[224] B. Le Guennic, W. Hieringer, A. Gorling, J. Autschbach, J. Phys. Chem. A 109 (2005) 4836.
[225] J. Neugebauer, E.J. Baerends, M. Nooijen, J. Autschbach, J. Chem. Phys. 122 (2005).
[226] M. Seth, T. Ziegler, J. Autschbach, J. Chem. Phys. 122 (2005).
[227] F. Neese, E.I. Solomon, Inorg. Chem. 38 (1999) 1847.
[228] D. Ganyushin, F. Neese, J. Chem. Phys. 128 (2008) 114117.
[229] J.A. Farrar, F. Neese, P. Lappalainen, P.M.H. Kroneck, M. Saraste, W.G. Zumft, A.J. Thomson, J. Am. Chem. Soc. 118 (1996) 11501.
[230] F. Neese, Electronic Structure and Spectroscopy of Novel Copper Chromophores in Biology, Universit y of Konstanz, Konstanz, 1997.
[231] M.E. Casida, in: D.P. Chong (Ed.), Recent Advances in Density Functional Methods, World Scientific, Singapore, 1995, p. 155.
[232] R. Bauernschmitt, R. Ahlrichs, Chem. Phys. Lett. 256 (1996) 454.
[233] R. Bauernschmitt, M. Haser, O. Treutler, R. Ahlrichs, Chem. Phys. Lett. 264 (1997) 573.
[234] R.E. Stratmann, G.E. Scuseria, J. Chem. Phys. 109 (1998) 8218.
[235] S.J.A. van Gisbergen, J.A. Groeneveld, A. Rosa, J.G. Snijders, E.J. Baerends, J. Phys. Chem. A 103 (1999) 6835.
[236] F. Neese, G. Olbrich, Chem. Phys. Lett. 362 (2002) 170.
[237] T.A. Stich, J. Seravalli, S. Venkateshrao, T.G. Spiro, S.W. Ragsdale, T.C. Brunold, J. Am. Chem. Soc. 128 (2006) 5010.
[238] T.A. Stich, M. Yamanishi, R. Banerjee, T.C. Brunold, J. Am. Chem. Soc. 127 (2005) 7660.
[239] T.A. Stich, N.R. Buan, J.C. Escalante-Semerena, T.C. Brunold, J. Am. Chem. Soc. 127 (2005) 8710.
[240] R. Schenker, M.T. Mock, M.T. Kieber-Emmons, C.G. Riordan, T.C. Brunold, Inorg. Chem. 44 (2005) 3605.
[241] A.T. Fiedler, P.A. Bryngelson, M.J. Maroney, T.C. Brunold, J. Am. Chem. Soc. 127 (2005) 5449.
[242] A. Fiedler, T.C. Brunold, Inorg. Chem. 44 (2005) 9322.
[243] K. Ray, T. Petrenko, K. Wieghardt, F. Neese, Dalton Trans. (2007) 1552.
[244] N. Lehnert, U. Cornelissen, F. Neese, T. Ono, Y. Noguchi, K. Okamoto, K. Fujisawa, Inorg. Chem. 46 (2007) 3916.
[245] C. Duboc, T. Phoeung, S. Zein, J. Pecaut, M.N. Collomb, F. Neese, Inorg. Chem. 46 (2007) 4905.
[246] A.K. Patra, E. Bill, E. Bothe, K. Chlopek, F. Neese, T. Weyhermüller, K. Stobie, M.D. Ward, J.A. McCleverty, K. Wieghardt, Inorg. Chem. 45 (2006) 7877.
[247] K. Ray, T. Weyhermüller, F. Neese, K. Wieghardt, Inorg. Chem. 44 (2005) 5345.
[248] L. Petit, P. Maldivi, C. Adamo, J. Chem. Theor. Comput. 1 (2005) 953.
[249] J. Mack, Y.K. Asano, N.M.J. Stillman, J. Am. Chem. Soc. 127 (2005) 17697.
[250] R. Bauernschmitt, M. Häser, O. Treutler, R. Ahlrichs, Chem. Phys. Lett. 264 (1997) 573.
[251] F. Furche, R. Ahlrichs, J. Chem. Phys. 121 (2004) 12772.
[252] C. Ko, D.K. Malick, D.A. Bradon, R.A. Friesner, T.J. Martinez, J. Chem. Phys. 128 (2008) 104103.
[253] T. Ziegler, F. Wang, J. Chem. Phys. 121 (2004) 12191.
[254] W.G. Han, T.Q. Liu, T. Lovell, L. Noodleman, Inorg. Chem. 45 (2006) 8533.
[255] L. Noodleman, E.J. Baerends, J. Am. Chem. Soc. 106 (1984) 2316.
[256] D.M. Adams, L. Noodleman, D.N. Hendrickson, Inorg. Chem. 36 (1997) 3966.
[257] K.W. Penfield, A.A. Gewirth, E.I. Solomon, J. Am. Chem. Soc. 107 (1985) 4519.
[258] C.A. Grapperhaus, E. Bill, T. Weyhermüller, F. Neese, K. Wieghardt, Inorg. Chem. 40 (2001) 4191.
[259] K. Meyer, J. Bendix, N. Metzler-Nolte, T. Weyhermüller, K. Wieghardt, J. Am. Chem. Soc. 120 (1998) 7260.
[260] A.B.P. Lever, Inorganic Electronic Spectroscopy, Elsevier, Amsterdam, 1968.
[261] A.C. Albrecht, J. Chem. Chem. 34 (1961) 1476.
[262] J. Tang, A.C. Albrecht, in: H.A. Szymanski (Ed.), Raman Spectroscopy, Theory and Practice, vol. 2, Plenum Press, New York, 1970, p. 33.
[263] T. Petrenko, F. Neese, J. Chem. Phys. 127 (2007) 164319.
[264] A.B. Myers, R.A. Mathies, D.J. Tannor, E.J. Heller, J. Chem. Phys. 77 (1982) 3857.
[265] D.J. Tannor, E.J. Heller, J. Chem. Phys. 77 (1982) 202.
[266] E.J. Heller, R.L. Sundberg, D. Tannor, J. Phys. Chem. 86 (1982) 1822.
[267] S.Y. Lee, E.J. Heller, J. Chem. Phys. 71 (1979) 4777.
[268] H.-C. Jankowiak, J.L. Stuber, R. Berger, J. Chem. Phys. 127 (2007) 234101.
[269] M. Dierksen, S. Grimme, J. Chem. Phys. 120 (2004) 3544.
[270] M. Dierksen, S. Grimme, J. Phys. Chem. A 108 (2004) 10225.
[271] A.B. Myers, R.A. Mathies, in: T.G. Spiro (Ed.), Biological Applications of Raman Spectroscopy, Wiley, New York, 1987, p. 1.
[272] A.B. Myers, Acc. Chem. Res. 30 (1997) 519.
[273] A.B. Myers, Chem. Rev. 96 (1996) 911.
[274] T. Petrenko, K. Ray, K.E. Wieghardt, F. Neese, J. Am. Chem. Soc. 128 (2006) 4422.
[275] J.C. Slater, Adv. Quant. Chem. 6 (1972) 1.
[276] J.F. Janak, Phys. Rev. B 18 (1978) 7165.
[277] J.W.D. Connolly, H. Siegbahn, U. Gelius, C. Nordling, J. Chem. Phys. 58 (1973) 4265.
[278] M. Stener, A. Lisini, P. Decleva, Chem. Phys. Lett. 191 (1995) 141.
[279] C.-H. Hu, D.P. Chong, Chem. Phys. Lett. 262 (1995) 729.
[280] C.-H. Hu, D.P. Chong, Chem. Phys. Lett. 262 (1996) 733.
[281] M. Cavalleri, H. Ogasawara, L.G.M. Pettersson, A. Nilsson, Chem. Phys. Lett. 364 (2002) 363.
[282] S. DeBeer, D.W. Randall, A.M. Nersissian, J.S. Valentine, B. Hedman, K.O. Hodgson, E.I. Solomon, J. Phys. Chem. B 104 (2000) 10814.
[283] S. DeBeer, P. Wittung-Stafshede, J. Leckner, G. Karlsson, J.R. Winkler, H.B. Gray, B.G. Malmstrom, E.I. Solomon, B. Hedman, K.O. Hodgson, Inorg. Chim. Acta 297 (2000) 278.
[284] S.D. George, M. Metz, R.K. Szilagyi, H.X. Wang, S.P. Cramer, Y. Lu, W.B. Tolman, B. Hedman, K.O. Hodgson, E.I. Solomon, J. Am. Chem. Soc. 123 (2001) 5757.
[285] R.K. Szilagyi, B.S. Lim, T. Glaser, R.H. Holm, B. Hedman, K.O. Hodgson, E.I. Solomon, J. Am. Chem. Soc. 125 (2003) 9158.
[286] A. Dey, T. Glaser, J.J.G. Moura, R.H. Holm, B. Hedman, K.O. Hodgson, E.I. Solomon, J. Am. Chem. Soc. 126 (2004) 16868.
[287] A. Dey, R.K. Hocking, P. Larsen, A.S. Borovik, K.O. Hodgson, B. Hedman, E.I. Solomon, J. Am. Chem. Soc. 128 (2006) 9825.
[288] R. Sarangi, N. Aboelella, K. Fujisawa, W.B. Tolman, B. Hedman, K.O. Hodgson, E.I. Solomon, J. Am. Chem. Soc. 128 (2006) 8286.
[289] K. Ray, S.D. George, E.I. Solomon, K. Wieghardt, F. Neese, Chem. Eur. J. 13 (2007) 2783.
[290] S. DeBeer George, T. Petrenko, F. Neese, Inorg. Chim. Acta 361 (2007) 965.

[291] J.J. Rehr, E.A. Stern, R.L. Martin, E.R. Davidson, Phys. Rev. B 17 (1978) 560.
[292] F. Neese, B. Hedman, K.O. Hodgson, E.I. Solomon, Inorg. Chem. 38 (1999) 4854.
[293] R. Kapre, K. Ray, I. Sylvestre, T. Weyhermueller, S.D. George, F. Neese, K. Wieghardt, Inorg. Chem. 45 (2006) 3499.
[294] S. DeBeer George, T. Petrenko, F. Neese, J. Phys. Chem. A, submitted for publication.
[295] S. DeBeer George, J.F. Berry, F. Neese, Phys. Chem. Chem. Phys., in press, doi:10.1039/b801803k.
[296] J. Yano, J. Robblee, Y. Pushkar, M.A. Marcus, J. Bendix, J.M. Workman, T.J. Collins, E.I. Solomon, S.D. George, V.K. Yachandra, J. Am. Chem. Soc. 129 (2007) 12989.
[297] W.J. Song, M.S. Seo, S.D. George, T. Ohta, R. Song, M.J. Kang, T. Tosha, T. Kitagawa, E.I. Solomon, W. Nam, J. Am. Chem. Soc. 129 (2007) 1268.
[298] R. Sarangi, S.D. George, D.J. Rudd, R.K. Szilagyi, X. Ribas, C. Rovira, M. Almeida, K.O. Hodgson, B. Hedman, E.I. Solomon, J. Am. Chem. Soc. 129 (2007) 2316.
[299] J.S. Pap, F.L. Benedito, E. Bothe, E. Bill, S.D. George, T. Weyhermüller, K. Wieghardt, Inorg. Chem. 46 (2007) 4187.
[300] R.R. Kapre, E. Bothe, T. Weyhermuller, S.D. George, K. Wieghardt, Inorg. Chem. 46 (2007) 5642.
[301] R.R. Kapre, E. Bothe, T. Weyhermuller, S.D. George, N. Muresan, K. Wieghard, Inorg. Chem. 46 (2007) 7827.
[302] R.R. Kapre, E. Bothe, T. Weyhermüller, S.D. George, K. Wieghardt, Inorg. Chem. 46 (2007) 5642.
[303] G.E. Pake, T.L. Estle, The Physical Principles of Electron Paramagnetic Resonance, W.A. Benjamin Inc., London, 1973.
[304] N.M. Atherton, Principles of Electron Spin Resonance, 2nd ed., Ellis Horwood, Prentice-Hall, New York, 1993.
[305] C.J. Ballhausen, Introduction to Ligand Field Theory, McGraw-Hill, New Yowrk, 1962.
[306] C.J. Ballhausen, H.B. Gray, Molecular Orbital Theory, Benjamin, New York, 1964.
[307] J.S. Griffith, The Theory of Transition Metal Ions, Camebridge University press, Camebridge, 1964.
[308] D. Reinen, M. Atanasov, W. Massa, Z. Anorg. Allg. Chem. 632 (2006) 1375.
[309] M. Atanasov, C.A. Daul, M.M. Rohmer, T. Venkatachalam, Chem. Phys. Lett. 427 (2006) 449.
[310] M. Atanasov, P. Comba, C.A. Daul, J. Phys. Chem. A 110 (2006) 13332.
[311] M. Atanasov, C. Rauzy, P. Baettig, C. Daul, Int. J. Quant. Chem. 102 (2005) 119.
[312] M. Atanasov, C.A. Daul, Comp. Rend. Chim. 8 (2005) 1421.
[313] M. Atanasov, C. Daul, H.U. Gudel, T.A. Wesolowski, M. Zbiri, Inorg. Chem. 44 (2005) 2954.
[314] M. Atanasov, C. Daul, Chimia 59 (2005) 504.
[315] M. Atanasov, C.A. Daul, C. Rauzy, Chem. Phys. Lett. 367 (2003) 737.
[316] M. Atanasov, C.A. Daul, Chem. Phys. Lett. 379 (2003) 209.
[317] M. Atanasov, C.A. Daul, Chem. Phys. Lett. 381 (2003) 584.
[318] F. Neese, E.I. Solomon, Inorg. Chem. 37 (1998) 6568.
[319] F. Neese, Int. J. Quant. Chem. 83 (2001) 104.
[320] F. Neese, J. Chem. Phys. 115 (2001) 11080.
[321] F. Neese, J. Chem. Phys. 118 (2003) 3939.
[322] F. Neese, Chem. Phys. Lett. 380 (2003) 721.
[323] F. Neese, in: M. Kaupp, M. Bühl, V. Malkin (Eds.), The Quantum Chemical Calculation of NMR and EPR Properties, Wiley–VCH, Heidelberg, 2004, p. 541.
[324] F. Neese, Magn. Reson. Chem. 42 (2004) S187.
[325] F. Neese, J. Chem. Phys. 127 (2007) 164112.
[326] F. Neese, E.I. Solomon, in: J.S. Miller, M. Drillon (Eds.), Magnetoscience—From Molecules to Materials, vol. IV, Wiley VCH, Weinheim, 2003, p. 345.
[327] S. Sinnecker, F. Neese, J. Phys. Chem. A 110 (2006) 12267.
[328] F. Neese, J. Am. Chem. Soc. 128 (2006) 10213.
[329] D. Ganyushin, F. Neese, J. Chem. Phys. 125 (2006) 024103.
[330] R. Takeda, S. Mitsuo, S. Yamanaka, K. Yamaguchi, Polyhedron 24 (2005) 2238.
[331] M. Shoji, K. Koizumi, T. Hamamoto, T. Taniguchi, R. Takeda, Y. Kitagawa, T. Kawakami, M. Okumura, S. Yamanaka, K. Yamaguchi, Polyhedron 24 (2005) 2708.
[332] O. Loboda, B. Minaev, O. Vahtras, B. Schimmelpfennig, H. Agren, K. Ruud, D. Jonsson, Chem. Phys. 286 (2003) 127.
[333] O. Vahtras, O. Loboda, B. Minaev, H. Agren, K. Ruud, Chem. Phys. 279 (2002) 133.
[334] R. Reviakine, A.V. Arbuznikov, J.-C. Tremblay, C. Remenyi, O.L. Malkina, I. Malkin, M. Kaupp, J. Chem. Phys. 125 (2006) 054110.
[335] O. Loboda, B. Minaev, O. Vahtras, K. Ruud, H. Agren, J. Chem. Phys. 119 (2003) 3120.
[336] J. Mählmann, M. Klessinger, Int. J. Quant. Chem. 77 (2000) 446.
[337] B. Bomfleur, M. Sironi, M. Raimondi, J. Voitländer, J. Chem. Phys. 112 (2000) 1066.
[338] Z. Havlas, J. Michl, Perkin Trans. (1999) 2299.
[339] C. Ribbing, K. Pierloot, A. Ceulemans, Inorg. Chem. 37 (1998) 5227.
[340] P.R. Surjan, K. Nemeth, M. Kallay, J. Mol. Struct. Theochem 398 (1997) 293.
[341] P.R. Surjan, K. Nemeth, M. Bennati, A. Grupp, M. Mering, Chem. Phys. Lett. 251 (1996) 115.
[342] A. Pullmann, E. Kochanski, Int. J. Quant. Chem. IS (1967) 251.
[343] F. Neese, in: B. Gilbert (Ed.), Specialist Reports on EPR Spectroscopy, Royal Society of Chemistry, London, 2007, p. 73.
[344] M. Kaupp, in: A. Lund, M. Shiotani (Eds.), EPR Spectroscopy of Free Radicals in Solids. Trends in Methods and Applications, Kluwer, Dordrecht, 2002.
[345] S. Patchkovskii, G. Schreckenbach, in: M. Kaupp, V. Malkin, M. Bühl (Eds.), Calculation of NMR and EPR Parameters, Wiley–VCH, Weinheim, 2004, p. 505.
[346] B.A. Hess, C.M. Marian, U. Wahlgren, O. Gropen, Chem. Phys. Lett. 251 (1996) 365.
[347] A. Berning, M. Schweizer, H.J. Werner, P.J. Knowles, P. Palmieri, Mol. Phys. 98 (2000) 1823.
[348] A. Nicklass, K.A. Peterson, A. Berning, H.J. Werner, P.J. Knowles, J. Chem. Phys. 112 (2000) 5624.
[349] F. Neese, J. Chem. Phys. 122 (2005) 034107.
[350] F. Neese, J. Phys. Chem. A 105 (2001) 4290.
[351] A. Schweiger, G. Jeschke, Principles of Pulse Electron Paramagnetic Resonance, Oxford University Press, Oxford, 2001.
[352] C.P. Slichter, Principles of magnetic resonance, Springer, Heidelberg, 1990.
[353] M. Kaupp, V. Malkin, M. Bühl (Eds.), The Quantum Chemical Calculation of NMR and EPR Properties, Wiley–VCH, Heidelberg, 2004.
[354] F. London, J. Phys. Radium 8 (1937) 397.
[355] R. Ditchfield, Mol. Phys. 27 (1974) 789.
[356] K. Wolinski, J.F. Hinton, P. Pulay, J. Am. Chem. Soc. 112 (1990) 8251.
[357] S. Kossmann, K.B.F. Neese, Mol. Phys. 105 (2007) 2049.
[358] M. Kaupp, R. Reviakine, O.L. Malkina, A. Arbuznikov, B. Schimmelpfennig, V. Malkin, J. Comput. Chem. 23 (2001) 794.
[359] X.R. Sun, H. Chun, K. Hildenbrand, E. Bothe, T. Weyhermüller, F. Neese, K. Wieghardt, Inorg. Chem. 41 (2002) 4295.
[360] S. Zein, F. Neese, J. Phys. Chem. A, 2008, in press.
[361] S. Zein, C. Duboc, W. Lubitz, F. Neese, Inorg. Chem. 47 (2007) 134.
[362] J.C. Schöneboom, F. Neese, W. Thiel, J. Am. Chem. Soc. 127 (2005) 5840.
[363] O. Pestovsky, S. Stoian, E.L. Bominaar, X.P. Shan, E. Munck, L. Que Jr., A. Bakac, Angew. Chem. Int. Ed. 44 (2005) 6871.
[364] M. Atanasov, P. Comba, C.A. Daul, F. Neese, in: J. Boeyens, J. Ogilvie (Eds.), Models, Mysteries and Magic of Molecules, Springer, Heidelberg, 2008.
[365] M.L. Munzarova, M. Kaupp, J. Phys. Chem. A 103 (1999) 9966.
[366] M.L. Munzarova, P. Kubacek, M. Kaupp, J. Am. Chem. Soc. 122 (2000) 11900.
[367] S. Kababya, J. Nelson, C. Calle, F. Neese, D. Goldfarb, J. Am. Chem. Soc. 128 (2006) 2017.
[368] M. Bühl, M. Kaupp, O.L. Malkina, V.G. Malkin, J. Comput. Chem. 20 (1999) 91.
[369] M. Bühl, in: M. Kaupp, V. Malkin, M. Bühl (Eds.), Calculation of NMR and EPR Parameters, Wiley–VCH, Weinheim, 2004, p. 421.
[370] M. Bühl, Inorg. Chem. 44 (2005) 6277.
[371] M.P. Waller, M. Bühl, K.R. Geethalakshmi, D.Q. Wang, W. Thiel, Chem. Eur. J. 13 (2007) 4723.
[372] J. Vaara, O.L. Malkina, H. Stoll, V.G. Malkin, M. Kaupp, J. Chem. Phys. 114 (2001) 61.
[373] M. Kaupp, C. Rovira, M. Parrinello, J. Phys. Chem. B 104 (2000) 5200.
[374] M. Kaupp, C. Aubauer, G. Engelhardt, T.M. Klapotke, O.L. Malkina, J. Chem. Phys. 110 (1999) 3897.
[375] R. Salzmann, M. Kaupp, M.T. McMahon, E. Oldfield, J. Am. Chem. Soc. 120 (1998) 4771.
[376] J.H. Mao, Y. Zhang, E. Oldfield, J. Am. Chem. Soc. 124 (2002) 13911.
[377] Z. Rinkevicius, J. Vaara, L. Telyatnyk, O. Vahtras, J. Chem. Phys. 118 (2003) 2550.
[378] S. Moon, S. Patchkovskii, in: M. Kaupp, V. Malkin, M. Bühl (Eds.), Calculation of NMR and EPR Parameters, Wiley–VCH, Weinheim, 2004, p. 325.
[379] P. Gütlich, J. Ensling, in: E.i. Solomon, A.B.P. Lever (Eds.), Inorganic Electronic Structure and Spectroscopy, Wiley, New York, 1999, p. 161.
[380] P. Gütlich, R. Link, A. Trautwein, Mössbauer Spectroscopy and Transition Metal Chemistry, Springer, Heidelberg/New York, 1978.
[381] W.G. Han, T.Q. Liu, T. Lovell, L. Noodleman, J. Comput. Chem. 27 (2006) 1292.
[382] Y. Zhang, J.H. Mao, E. Oldfield, J. Am. Chem. Soc. 124 (2002) 7829.
[383] Y. Zhang, J. Mao, E. Oldfield, J. Am. Chem. Soc. 124 (2002) 7829.
[384] F. Neese, Inorg. Chim. Acta 337C (2002) 181.
[385] S. Sinnecker, L.D. Slep, E. Bill, F. Neese, Inorg. Chem. 44 (2005) 2245.
[386] T.Q. Liu, T. Lovell, W.G. Han, L. Noodleman, Inorg. Chem. 42 (2003) 5244.
[387] T. Lovell, J. Li, D.A. Case, L. Noodleman, J. Am. Chem. Soc. 124 (2002) 4546.
[388] T. Lovell, W.G. Han, T. Liu, L. Noodleman, J. Am. Chem. Soc. (2002) 5890.
[389] V.V. Vramasu, E.L. Bominaar, J. Meyer, E. Münck, Inorg. Chem. 41 (2002) 6358.
[390] K. Ray, A. Begum, T. Weyhermüller, S. Piligkos, J. van Slageren, F. Neese, K. Wieghardt, J. Am. Chem. Soc. 127 (2005) 4403.
[391] F. Neese, J. Inorg. Biol. Chem. 100 (2006) 716.
[392] M. Filatov, J. Chem. Phys. 127 (2007).
[393] W.G. Han, T.Q. Liu, T. Lovell, L. Noodleman, J. Inorg. Biochem. 100 (2006) 771.
[394] W.G. Han, T.Q. Liu, T. Lovell, L. Noodleman, J. Am. Chem. Soc. 127 (2005) 15778.
[395] T.Q. Liu, T. Lovell, W.G. Han, L. Noodleman, Inorg. Chem. 43 (2004) 6858.
[396] W.G. Han, T. Lovell, T.Q. Liu, L. Noodleman, Inorg. Chem. 43 (2004) 613.
[397] W.G. Han, T. Lovell, T.Q. Liu, L. Noodleman, Inorg. Chem. 42 (2003) 2751.
[398] T. Lovell, J. Li, D.A. Case, L. Noodleman, J. Biol. Inorg. Chem. 7 (2002) 735.
[399] T. Lovell, W.G. Han, T.Q. Liu, L. Noodleman, J. Am. Chem. Soc. 124 (2002) 5890.
[400] T. Lovell, J. Li, L. Noodleman, Inorg. Chem. 40 (2001) 5251.
[401] T. Lovell, J. Li, T.Q. Liu, D.A. Case, L. Noodleman, J. Am. Chem. Soc. 123 (2001) 12392.
[402] Y. Zhang, E. Oldfield, J. Am. Chem. Soc. 126 (2004) 9494.
[403] Y. Zhang, E. Oldfield, J. Phys. Chem. A 107 (2003) 4147.
[404] Y. Zhang, E. Oldfield, J. Phys. Chem. B 107 (2003) 7180.
[405] Y. Zhang, W. Gossman, E. Oldfield, J. Am. Chem. Soc. 125 (2003) 16387.
[406] Y. Zhang, J.H. Mao, N. Godbout, E. Oldfield, J. Am. Chem. Soc. 124 (2002) 13921.
[407] S. Stoian, O. Pestovsky, E.L. Bominaar, E. Münck, L. Que Jr., A. Bakac, ICBIC-12, Minneapolis, 2005.

[408] C.V. Sastri, M.J. Park, T. Ohta, T.A. Jackson, A. Stubna, M.S. Seo, J. Lee, J. Kim, T. Kitagawa, E. Munck, L. Que Jr., W. Nam, J. Am. Chem. Soc. 127 (2005) 12494.
[409] M.P. Jensen, M. Costas, R.Y.N. Ho, J. Kaizer, A. Mairatai Payeras, E. Munck, L. Que Jr., J.-U. Rohde, A. Stubna, J. Am. Chem. Soc. 127 (2005) 10512.
[410] J. Kaizer, E.J. Klinker, N.Y. Oh, J.-U. Rohde, W.J. Song, A. Stubna, J. Kim, E. Munck, W. Nam, L. Que Jr., J. Am. Chem. Soc. 126 (2004) 472.
[411] M.H. Lim, J.U. Rohde, A. Stubna, M.R. Bukowski, M. Costas, R.Y.N. Ho, E. Munck, W. Nam, L. Que, Proc. Natl. Acad. Sci. U.S.A. 100 (2003) 3665.
[412] T. Petrenko, S. DeBeer George, N. Aliaga-Alcalde, E. Bill, B. Mienert, Y. Xiao, Y. Guo, W. Sturhahn, S.P. Cramer, K. Wieghardt, F. Neese, J. Am. Chem. Soc. 129 (2007) 11053.
[413] J.F. Berry, E. Bill, R. Garcia-Serres, F. Neese, T. Weyhermüller, K. Wieghardt, Inorg. Chem. 45 (2006) 2027.
[414] J.F. Berry, E. Bill, E. Bothe, F. Neese, K. Wieghardt, J. Am. Chem. Soc. 128 (2006) 13515.
[415] J.F. Berry, E. Bill, E. Bothe, S.D. George, B. Mienert, F. Neese, K. Wieghardt, Science 312 (2006) 1937.
[416] S.C. Bart, K. Chlopek, E. Bill, M.W. Bouwkamp, E. Lobkovsky, F. Neese, K. Wieghardt, P.J. Chirik, J. Am. Chem. Soc. 128 (2006) 13901.
[417] V.K.K. Praneeth, F. Neese, N. Lehnert, Inorg. Chem. 44 (2005) 2570.
[418] N. Aliaga-Alcade, S. DeBeer George, E. Bill, K. Wieghardt, F. Neese, Angew. Chem. Int. Ed. 44 (2005) 2908.
[419] R. Garcia Serres, C.A. Grapperhaus, E. Bothe, E. Bill, T. Weyhermüller, F. Neese, K. Wieghardt, J. Am. Chem. Soc. 126 (2004) 5138.
[420] L.D. Slep, F. Neese, Angew. Chem.-Int. Ed. 42 (2003) 2942.
[421] L.D. Slep, A. Mijovilovich, W. Meyer-Klaucke, T. Weyhermüller, E. Bill, E. Bothe, F. Neese, K. Wieghardt, J. Am. Chem. Soc. 125 (2003) 15554.
[422] P. Ghosh, E. Bill, T. Weyhermüller, F. Neese, K. Wieghardt, J. Am. Chem. Soc. 125 (2003) 1293.
[423] A.X. Trautwein, F.E. Harris, A.J. Freeman, J.P. Desclaux, Phys. Rev. B 11 (1975) 4101.
[424] G.K. Shenoy, F.E. Wagner (Eds.), Mössbauer Isomer Shifts, North-Holland, Amsterdam, 1978.
[425] V. Starovoitova, T.E. Budarz, G.R.A. Wyllie, W.R. Scheidt, W. Sturhahn, E.E. Alp, E.W. Prohofsky, S.M. Durbin, J. Phys. Chem. B 110 (2006) 13277.
[426] W.Q. Zeng, N.J. Silvernail, D.C. Wharton, G.Y. Georgiev, B.M. Leu, W.R. Scheidt, J.Y. Zhao, W. Sturhahn, E.E. Alp, J.T. Sage, J. Am. Chem. Soc. 127 (2005) 11200.
[427] B.M. Leu, M.Z. Zgierski, G.R.A. Wyllie, M.K. Ellison, W.R. Scheidt, W. Sturhahn, E.E. Alp, S.M. Durbin, J.T. Sage, J. Phys. Chem. Solids 66 (2005) 2250.
[428] B.M. Leu, M.Z. Zgierski, G.R.A. Wyllie, W.R. Scheidt, W. Sturhahn, E.E. Alp, S.M. Durbin, J.T. Sage, J. Am. Chem. Soc. 126 (2004) 4211.
[429] H. Paulsen, V. Schünemann, A.X. Trautwein, H. Winkler, Coord. Chem. Rev. 249 (2005) 255.
[430] H. Paulsen, P. Wegner, H. Winkler, J.A. Wolny, L.H. Bottger, A.X. Trautwein, C. Schmidt, V. Schünemann, G. Barone, A. Silvestri, G. La Manna, A.I. Chumakov, I. Sergueev, R. Ruffer, Hyperfine Interact. 165 (2005) 17.
[431] A.X. Trautwein, P. Wegner, H. Winkler, H. Paulsen, V. Schünemann, C. Schmidt, A.I. Chumakov, R. Ruffer, Hyperfine Interact. 165 (2005) 295.
[432] T. Petrenko, W. Sturhahn, F. Neese, Hyperfine Interact. (2008), doi:10.1007/s10751-008-9600-5.
[433] P. Gütlich, H.A. Goodwin, Top. Curr. Chem. 233–235 (2004).
[434] S. Zein, S.A. Borshch, P. Fleurat-Lessard, M.E. Casida, H. Chermette, J. Chem. Phys. 126 (2007).
[435] G. Ganzenmuller, N. Berkaine, A. Fouqueau, M.E. Casida, M. Reiher, J. Chem. Phys. 122 (2005).
[436] A. Fouqeau, M.E. Casida, L.M. Lawson, A. Hauser, F. Neese, J. Chem. Phys. 122 (2005) 044110.
[437] L.M.L. Daku, A. Vargas, A. Hauser, A. Fouqueau, M.E. Casida, ChemPhysChem 6 (2005) 1393.
[438] A. Fouqueau, S. Mer, M.E. Casida, L.M.L. Daku, A. Hauser, T. Mineva, F. Neese, J. Chem. Phys. 120 (2004) 9473.
[439] G. Brehm, M. Reiher, B. Le Guennic, M. Leibold, S. Schindler, F.W. Heinemann, S. Schneider, J. Raman Spectrosc. 37 (2006) 108.
[440] M. Reiher, Inorg. Chem. 41 (2002) 6928.
[441] G. Brehm, M. Reiher, S. Schneider, J. Phys. Chem. A 106 (2002) 12024.
[442] M. Reiher, O. Salomon, B.A. Hess, Theor. Chem. Acc. 107 (2001) 48.
[443] K.L. Ronayne, H. Paulsen, A. Hofer, A.C. Dennis, J.A. Wolny, A.I. Chumakov, V. Schünemann, H. Winkler, H. Spiering, A. Bousseksou, P. Gutlich, A.X. Trautwein, J.J. McGarvey, Phys. Chem. Chem. Phys. 8 (2006) 4685.
[444] L.H. Bottger, A.I. Chumakov, C.M. Grunert, P. Gutlich, J. Kusz, H. Paulsen, U. Ponkratz, V. Rusanov, A.X. Trautwein, J.A. Wolny, Chem. Phys. Lett. 429 (2006) 189.
[445] G. Lemercier, N. Brefuel, S. Shova, J.A. Wolny, F. Dahan, M. Verelst, H. Paulsen, A.X. Trautwein, J.P. Tuchagues, Chem. Eur. J. 12 (2006) 7421.
[446] H. Paulsen, A.X. Trautwein, Spin Crossover Transit. Met. Compd. Iii (2004) p197.
[447] H. Paulsen, A.X. Trautwein, J. Phys. Chem. Solids 65 (2004) 793.
[448] S. Larsson, K. Stahl, M.C. Zerner, Inorg. Chem. 25 (1986) 3033.
[449] K. Pierloot, S. Vancoillie, J. Chem. Phys. 125 (2006).
[450] A. Fouqueau, M.E. Casida, L.M.L. Daku, A. Hauser, F. Neese, J. Chem. Phys. 122 (2005).
[451] R. Szylagi, M. Metz, E.I. Solomon, J. Phys. Chem. A 106 (2002) 2994.
[452] M. Filatov, S. Shaik, J. Chem. Phys. 110 (1999) 116.
[453] P. Deloth, P. Cassoux, J.P. Daudey, J.P. Malrieu, J. Am. Chem. Soc. 103 (1981) 4007.
[454] J. Cabrero, C. de Graaf, E. Bordas, R. Caballol, J.P. Malrieu, Chem. Eur. J. 9 (2003) 2307.
[455] M. Reguero, R. Caballol, J.L. Heully, J.P. Malrieu, Chem. Phys. Lett. 265 (1997) 621.
[456] C.J. Calzado, J.P. Malrieu, J. Cabrero, R. Caballol, J. Phys. Chem. A 104 (2000) 11636.
[457] J. Cabrero, C.J. Calzado, D. Maynau, R. Caballol, J.P. Malrieu, J. Phys. Chem. A 106 (2002) 8146.
[458] C.J. Calzado, J. Cabrero, J.P. Malrieu, R. Caballol, J. Chem. Phys. 116 (2002) 3985.
[459] C.J. Calzado, J. Cabrero, J.P. Malrieu, R. Caballol, J. Chem. Phys. 116 (2002) 2728.
[460] I. Moreira, N. Suaud, N. Guihery, J.P. Malrieu, R. Caballol, J.M. Bofill, F. Illas, Phys. Rev. B 66 (2002).
[461] F. Illas, I.D.R. Moreira, C. de Graaf, V. Barone, Theor. Chem. Acc. 104 (2000) 265.
[462] C. de Graaf, E.D.R. Moreira, F. Illas, O. Iglesias, A. Labarta, Phys. Rev. B 66 (2002).
[463] D. Munoz, C. De Graaf, F. Illas, J. Comput. Chem. 25 (2004) 1234.
[464] C. Sousa, C. de Graaf, N. Lopez, N.M. Harrison, F. Illas, J. Phys. Condens. Matter 16 (2004) S2557.
[465] E. Schreiner, N.N. Nair, R. Pollet, V. Staemmler, D. Marx, Proc. Natl. Acad. Sci. U.S.A. 104 (2007) 20725.
[466] L. Noodleman, J. Chem. Phys. 74 (1981) 5737.
[467] G. Jonkers, C.A. Delange, L. Noodleman, E.J. Baerends, Mol. Phys. 46 (1982) 609.
[468] L. Noodleman, J.G. Norman, J.H. Osborne, A. Aizman, D.A. Case, J. Am. Chem. Soc. 107 (1985) 3418.
[469] L. Noodleman, E.R. Davidson, Chem. Phys. 109 (1986) 131.
[470] J.C. Slater, The Quantum Theory of Atomic Structure, vol. II, McGraw-Hill, New York, 1960.
[471] C. Kolczewski, K. Fink, V. Staemmler, Int. J. Quant. Chem. 76 (2000) 137.
[472] K. Fink, C. Wang, V. Staemmler, Inorg. Chem. 38 (1999) 3847.
[473] K. Fink, C. Wang, V. Staemmler, Int. J. Quant. Chem. 65 (1997) 633.
[474] C. Wang, K. Fink, V. Staemmler, Chem. Phys. 201 (1995) 87.
[475] C. Wang, K. Fink, V. Staemmler, Chem. Phys. 192 (1995) 25.
[476] K. Fink, R. Fink, V. Staemmler, Inorg. Chem. 33 (1994) 6219.
[477] V.M. Garcia, O. Castell, R. Caballol, J.P. Malrieu, Chem. Phys. Lett. 238 (1995) 222.
[478] J. Miralles, O. Castell, R. Caballol, J.P. Malrieu, Chem. Phys. 172 (1993) 33.
[479] F. Neese, J. Phys. Chem. Solids 65 (2004) 781.
[480] V.N. Staroverov, E.R. Davidson, J. Am. Chem. Soc. 122 (2000) 7377.
[481] V.N. Staroverov, E.R. Davidson, Chem. Phys. Lett. 330 (2000) 161.
[482] M. Head-Gordon, Chem. Phys. Lett. 372 (2003) 508.
[483] K. Yamaguchi, Y. Takahara, T. Fueno, in: V.H. Smith (Ed.), Applied Quantum Chemistry, V. Reidel, Dordrecht, 1986, p. 155.
[484] T. Soda, Y. Kitagawa, T. Onishi, Y. Takano, Y. Shigeta, H. Nagao, Y. Yoshika, K. Yamaguchi, Chem. Phys. Lett. 319 (2000) 223.
[485] L. Noodleman, D. Post, E.J. Baerends, Chem. Phys. 64 (1982) 159.
[486] L. Noodleman, Inorg. Chem. 27 (1988) 3677.
[487] L. Noodleman, D.A. Case, A. Aizman, J. Am. Chem. Soc. 110 (1988) 1001.
[488] E. Ruiz, S. Alvarez, J. Cano, V. Polo, J. Chem. Phys. 123 (2005) 164110.
[489] C. Adamo, V. Barone, A. Bencini, R. Broer, M. Filatov, N.M. Harrison, F. Illas, J.P. Malrieu, I.D.R. Moreira, J. Chem. Phys. 124 (2006).
[490] E. Ruiz, S. Alvarez, J. Cano, V. Polo, J. Chem. Phys. 123 (2006) 107102.
[491] J.H. Wang, A.D. Becke, V.H. Smith, J. Chem. Phys. 102 (1995) 3477.
[492] A.J. Cohen, D.J. Tozer, N.C. Handy, J. Chem. Phys. 126 (2007).
[493] J. Li, L. Noodleman, D.A. Case, in: E.I. Solomon, A.B.P. Lever (Eds.), Inorganic Electronic Structure and Spectroscopy, vol. I, John Wiley & Sons, New York, 1999, p. 661.
[494] D. Herebian, K.E. Wieghardt, F. Neese, J. Am. Chem. Soc. 125 (2003) 10997.
[495] A.T. Amos, G.G. Hall, Proc. R. Soc. Ser. A 263 (1961) 483.
[496] H.F. King, R.E. Stanton, H. Kim, R.E. Wyatt, R.G. Parr, J. Chem. Phys. 47 (1967) 1936.
[497] G. Trinquier, J.P. Malrieu, I. Garciacuesta, J. Am. Chem. Soc. 113 (1991) 6465.
[498] W.A. Goddard, T.H. Dunning, W.J. Hunt, P.J. Hay, Acc. Chem. Res. 6 (1973) 368.
[499] A.I. Krylov, Chem. Phys. Lett. 338 (2001) 375.
[500] Y.H. Shao, M. Head-Gordon, A.I. Krylov, J. Chem. Phys. 118 (2003) 4807.
[501] A. de la Lande, V. Moliner, O. Parisel, J. Chem. Phys. 126 (2007) 035102.
[502] I. Rudra, Q. Wu, T. Van Voorhis, J. Chem. Phys. 124 (2006).
[503] R. Bastardis, N. Guihery, N. Suaud, Phys. Rev. B 75 (2007).
[504] R. Bastardis, N. Guihery, C. de Graaf, Phys. Rev. B 76 (2007).
[505] R. Bastardis, N. Guihery, N. Suaud, C. de Graaf, J. Chem. Phys. 125 (2006).
[506] R. Bastardis, N. Guihery, C. de Graaf, Phys. Rev. B 74 (2006).
[507] Y. Komiyama, E.C. Lingafelter, Acta Cryst. 17 (1964) 1145.
[508] R.J. Bartlett, I.V. Schweigert, V.F. Lotrich, J. Mol. Struct. Theochem. 771 (2006) 1.
[509] S. Grimme, Angew. Chem. 118 (2006) 4576.
[510] T. Ziegler, Chem. Rev. 91 (1991) 651.
[511] R. vanLeeuwen, O. V. Gritsenko, E. J. Baerends, in Density Functional Theory I, vol. 180, 1996, pp. 107.
[512] E.J. Baerends, O.V. Gritsenko, R. van Leeuwen, in: B.B. Laird, R.B. Ross, T. Ziegler (Eds.), Chemical Applications of Density-Functional Theory, American Chemical Society, Washington DC, 1996.
[513] A.V. Astashkin, F. Neese, A.M. Raitsimaring, J.J.A. Cooney, E. Bultman, J.H. Enemark, J. Am. Chem. Soc. 127 (2005) 16713.
[514] M. Mader-Cosper, F. Neese, A.V. Astashkin, M.A. Carducci, A.M. Raitsimring, J.H. Enemark, Inorg. Chem. 44 (2005) 1290.
[515] J. Fritscher, P. Hrobarik, M. Kaupp, J. Phys. Chem. B 111 (2007) 4616.